DEPARTAMENTO DE CIÊNCIAS DA VIDA

FACULDADE DE CIÊNCIAS E TECNOLOGIA
UNIVERSIDADEDE COIMBRA

Ketone Bodies as Brain Substrates

Dissertação apresentada à Universidade de Coimbra para cumprimento dos requisitos necessários à obtenção do grau de Mestre em Bioquímica, realizada sob a orientação científica do Professor Doutor John G. Jones (CNC/Biocant- UC-Biotech) e do Professor Doutor Ângelo Tomé (Universidade de Coimbra)

Paula Sofia Valente da Silva

2015

When a door closes, you open it back.
That's how doors work...

Acknowledgments/Agradecimentos

To Professor John G. Jones, for accepting me in his group all those years ago and for never giving up on me. For all his time and patience, and for trusting me with this project, for all the motivation and for always seeing the potential in me. For helping me grow, as a person and as a scientist, and for showing me that what makes a good scientist is the ability to always be amazed by new discoveries. For being an amazing supervisor. Also, thanks for the beer!

To Professor Rodrigo Cunha, for accepting this partnership and being part of this project, and welcoming me to the Purines group. For all the fruitful meeting and discussions, and the smacks on the head when I needed them.

To doctor Attila Köfalvi, for giving me a place to do my experiments and making me feel like one of his own students! For all the discussions, the laughs and the shared frustrations.

To Professor Rui de Carvalho, for all his help with the analysis and the "borrowed" standards. For the fruitful discussions and for taking a special interest in me and my work.

To all of my colleagues of the "Intermediary Metabolism" Group, in particular to Margarida for all the rides to Cantanhede – and also the gossip that got us through lunch and coffee breaks.

To all of my colleagues at the "Purines at CNC" Group, in particular to Cristina Lemos and Anna, for helping me keep my sanity when all seemed lost – and for rejoicing with me in my little victories. For all the teas, the talks, the laughs and the cries. To Carolina Xavier, with whom it is an absolute joy to work with! To Daniel Rial, for all the help, the jokes and for never thinking my questions were stupid. To Filipe Matheus, for kindly supplying the 6-OHDA rats. To Henrique Silva, who can fix pretty much everything around the lab and keeps our experiments running. To António for, well, for being António.

To Yarmo, for all his curiosity and neverending questions, reminding me why we love science so much!

Aos meus amigos, de Coimbra e do Entroncamento, que me ajudaram a ser o que sou hoje: à Catarina Cajada, que sofreu tanto como eu com esta tese e ouviu as minha infinitas lamentações quando tudo corria mal com infinita paciência; ao Rudolfinho, ao Nini Faloan, ao Cerca, à Minês, ao Scratcha (pelas revisões … e pelos scratchas), à Daniela, ao Tiago alfa, ao Tiago beta, à Cláudia, à minha (sempre) caloirinha Rita Leão e ao meu caloiro André Santiago. Ao Mário Carvalho pelos cafés espontâneos e conversas intermináveis.

Um agradecimento muito especial à Isabel, por toda a ajuda, companheirismo e conselhos. I could not have made it without you giiirl!

À Luísa, por de vez em quando me fazer sair para ver a luz do sol e comer um pastelinho, e me relembrar constantemente que nunca é tarde para perseguirmos os nossos sonhos. Pela sua imensa, eterna e contagiante alegria de simplesmente ser e viver! Pela sua forma muito própria de ver sempre o mundo como algo novo e fantástico a explorar.

Ao meu querido Paulo, um agradecimento muito especial, por me aturar em todos os bons e maus momentos, por sempre me fazer ver o silver lining, por todo o apoio e amor incondicional que me dá e por acreditar em mim pelos dois quando eu não acreditei em mim mesma. Por estar tão, tão perto, mesmo estando longe.

À família do Paulo, em especial à mãe Alda, à irmã Margarida e aos primos Firefox, por me acolherem como se fosse da família.

Aos meus pais, Carlos e Antónia, que sempre me apoiaram e ajudaram incondicionalmente, e sempre fizeram de tudo para que nada me faltasse. A eles que há 18 anos atrás correram a cidade porque tudo o que eu queria pelo Natal era um microscópio. Por manterem sempre esse meu sonho vivo, e por constantemente me lembrarem que eu podia ser o que quisesse "quando fosse grande".

À minha irmã, por de vez em quando me "salvar" do amor dos meus pais. Por ser minha irmã e fazer essas coisas de irmãs. E depois mais ainda.

Aos meus avós, Cuca e Mimi, que durante estes anos em Coimbra me deram mais do que cama, comida e roupa lavada, trataram de mim, mimaram-me e fizeram-me sentir em casa. Garantiram que nunca me faltasse nada, fosse gelado, chocolates, bolachinhas ou miminhos. Ou comida da avó!

A todos os cientistas e investigadores que fazem da ciência algo belo, onde as descobertas são partilhadas com alegria, onde a curiosidade é fomentada, e a sede de saber sempre mais e "porquê" fala sempre mais alto. Que nunca nos falte essa curiosidade infantil, essa sede do saber, e o amor à camisola (ou melhor, à bata?)

Muito obrigado.

Index

Abreviations

°C – degrees Celsius

^{12}C – carbon 12

^{13}C – carbon 13

$^{13}C3$ – carbon 3 labeled as ^{13}C

$^{13}C4$ – carbon 4 labeled as ^{13}C

^{1}H - proton

$^{1}J_{C-H}$ – heteronuclear (C-H) coupling constant J from interactions 1 atomic bond apart

$^{2}J_{C-H}$ – heteronuclear (C-H) coupling constant J from interactions 2 atomic bonds apart

^{2}H– deuterium

^{31}P – phosphorous 31

3HB – 3-D-β-hydroxybutyrate

3-KT – 3-kethotiolase

4-AP – 4 aminopyridine

6-OHDA – 6-hydroxydopamine

AcAc – acetoacetate

AceSS1– acetyl-coA synthetase isoform 1

AceSS2– acetyl-coA synthetase isoform 2

Acetyl-coA – acetyl-coenzyme A

ACSF – artificial cerebral-spinal fluid

ADP – adenosine diphosphate

Ala – alanine

AP – antero-posterior

ATP – adenosine triphosphate

BBB – blood brain barrier

BCA – Bicinchoninic Acid

BSA – bovine serum albumin

coA – coenzyme A

CPT 1 - carnitine palmitoyltransferase 1

Cre – creatine

D₂O – deuterated water

DV – dorso-ventral

Fc0 – fraction of glutamate pool that originated in acetyl-coA without any ^{13}C label

Fc1 – fraction of glutamate pool that originated in acetyl-coA labeled with ^{13}C in carbon 1

Fc2 – fraction of glutamate pool that originated in acetyl-coA labeled with ^{13}C in carbon 2

Fc3 – fraction of glutamate pool that originated in acetyl-coA labeled with ^{13}C in both carbons

GABA – γ-aminobutyric acid

GABA C2D12 - doublet in the carbon 2 region, due to ^{13}C label in the adjacent C1

GABA C2S - GABA labeled with ^{13}C only in carbon 2 giving rise to a Singlet peak

GLUT1 – glucose transporter protein 1

GLUT3 – glucose transporter protein 3

Glutamate C3 – glutamate labeled ^{13}C in carbon 3, regardless of other existing ^{13}C labels on adjacent carbons

Glutamate C4 – glutamate labeled with ^{13}C in carbon 4, regardless of other existing ^{13}C labels on adjacent carbons

Glutamate C4D34 - doublet in the carbon 4 region, due to ^{13}C label in the adjacent C3

Glutamate C4Q – quartet in the carbon 4 region, due to label in the adjacent C5 and the adjacent C3

Glutamate C5D45 – doublet in the carbon 5 region, due to ^{13}C label in the adjacent C4

Glutamate C5S – glutamate labeled with ^{13}C only in carbon 5 giving rise to a Singlet peak

H₂O₂ – hydrogen peroxide

HBD – 3-D-β-hydroxybutyrate dehydrogenase

HL – HMG-coa lyase

HMG-coa - 3-hydroxy-3-methylglutaryl CoA

ip – intraperitoneally

J – apparent coupling constant J

KB- Ketone Bodies

KD – Ketogenic Diet

KOH – potassium hydroxide

Lac – lactate

LCFA – long chain fatty acids

LDH – lactate dehydrogenase

MAT – methylacetoacetyl-coA thiolase

MCT – monocarboxylate transporter protein

MCTr – medium chain triglycerides

mHS - HMG-coa synthase

ML – medium-lateral

MPP+–1-methyl-4-phenylpyridinium

MPTP–1-methyl-4-phenyl-1,2,3,6-tetrahydropyridine

MRS – Magnetic Resonance Spectroscopy

N - nitrogen

NAA – N-acetyl-aspartate

NAD⁺ - oxidated form of nicotinamide adenine dinucleotide

NADH - reduced form of nicotinamide adenine dinucleotide

NADP⁺ - oxidated form of nicotinamide adenine dinucleotide phosphate

NADPH – reduced form of nicotinamide adenine dinucleotide phosphate

NEFA – non-esterified fatty acids

NMR – Nuclear Magnetic Resonance

NR – non-recirculating

OCT – 3-oxoacid-coa transferase

PC – pyruvate carboxylase

PCA – perchloric acid

PCre – phosphocreatine

PD – Parkinson's disease

PDH – pyruvate dehydrogenase

ppm – parts per million

Pyr – pyruvate

Rec – recirculating

ROS – reactive oxygen species

SCOT – succinil-coa oxoacid transferase

SN – Substantia Nigra

TSP – trimethylsilyl propanoic acid

VLDL– very low density lipoproteins

WT – Wild Type

ΔG' – Gibbs free energy

Abstract

Since their discovery as a marker for diabetic ketoacidosis, ketone bodies have become known for their therapeutic role as effective agents in refractory epilepsy and a diet specifically designed to increase ketone bodies' levels in circulation has been often prescribed as treatment. In the classical ketogenic diet, intake of even small additional amounts of carbohydrates drastically drops the level of circulating ketone bodies and abolishes their therapeutical effects (in epilepsy, the immediate re-appearance of seizures is the most obvious sign of reversal). Novel dietary supplements have been developed to produce ketone bodies under less restrictive dietary conditions and are able to generate a significant amount of ketone bodies even in the presence of considerable dietary carbohydrate.

Since previous studies of cerebral ketone body utilization had always been performed under conditions of low glucose availability, the aim of this project was to evaluate the competition between glucose and ketone bodies for cerebral energy production with saturating concentrations of both substrates and probe for possible cell-type substrate preference.

Thus, we evaluated the contribution of saturating (5mM) levels of the ketone body 3-hydroxybutyrate (3HB) to cerebral energy generation in the presence of non-limiting glucose levels (5mM) in hippocampal slices. Following administration of selectively ^{13}C-enriched exogenous glucose, ketone bodies and lactate/pyruvate, we used ^{13}C-NMR isotopomer analysis of tissue glutamate and GABA to determine the contribution of each substrate to glutamatergic and GABA-ergic Krebs cycle utilization. We demonstrated that 3HB effectively competed with glucose for acetyl-coA formation in both metabolic compartments, but with greater efficacy in the glutamatergic compared to the GABA-ergic compartment.

3HB did not decrease lactate/pyruvate utilization for Krebs cycle oxidation, suggesting that it did not downregulate pyruvate oxidation to acetyl-coA via pyruvate dehydrogenase. Instead, it may downregulate glycolysis upstream of PDH, a hypothesis supported by the observation that levels of superfusate lactate derived from glycolysis of the ^{13}C-enriched glucose substrate showed a strong tendency to be reduced in the presence of the ketone body. Ketone bodies also seem to contribute to a more reduced cytosolic redox state as revealed by higher tissue lactate/alanine ratios when 3HB was included as a substrate.

Brain slice preparations also secreted a significant amount of acetate into the superfusion medium. All four possible isotopomers of acetate ($[1-^{13}C]$, $[2-^{13}C]$, $[U-^{13}C]$ and $[U-^{12}C]$acetate) were resolved by ^{1}H NMR of superfusate samples. Acetate ^{13}C-isotopomers originating from $[1-^{13}C]$glucose, $[U-^{13}C]$glucose, $[3-^{13}C]$lactate and $[2-^{13}C]$lactate/pyruvate were observed, but in experiments where $[U-^{13}C]$3HB was present, its predicted $[U-^{13}C]$acetate product was never detected. Hence, we conclude that this acetate was derived from a metabolic pool that was not in exchange with acetyl-CoA that was derived from 3HB oxidation. While not contributing any carbons to secreted acetate, the presence of 3HB seemed to attenuate its production. Further experiments are needed to identify the enzymes and cell compartments that are involved in its production.

Keywords: brain metabolism; Krebs cycle; ketone bodies; NMR spectroscopy

Sumário

Desde a sua descoberta como um marcador de cetoacidose diabética, os corpos cetónicos tornaram-se conhecidos pelo seu papel terapêutico em epilepsia refractária, e uma dieta desenhada especificamente para aumentar os níveis de corpos cetónicos em circulação tem sido prescrita como tratamento. Na dieta cetogénica clássica, o consumo de pequenas quantidades de hidratos de carbono diminui drasticamente os níveis de corpos cetónicos em circulação e suprime o seu efeito terapêutico (em pacientes epilépticos, o re-aparecimento imediato das convulsões é o sinal mais óbvio de reversão). Têm sido desenvolvidos novos suplementos dietéticos para produzir corpos cetónicos sob condições alimentares menos restritas, e estes são capazes de gerar uma quantidade significativa de corpos cetónicos mesmo na presença de níveis de carbohidratos consideráveis.

Dado que os estudos prévios sobre a utilização cerebral de corpos cetónicos foram sempre realizados com baixa disponibilidade de glucose, o objectivo deste trabalho foi o de avaliar a competição entre glucose e corpos cetónicos para a produção de energia cerebral em condições saturantes de ambos os substratos, e explorar possíveis preferências ao nível de tipo de célula.

Assim, avaliámos a contribuição de concentrações saturantes (5mM) do corpo cetónico 3-hidroxibutirato (3HB) para a produção energética cerebral na presença de níveis de glucose não-restritivos (5mM) em fatias de hipocampo. Após a administração de glucose, lactato/piruvato e corpos cetónicos selectivamente marcados com ^{13}C, analisámos os isotopómeros de glutamato e GABA por ^{13}C-RMN para determinar a contribuição de cada substrato para a oxidação no ciclo de Krebs nos neurónios glutamatergicos e GABAérgicos, respectivamente. Demonstrámos que o 3HB compete eficazmente com a glucose para a formação de acetil-coA em ambos os compartimentos, mas com maior eficácia no compartimento glutamatérgico, quando comparado com o compartimento GABAérgico.

O 3HB não diminuiu a utilização de lactato/piruvato pelo ciclo de Krebs, sugerindo que não diminui a oxidação do piruvato a acetil-coA via piruvato desidrogenase. Em vez disso, poderá diminuir o fluxo glicolítico acima da pirvato desidrogenase, uma hipótese suportada pela observação de que os níveis de lactato proveniente da glucose marcada no superfusato mostram uma forte tendência para serem mais baixos na presença do corpo cetónico. Os corpos cetónicos também parecem contribuir para um estado citosólico mais reduzido, demonstrado pelo maior rácio lactato/alanina observado quando o 3HB era incluído como substrato.

As fatias de estruturas cerebrais também parecem excretar uma quantidade significativa de acetato para o meio superfusato. Todos os isotopómeros possíveis do acetato ([1-^{13}C], [2-^{13}C], [U-^{13}C] e [U-^{12}C]acetato) foram determinados no superfusato por ^{1}H RMN. Foram observados os isotopómeros de ^{13}C de acetato proveniente de [1-^{13}C]glucose, [U-^{13}C]glucose, [3-^{13}C]lactato e [2-^{13}C]lactato/piruvato mas nas experiências em que [U-^{13}C]3HB estava presente, o esperado [U-^{13}C]acetato nunca foi observado. Deste modo, concluímos que este acetato é formado de um compartimento metabólico que não está em contacto com o acetil-coA derivado da oxidação de 3HB. Ainda que não contribuindo para a formação de acetato, a presença do 3HB pareceu atenuar a sua produção. Serão necessárias mais experiências para identificar as enzimas e compartimentos celulares envolvidos na produção de acetato.

1. Introduction

1.1. Ketone Bodies: an overview

Ketone bodies (KB) are a class of metabolites that are synthesized in the liver from fatty-acid derived acetyl-coA (Fig.1.1). They were first discovered in the late 19th century in the urine of patients in diabetic coma and soon associated with the symptoms that we now refer to as "diabetic ketoacidosis" (Vanitallie & Nufert 2003). In diabetic ketoacidosis, ketone bodies' levels in blood can rise up to 25mM which results in severe acidosis and consequent death if untreated (Laffel 1999; Veech et al. 2001; Veech 2004).

Fatty acids

Acetyl CoA
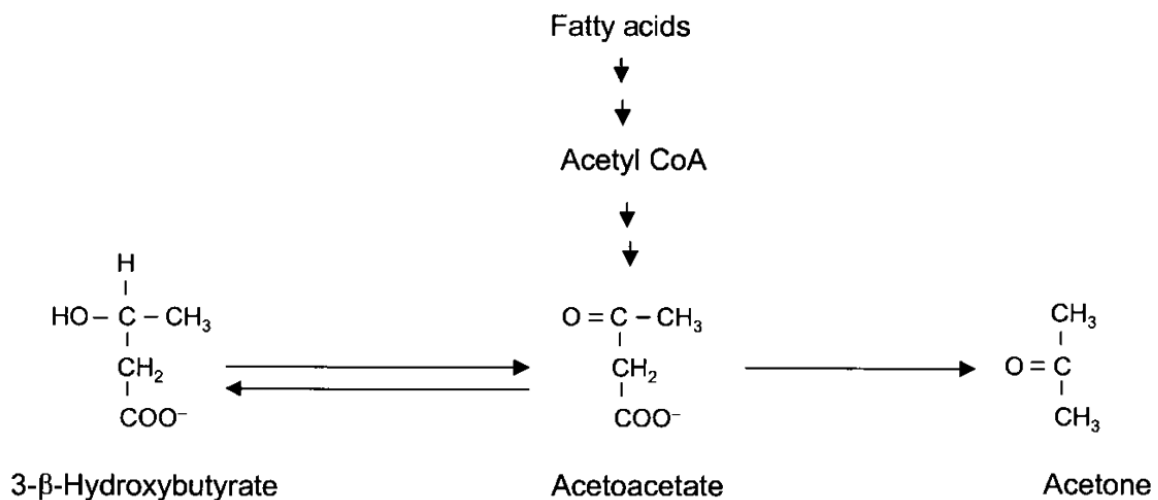
Fig.1.1 Structure of the main ketone bodies, 3-β-hydroxybutyrate, acetoacetate and acetone.
Figure from Laffel 1999

However, it is now well established that a mild, controlled ketosis may have beneficial effects (Veech et al. 2001; Vanitallie & Nufert 2003; Veech 2004; Hashim & Vanitallie 2014). Particularly, ketone bodies have been widely reported as helping to control seizures in retractable epilepsy (Kinsman et al. 1992; Erecińska et al. 1996; Daikhin & Yudkoff 1998; Puchowicz et al. 2000; Vanitallie & Nufert 2003; Ma et al. 2007; Hasebe et al. 2010). In the early 20th century, epilepsy was believed to be caused by intestinal intoxication, and fasting was prescribed as a treatment (Veech et al. 2001). In 1921, Russel Wilder came to the conclusion that ketone bodies themselves were the effective agent, and proposed that the same effects could be achieved from a high fat-low carbohydrate diet (Wilder 1921). The "ketogenic diet" (KD) is also known as the 4:1 diet because it provides a ratio of approximately 4 parts (by weight) fat to 1 part (by weight) of a mixture of protein and carbohydrate. In practice, it means a daily uptake of 1g of protein/kg body weight (considerably less in adults), 10 to 15g of carbohydrate, and the remainder of the calories as fat (Wilder 1921; Vanitallie & Nufert 2003; Veech 2004; Hallböök et al. 2012).

With the development of anti-epileptic drugs, the ketogenic diet became less prescribed as treatment. Nonetheless, there are still many cases of retractable epilepsy for which current anti-epileptic drugs are ineffective, and ketogenic diets are indicated. For example it was reported that for a group of patients with refractory epilepsy to over 6 anti-epileptic drugs and reporting over 20 seizures a day, a ketogenic diet had beneficial effects. 20% of these patients had virtually complete seizure control, while in 38% of the patients, seizure frequency was reduced by half (Kinsman et al. 1992). In animal models, ketogenic feeding was shown to significantly increase the threshold against seizures induced either chemically via pentylenetetrazol infusion or electrically via the electroconvulsive shock test (Thavendiranathan et al. 2003). In resolving epilepsy resulting from GLUT1 deficiency (the major glucose transporter across the blood-brain barrier), ketone bodies were hypothesized to provide an alternative substrate for energy generation, thereby compensating for low glucose uptake (Veech et al. 2001; Veech 2004; Marin-Valencia et al. 2012).The mechanism of action of ketone bodies in resolving other forms of epilepsy remains unknown (Veech et al. 2001; Laffel 1999; Vanitallie & Nufert 2003; McNally & Hartman 2012); some authors have cited the effects of increased brain inhibitory neurotransmitter gamma-aminobutyric acid (GABA) (Erecińska et al. 1996; Daikhin & Yudkoff 1998; Yang et al. 2007; Kang & Macdonald 2009; McNally & Hartman 2012; Kernig et al. 2012). Others have attributed the therapeutic efficacy of the ketogenic diet to a decrease in circulating blood glucose (Greene et al. 2001). It is accepted that the metabolism of KB in the brain is likely to improve the overall energy cellular state since ATP/ADP ratio is significantly increased in the brain of rats fed a high-fat diet. This improves the maintenance of Na^+ and Ca^{2+}gradients thereby decreasing the resting membrane potential and inhibiting the synchronous neuronal discharge characteristic of epilepsy. This may, at least partially, explain the increased neuronal stability that develops during chronic ketosis (Vanitallie & Nufert 2003; Veech 2004).

Recently, ketone bodies have become the focus of attention regarding their neuroprotective and antioxidant roles, particularly in neurodegenerative diseases such as Alzheimer's disease (Henderson 2008; Henderson & Poirier 2011) as well conditions of limited glucose delivery. This may be due in part to their capacity to supplement compromised cerebral energy generation from glucose. As an example, KB were shown to increase survival in a rodent model of bilateral carotid occlusion and hypoxia (Suzuki et al. 2001).

Unlike glucose, which can be oxidized for energy via acetyl-CoA or supply anaplerotic carbons via pyruvate carboxylase (PC), four-carbons KB such as 3-hydroxybutyrate (3HB) and acetoacetate (AcAc) can only be converted to acetyl-coA. Hence, their utilization by the Krebs cycle is limited to that of energy production and they cannot increase the overall pool sizes of Krebs cycle metabolites and associated amino acids. However, it is possible that through bypassing pyruvate dehydrogenase-mediated control of acetyl-coA production, they can cause a redistribution of these metabolite pools resulting in increased GABA levels (Fig.1.2).
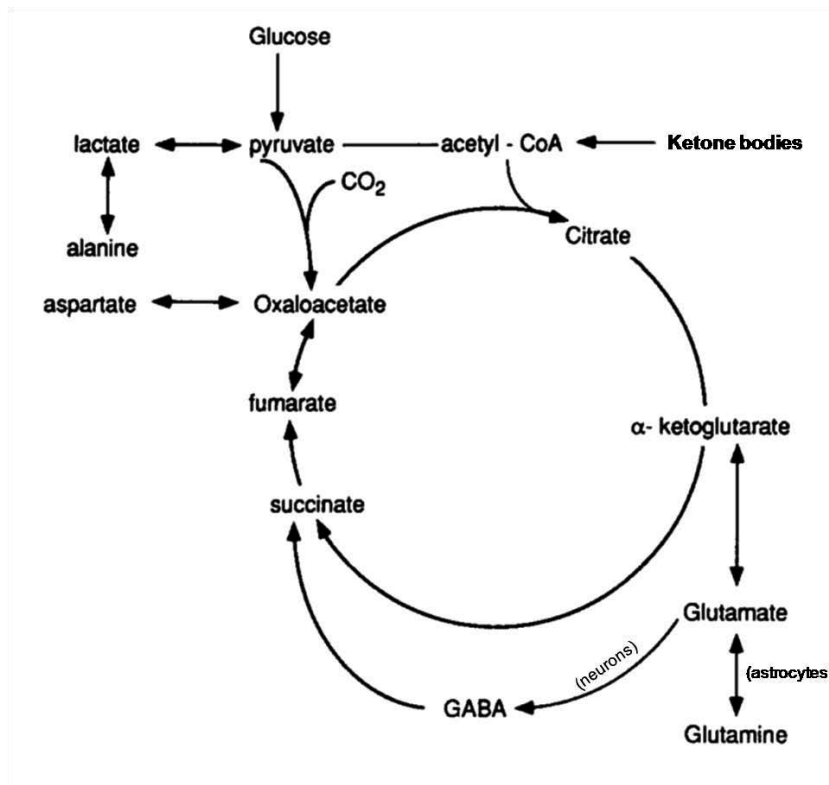
Fig.1.2 Brain metabolism of ketone bodies to glutamate and GABA. The metabolism of ketone bodies to acetyl-coA causes increased citrate synthase activity, reducing the pool of oxaloacetate, which is being used for citrate synthesis. The reduction of [oxaloacetate] results in less transamination of glutamate, which requires oxaloacetate as a reactant. More glutamate then becomes available to the glutamate decarboxylase reaction, leading to enhanced GABA synthesis.
(figure adapted from Lapidots & Gopher 1994)

There are, however, some studies that show no changes in GABA levels from whole brain samples of rodents fed a ketogenic diet, inconsistent with an increase in GABA synthesis (Yudkoff et al. 2005; Melø et al. 2006; McNally & Hartman 2012). In vitro patch clamp studies of post-synaptic GABA$_A$ receptors of rat hippocampal neurons reported no changes in receptor activity in the presence of extracellular 2 mM 3HB or 1 mM AcAc (Thio et al. 2000).

In animal studies, the serum concentrations of ketone bodies that are attained during ketogenic interventions of epilepsy range from 2 to 7 mM (Vanitallie & Nufert 2003; Veech 2004). However, much smaller blood ketone body levels (0.19 – 0.36mM) were reported to produce a therapeutic response in children with acyl-coA dehydrogenase deficiency (Hove et al. 2003). In another study, full control over epileptic seizures was obtained in epileptic patients under a ketogenic diet, and brain acetone levels were approximately 0.7 mM (Seymour et al. 1999). These data suggest that humans and rats may have attain different degrees of ketotosis from ketogenic diets, possibly explaining the different anticonvulsant profiles observed in animal seizure models.

In 1958, Johnson and colleagues came to the conclusion that after overnight fasting there are always measurable concentrations of KB in serum (~0.7mM) and a residual KB appearance in

urine (0.9-2.8μmol/min). They also observed that moderate daily physical activity seems to increase the capacity of muscle to use KB (Johnson et al. 1958). Prolonged exercise is now known to be associated with mild hyperketonemia, with ketone body levels rising up to 2 mM. Under these conditions there is significant oxidation of KB by peripheral tissue, including skeletal muscle (Laffel 1999; Vanitallie & Nufert 2003). It has also been shown in suckling rodents that KB derived from oxidation of the fatty acids contained in maternal milk represent a significant source of energy, particularly for the developing brain (Hawkins et al. 1971; Vannucci & Simpson 2003; Pierre & Pellerin 2005).

1.2. Physiology of Ketogenesis

Ketosis may be seen as the response of tissue to carbohydrate deprivation during starvation or as a result of insulin deficiency. The formation of ketone bodies, ketogenesis, is stimulated by a high glucagon/insulin ratio (as happens in fasting and Type 1 diabetes) through activation of lipolysis of the adipocyte tissue and β-oxidation in the liver (Laffel 1999). Fatty acids enter the hepatocytes' mitochondria as fatty acyl-coA and undergo β-oxidation to acetyl-coA. Then, acetoacetyl-coA is formed (catalyzed by 3-kethotiolase – 3KT), and converted to 3-hydroxy-3-methylglutaryl-coA (HMG CoA) by HMG-coA synthase (mHS). This step is stimulated under conditions of starvation, low levels of insulin, and the consumption of a high fat diet. Acetoacetate is then formed, in a step catalyzed by HMG-coA lyase (HL). Acetoacetate is reduced to 3HB by 3-hydroxybutyrate dehydrogenase (HBD), or undergoes spontaneous decarboxylation, forming acetone (Fig.1.3) (Laffel 1999; Vanitallie & Nufert 2003). 3-hydroxybutyrate dehydrogenase (HBD) is a phosphatidylcholine-dependent enzyme.

During the reduction step of AcAc to 3HB catalyzed by HBD, NADH is oxidized to NAD^+, and as a consequence, the ultimate ratio of 3HB to AcAc (KB ratio) in the blood is dependent on the redox potential (i.e. the $NADH/NAD^+$ ratio) within hepatic mitochondria. This KB ratio is often used as an indirect indicator of the redox state of the hepatocyte mitochondria (Laffel 1999), whereas lactate/pyruvate ratio is used as an indicator of cytosolic redox state (Cruz et al. 2001; Alves et al. 2011).
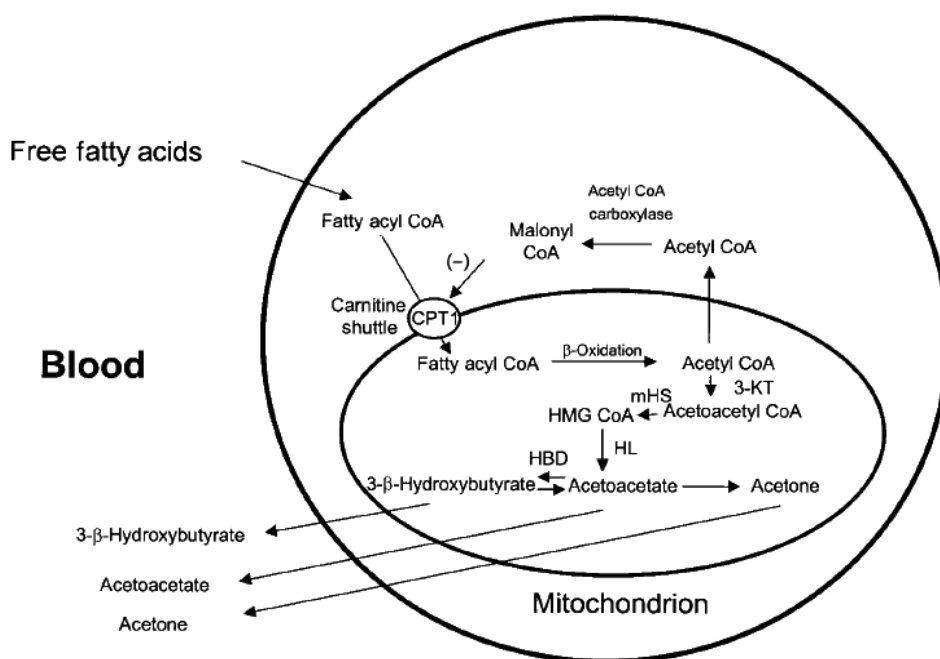
Fig.1.3 Ketone bodies formation from fatty acids. Fatty acyl-coA is transported into mitochondria via the carnitine shuttle, driven by carnitine palmitoyltransferase 1 (CPT 1). Excess of acetyl-coA is converted to acetoacetate via 3-ketothiolase (3-KT), HMG CoA synthase (mHS) and HMG CoA lyase (HL). Acetoacetate is reduced to 3HB by 3HB dehydrogenase (HBD), and acetone is formed by the spontaneous decarboxylation of acetoacetate. Acetyl-coA carboxylase catalyzes the production of malonyl-coA from acetyl-coA. Malonyl-coA inhibits CPT1, so if excess acetyl-coA is shunt to ketone bodies' production, there will be decreased activity of acetyl-coA carboxylase and increased transport of fatty acids into the mitochondria. Acetyl-coA carboxylase activity is also upregulated by insulin. In low insulin conditions such as Diabetes Type1 or fasting there is no production of malonyl-coA, hence CPT 1 is not inhibited.
Figure from Laffel 1999

KB supply 2 to 6% of the body's energetic needs after an overnight fast and 30 to 40% after a 3-day fast (Laffel 1999; Vanitallie & Nufert 2003). When people are deprived of food for 3 days or longer, they become hyperketonemic, with ketone bodies concentration in blood reaching levels up to 5-7mM (Vanitallie & Nufert 2003; Veech 2004; Hashim & Vanitallie 2014) and liver production of KB achieves 150g/day (Veech 2004). In healthy individuals, the buffering capacity of blood is capable of dealing with this level of ketoacidosis (Hashim & Vanitallie 2014). Bates and colleagues showed that in starved rats, the mean total KB concentration in the blood rises about 11-fold compared to fed animals (Bates et al. 1968). This is essential to preserve muscular mass from being consumed by providing non-glucose substrate for the brain and preventing muscle protein breakdown for glucose synthesis. Thus, humans can survive for up to 2 months without food, compared to an estimated 2–3 weeks if ketone bodies were not available (Veech et al. 2001; Vanitallie & Nufert 2003).

1.3. Ketone Bodies as alternative brain fuels to glucose

The human brain has a high energy demand: it represents 2% of body weight but accounts for about 20% of whole-body oxygen and glucose consumption (Veech et al. 2001; Vanitallie & Nufert 2003; Pellerin 2010). Most of the neural ATP and NADPH produced are used to maintain the electrochemical (Na^+/K^+) gradient needed for electrical and chemical signaling and to restore membrane resting potential after depolarization by the Na^+, K^+-ATPase. The remainder is used to recycle neurotransmitters (Castro et al. 2009). The brain also consumes other substrates including lactate and pyruvate (Bouzier et al. 2000; Hassel & Bråthe 2000; Bergersen et al. 2001; Bouzier-Sore et al. 2002; Vannucci & Simpson 2003; Pierre & Pellerin 2005; Pellerin 2010; Dienel 2012) but non-esterified fatty acids are unable to cross the blood-brain barrier (BBB), and are therefore unavailable as an energy source even when blood glucose levels are low (Laffel 1999; Vanitallie & Nufert 2003). With glucose as the main source of energy and with very little endogenous carbohydrate stored as glycogen, there is a need for constant cerebral glucose uptake (Lapidots & Gopher 1994).

Protein catabolism would be a feasible source of energy for a short period of time. Theoretically, 57 g of glucose can be derived from 100 g of protein breakdown. Generation of the required 100 to 150 g of glucose/day for sustenance of the brain would require the gluconeogenic breakdown of about 172 to 259 g/day of body protein, representing an unsustainable loss of lean body mass. In fact, during prolonged fasting 4–9 g of nitrogen per day are excreted. If we assume that 1 g of urinary nitrogen corresponds to 6.25 g of protein catabolism, this rate of urinary nitrogen appearance represents the catabolism of 25–55 g protein/day. This amount of protein catabolism could supply between 17 and 32 g of glucose for the brain per day which is far below the daily requirement (Gamble et al. 1923; Owen et al. 1967; Vanitallie & Nufert 2003; Veech 2004).

Ketone bodies were found to replace glucose as the brain's main fuel during prolonged fasting in 1967 (Owen et al. 1967). They are uptaken via monocarboxylate transporters (MCTs) through the BBB (Bouzier-Sore et al. 2002; Vannucci & Simpson 2003; Pierre & Pellerin 2005; Pellerin 2010; Hashim & Vanitallie 2014). During starvation, increased KB levels in blood are partially due to a decrease in KB utilization by skeletal muscles thereby sparing KB to fuel the brain (see Table 1-1). Glucose utilization in the brain drops to 1/3 of the values for the fed state, with KB filling the energy gap (Owen et al. 1967; Laffel 1999; Vanitallie & Nufert 2003) for both neurons and astrocytes, with higher rates of utilization for neurons (70% of total KB consumption) than for astrocytes (30%) (Jiang et al. 2011). During prolonged fasting, blood glucose concentrations can decrease to below 1mM without either convulsions or any notable impairment of cognitive function (Cahill & Aoki 1980; Veech 2004). Interestingly, some early studies have shown that even in the presence of glucose, the brain is able to metabolize KB in significant amounts (Hawkins et al. 1971; Pan et al. 2002; Henderson & Poirier 2011), showing that KB utilization may be independent of the nutritional state.

Table 1-1 Proportion of brain energy metabolism supported by ketone bodies, as a function of plasma ketone bodies concentration (in mM). From Hashim & Vanitallie 2014

0.3-0.5 mM (12-24 hr fast): 3-5%
1.5 mM (2-3-day fast): 18%
5 mM (8-day fast): 60%
7 mM (≥ 20-day fast): >60%

In stress situations such as ischemia, trauma or low glucose, the brain adapts by increasing the expression and activities of enzymes and transporters for KB metabolism (Vanitallie & Nufert 2003; Prins 2008; Jiang et al. 2011). There is increased transport from the blood through MCTs (Jiang et al. 2011) as it has been demonstrated in the brain of starved rats and an upregulation of 3-oxoacid-CoA transferase (OCT) activity (Vanitallie & Nufert 2003). Succinyl-coa-oxoacid transferase (SCOT) is the enzyme responsible for the conversion of AcAc back into acetoacetyl-coA, and is the rate-determining step in ketolysis (Fig.1.4). SCOT activity is highest in the heart and kidney, central nervous system and skeletal muscle, with only residual activity in the liver. SCOT activity is down-regulated by high (>5 mM) intracellular levels of acetoacetyl-coA. This phenomenon is responsible for the observed increase in circulating levels of ketone bodies during the early phases of starvation (3 days to 2 weeks), despite relatively constant rates of hepatic ketogenesis during this period. The acetoacetyl-coA produced is then cleaved by methylacetoacetyl-coA thiolase (MAT), producing free acetyl-coA, which can then enter the Krebs cycle (Laffel 1999).
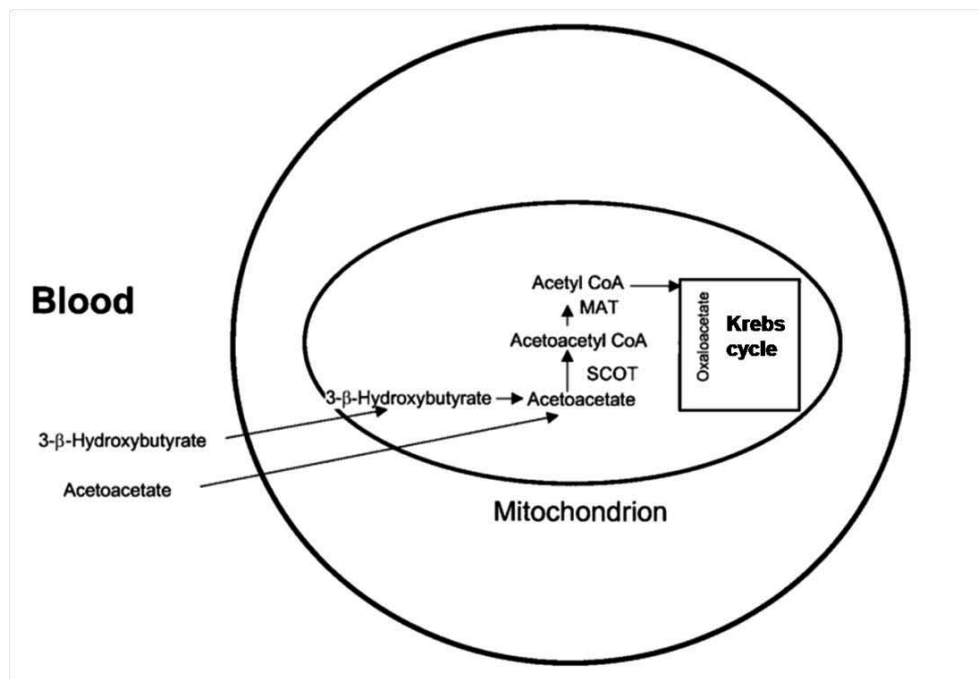

Fig.1.4 Utilization of ketone bodies in extra-hepatic tissues, particularly the brain. 3-β-hydroxybutyrate and acetoacetate enter the cells by the monocarboxylic transport proteins and enter the Krebs cycle after being converted to acetyl-coA by succinyl-coA-oxoacid transferase (SCOT) and methylacetoacetyl-coA thiolase (MAT). Figure adapted from Laffel 1999

A study of acute hyperketonemia in overnight-fasted humans infused intravenously with [2,4-^{13}C$_2$]3HB revealed a dynamic enrichment pattern of brain glutamate and glutamine labeling similar to that from [1-^{13}C]glucose, indicating that oxidation of 3HB, like glucose, occurs mostly in neurons (Pan et al. 2002). Later experiments in rats support this hypothesis (Jiang et al. 2011; Chowdhury et al. 2014). Experiments in hyperketonic rats showed that 3HB is oxidized to a greater extent in neurons than in astrocytes (70:30), and follows a pattern closely similar to the metabolism of glucose, while Krebs cycle flux remained similar to values reported for normal rats (Jiang et al. 2011).

Neural lipid synthesis preferentially uses AcAc over glucose (Patel & Owen 1976; Koper et al. 1984). Both oligodendrocytes and astrocytes were shown to use AcAc for lipogenesis and cholesterogenesis, and the incorporation of AcAc in lipid synthesis exceeds glucose contributions (Koper et al. 1984). This suggests that some of the benefits of KB in brain lesion models may involve the more rapidly recuperation of damaged neurons.

The literature is contradictory about the effects of ketone bodies on brain glucose consumption. There are reports that KB do not reduce glucose oxidation (Zhang et al. 2013), whereas others report that glucose metabolism decreases with increasing oxidation, consistent with the down regulation of the glycolytic path at various levels such as phosphofructokinase and/or hexokinase (LaManna et al. 2009; Jiang et al. 2011).

1.4. Ketone bodies, Monocarboxylate Transporters and the Lactate-Shuttle Hypothesis

Ketone bodies are transported across cell membranes via MCTs – the monocarboxylate transporters. In newborn rodents, during the suckling period there is a high expression of these transporters in the brain, coinciding with active ketonegenis from the fat of maternal milk (Vannucci & Simpson 2003; Simpson et al. 2007). After weaning, MCT2 seems to be expressed predominantly in neurons. MCT4 appears to be astrocyte-specific and MCT1 is observed in brain capillaries (Bergersen et al. 2001; Pierre & Pellerin 2005; Hashim & Vanitallie 2014). Glucose transporters also seem to have tissue specificity. GLUT1 exists in the endothelial cells of capillaries, and to some extent in astrocytes (Bouzier-Sore et al. 2002; Simpson et al. 2007), whereas neurons seem to almost exclusively express GLUT3 (Leino et al. 1997; Bouzier-Sore et al. 2002; Simpson et al. 2007), although neuronal GLUT1 expression increases in response to environmental stressors or when neurons are placed in culture (Simpson et al. 2007).

The different MCT and GLUT isoform expression seems to suggest differential substrate preference between these types of cells. MCT2 has the highest affinity for lactate, with a K$_m$ of 0.7mM. MCT4 has the highest K$_m$ for lactate (35mM) and MCT1 has an intermediary affinity with a K$_m$ value of 3.5mM (Pellerin et al. 2005; Bergersen 2007). MCT4 has been well documented in

glycolytic muscle as an exporter of lactate, and some authors suggest it may have an analogous function in the brain (Bergersen et al. 2001; Bergersen et al. 2002; Pierre & Pellerin 2005), suggesting an astrocyte-to-neuron lactate shuttle hypothesis. Further supporting this hypothesis is the GLUT3 astrocyte localization, as GLUT3 is characteristic of cells with high rates of glucose metabolism (Simpson et al. 2007). Moreover, studies using labeled lactate show higher enrichments of labeling in GABA and glutamate pools in comparison to glutamine (Hassel & Bråthe 2000; Bouzier et al. 2000; Bouzier-Sore et al. 2002). This specific MCT distribution also explains the greater extent of KB oxidation by neurons than by astrocytes.

1.5. Ketogenic Diet

The ketogenic diet (KD) was invented to purposely increase circulating KB. It is also known as the "4:1 diet" because it provided a ratio of approximately 4 parts (by weight) fat to 1 part (by weight) of a mixture of protein and carbohydrate. In practice, it means a daily uptake of 1 g of protein/kg body weight (considerably less in adults), 10 to 15 g of carbohydrate, and the remainder of the calories as fat (Wilder 1921; Vanitallie & Nufert 2003; Veech 2004; Hallböök et al. 2012). In the ketogenic diet, the liver produces ketone bodies by shunting excess acetyl-coA to ketogenesis (McNally & Hartman 2012). One might argue that ketone bodies increase acetyl-coA production and thus should Krebs cycle flux, but in fact, ketone bodies' increased metabolism causes a depletion of free coenzyme A, by converting it to acetoacetyl-coA in β-oxidation. This induces a decrease of α-ketoglutarate dehydrogenase activity, since it requires free coA, and consequent reduction of flux throughout the rest of the cycle (Silver & Erecińska 1994; Daikhin & Yudkoff 1998). When applied properly, the KD should minimize circulating glucose levels without causing caloric restriction or malnutrition (Hallböök et al. 2012).

Although the high fat-low protein diet has been proved to have remarkable effects in epilepsy, it is not without downside. A common problem of following a high fat-low carbohydrate diet in adults is the elevation of triglycerides or cholesterol or both (Veech 2004): the mean blood cholesterol has been reported in levels over 250, significantly above the recommended levels (Veech 2004). Changing the fat portion by medium chain triglycerides (MCTr) may avoid these effects and give approximately equal results in reducing seizures (Vanitallie & Nufert 2003; Veech 2004). Another major problem with the classical ketogenic diet is that ingestion of even small amounts of carbohydrate cause insulin release and an immediate drop in ketone body levels (followed by seizures in epileptic patients) (Veech et al. 2001), since carbohydrates are metabolized to pyruvate, which is then converted to oxaloacetate, increasing acetyl-coA flux through the Krebs cycle and thus, decreasing the KB synthesis pathway. Ketone bodies' levels do not rise after ingestion of long chain triglycerides within a normal diet (with carbohydrates), but they do after MCTr ingestion (Bach et al. 1977). MCTr are fatty acids with between 6 and 12 carbons (Bach et al. 1977). They are well known to cause hyperketonemia in human, dogs (Bach et al. 1977), pigs and rats (Yeh & Zee 1975). One of the advantages of MCTr is that rather than

being incorporated into lipid synthesis in the liver via chain elongation, they are converted to ketone bodies regardless of nutritional state (Bach et al. 1977), with severe and long-lasting hyperketonemia developing rapidly (15-30min after ingestion) (Yeh & Zee 1975; Bach et al. 1977).

Early experiments show that MCTr-induced ketosis does not impair utilization of glucose by the liver: the level of plasma glucose was increased at 1 and 2 hours after MCTr plus glucose administration, but was decreased at 1 hour after administration of MCTr alone. The concentration of immune-reactive insulin in plasma was increased by MCTr but not by corn oil (long chain fatty acid) suggesting that MCTr stimulates insulin release by the pancreas (Yeh & Zee 1975). Of note, MCTr-induced hyperketonemia was slightly but significantly reduced when co-administrated with glucose (Yeh & Zee 1975).

Long-chain fatty acids (LCFA), insoluble in water, are absorbed by the lymphatic system in the form of chylomicrons. When they reach the liver they are preferentially incorporated into lipids synthesis, especially triglycerides. On the other hand, the medium-chain fatty acids, being water soluble, are directly transported through the portal vein in the form of NEFA (non-esterified fatty acids) bound to albumin. Hence they rapidly reach the liver, which takes them up almost completely and does not integrate them into triglyceride and VLDL (very low density lipoproteins) synthesis, but instead converts them to ketone bodies. This explains why an LCFA load increases plasma triglycerides while MCTr does not (Yeh & Zee 1975; Bach et al. 1977). Oxidation of fatty acids elevates acetyl-coA concentration and consequently increases the production of ketone bodies (Yeh & Zee 1975). Further supporting this idea, in liver slices of MCTr-fed rats, ketosis was depressed by administration of 4-pentenoic acid, a potent inhibitor of fatty acid oxidation. These results support the hypothesis that ketosis induced by MCTr results from rapid oxidation of medium chain fatty acids (Yeh & Zee 1975). Of note, ketonemia was considerably less severe in genetically obese rats than in control normal-weight rats (Bach et al. 1977).

Because of its more complete hydrolysis and rapid absorption, MCTr have replaced long-chain triglyceride in diets of patients with malabsorption syndrome. Also, cholesterol levels of several mammalian species were lower after MCTr feedings when compared to LCFA rich diets (Yeh & Zee 1975), but many of the children given MCTr diets complained of nausea, diarrhea, and occasional vomiting (Vanitallie & Nufert 2003; Veech 2004).

The newest classes of ketogenic substrates are the ketone esters. The prototype consists of two molecules of 3HB linked by esterification of the carboxyl functionality of one with the alcohol functionality of the other. On ingestion, the ester is hydrolyzed by intestinal esterases thereby directly releasing 3HB into the circulation and acutely raising blood 3HB levels.

1.6. Parkinson's disease

Recently, ketone bodies have received a lot of attention for their apparently neuroprotective role in neurodegenerative diseases, such as Parkinson's disease (PD). PD is characterized by a loss of dopaminergic neurons in the substantia nigra (SN), which can be up to 80% when clinical symptoms of the disease appear. Dopaminergic neurons' numbers normally decline with aging, but the rate of destruction is accelerated in patients with clinical Parkinsonism (Veech 2004). Symptoms include bradykinesia, rigidity and tremor (Veech 2004). Non-motor symptoms include depression, anxiety and cognitive impairment (Tadaiesky et al. 2008). This rapid destruction of neurons is thought to result from continued free radical damage to dopaminergic neurons, which are particularly sensitive to this toxicity given their high iron content. The disease is manageable for some time with L-dopa administration, but as damage and death of dopaminergic neurons continues, L-dopa therapy becomes either ineffective or limited by its toxicity (Veech 2004).

Mitochondrial impairment in dopamine neurons could lead to increased dependence on the glycolytic pathway for ATP production: reduced levels of high energy phosphates in SN and the striatum in early and advanced PD were observed (Hattingen et al. 2009), and it was shown in a MPTP mouse model of PD that energetic impairment is not due to diminishing of GLUT1 or MCT2 expression (Puchades et al. 2013). In this frame, mitochondrial dysfunction due to ROS damage could result in impaired energetic metabolism, which in turn would contribute to PD development.

As we previously suggested, ketone bodies can fulfill the energy gap, offering an attractive possibility for improving the quality of life of patients with these diseases, although its role may be more than just an energetic one: reports show that primary cultures of mesencephalic dopaminergic neurons exposed to MPP+ (a molecule that inhibits NADH dehydrogenase [complex 1] and causes oxygen free radical formation) can be protected from death by addition of 4 mM 3HB (Kashiwaya et al. 2000) and in a study using a rat PD model injected with 6-hydroxydopamine (6-OHDA), a ketogenic diet protected dopaminergic neurons of the SN against neurotoxicity (Cheng et al. 2009). Veech et al. suggest that 3HB probably acts by decreasing the source of mitochondrial oxygen radical formation by oxidizing the co-enzyme Q couple while at the same time reducing the redox potential of the NADP couple which, through glutathione, is the final detoxification step for H_2O_2 (Veech et al. 2001).

1.7. Nuclear Magnetic Resonance (NMR)

NMR spectroscopy is a non-destructive, non-invasive technique that provides detailed information on molecular structure, both for pure compounds and in complex mixtures as well as information on absolute or relative concentrations (Beckmann et al. 1995; Lindon et al. 2007;

Zwingmann & Leibfritz 2003), making it a useful tool for *in vivo* studies. The most commonly used atoms for NMR are ^{1}H, ^{2}H, ^{12}C, ^{13}C, ^{15}N and ^{31}P. NMR spectroscopy allows the detection of several compounds present in the sample, allowing a very complete analysis in one single spectrum.

1.7.1. ^{13}C NMR spectroscopy

The enrichment of molecules in ^{13}C has many advantages. ^{13}C natural abundance is very low, of about 1.1%, allowing the possibility of tagging a specific carbon position by selective enrichment with ^{13}C (Beckmann et al. 1995; Lindon et al. 2007). ^{13}C nucleus is a stable carbon isotope and hence is not subject to the radiation hazards related to radioactive tracers (Beckmann et al. 1995). To eliminate the splitting of the ^{13}C-signal that occurs due to J-coupling with attached hydrogens and to enhance the intensity of the resulting simplified ^{13}C-resonance via the nuclear Overhauser effect, continuous ^{1}H decoupling is applied (Lindon et al. 2007). The chemical shifts of ^{13}C within substrates and metabolites are dispersed over a wide range, so separate resonances for numerous metabolites can be simultaneously detected, identified and quantified without need for prior separation. Incorporation of labeling in specific carbons provides information about the fate of that specific carbon, and allows simultaneous monitoring of carbon fluxes through converging metabolic pathways, such as those that generate acetyl-coA for Krebs cycle utilization (Malloy et al. 1990; Badar-Goffer et al. 1990; Beckmann et al. 1995; Zwingmann & Leibfritz 2003).

Labeling with ^{13}C of two (or more) adjacent carbons results in homonuclear ^{13}C-^{13}C spin-spin couplings, which can provide even more biochemical information. The spin coupling is detected in the form of doublets (for two) or multiplets (for >2) adjacent carbons. This resonance splitting is a well-defined parameter known as the coupling constant **J** for each isotopomer, (Beckmann et al. 1995). Spin coupling gives information not only about which adjacent carbons are labeled, but also the ratio of labeling between them. With this information, and choosing carefully the labeling in the precursor molecules, it is possible to study substrate competition and preference; competition and contribution of alternative pathways, and fluxes that involve cycling of metabolites such as pyruvate (Beckmann et al. 1995),

^{13}C NMR Isotopomer analysis is limited to intracellular metabolites that are present in sufficient amounts to be detected, and typically include glutamate, glutamine, aspartate, alanine, lactate, or glucose. For NMR isotopic analysis of Krebs cycle intermediates, whose concentrations are typically too low for direct NMR observation, their more abundant amino-acid transamination products are analyzed. For this, it is assumed that glutamate accurately reflects the labeling of α-ketoglutarate, since the two metabolites are in a fast equilibrium via transamination. The same assumption is made for lactate and alanine, which reflect the labeling of pyruvate, and aspartate, which reflects the labeling of oxaloacetate (Beckmann et al. 1995; Carvalho et al. 1999).

1.7.2. ¹H NMR spectroscopy

Almost all metabolites possess a chemically-bound hydrogen that can be detected by ^{1}H NMR. While having a smaller chemical shift dispersion than ^{13}C NMR, signals from an array of metabolites can nevertheless be resolved in the ^{1}H NMR spectrum allowing a reasonably detailed profile of tissue metabolites to be obtained. ^{1}H NMR is also inherently more sensitive than ^{13}C NMR and can therefore detect lower levels of metabolites, including true Krebs cycle intermediates such as succinate and other low-abundance metabolites such as pyruvate. ^{1}H signal areas relate directly to the number of protons giving rise to that signal, hence absolute metabolite concentrations can be obtained from a ^{1}H NMR spectrum by adding an internal standard of known concentration whose resonance does not coincide with those of the sample metabolites (Lindon et al. 2007).

The concept of resolving complex metabolite ^{13}C-isotopomer distributions via spin-coupling interactions using ^{13}C NMR can also be extended to ^{1}H NMR as a result of heteronuclear J couplings between ^{13}C and neighboring ^{1}H nuclei (Beckmann et al. 1995). The ^{1}H signal splitting thus provides information about ^{13}C-enrichment of nearby carbons (Lindon et al. 2007) and determination of different metabolite ^{13}C-isotopomer populations. This is illustrated in Fig.1.5 for various isotopomers of lactate.
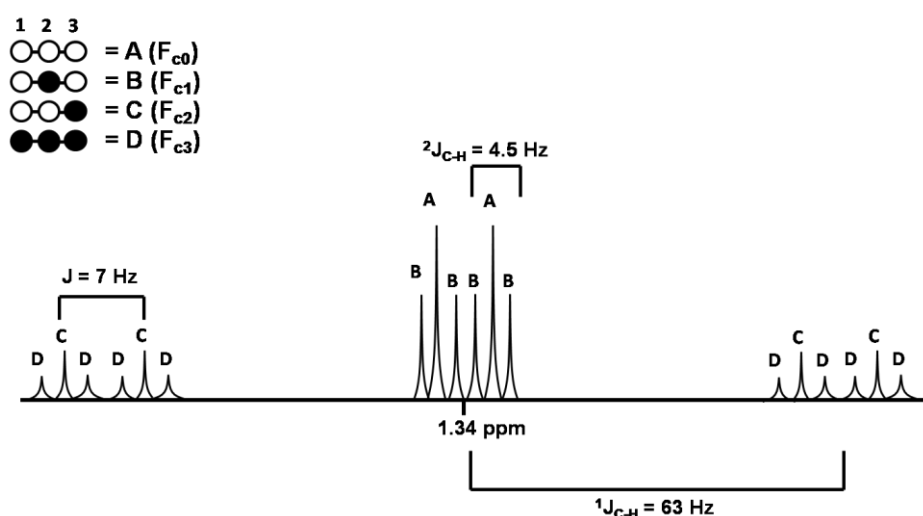
Fig.1.5 Different ^{13}C isotopomers of lactate give distinct peaks in the ^{1}H-NMR spectrum, with well-defined J-coupling constants.

Isotopomer information obtained by ^{1}H NMR analysis can be integrated with that obtained by ^{13}C NMR thereby maximizing the information content from the experiment and allowing more realistic and detailed descriptions of cellular and tissue metabolic fluxes to be obtained.

2. Aim of the Project

Despite all the research regarding ketone bodies as therapeutic agents in the brain, and ketone bodies formation from variations of the ketogenic diet, little information is known about the energetic metabolism changes occurring due to ketone bodies' presence, especially for dietary supplements designed to generate ketone bodies in the presence of sufficient dietary carbohydrate. As such, the main objectives of this study were:

i.   Understand how ketone bodies compete with glucose and lactate/pyruvate for acetyl-coA formation when none of the substrates is of limited supply and possible cell-type compartmentation;

ii. Investigate if time-dependent changes occur during the experimental time-frame, that can hint in the direction of substrate swap and/or other metabolic state changes;

iii. Explore the relationship between ketone body and glucose utilization in a pre-symptomatic model of Parkinson's disease.

3. Materials and Methods

3.1. Solutions and buffers

Modified ACSF solution	Re-suspension buffer for NMR
	53.7 mM NaH_2PO_4
124mM NaCl	46.3 mM Na_2HPO_4
2mM KCl	
1.25mM $NaH_2PO_4.H_2O$	
26 mM $NaHCO_3$	Standards:
1 mM $MgSO_4$	2.5mM pyrazine
2mM $CaCl_2$	1mM TSP
Diluted in ultra-pure H_2O	1mM sodium fumarate
The solution was continuously gassed with carbogen (95% O_2/5% CO_2) to maintain oxygen supply and pH~7.	Diluted in D_2O >99%

Isotopomers

	Distributor	Catalog nr.
[1-^{13}C]glucose	Isotec ™ (Sigma-Aldrich)	EW0772
[2-^{13}C]lactate	Sigma-Aldrich	589209
[2-^{13}C]pyruvate	Sigma-Aldrich	490725-500mg
[U-^{13}C]3-hydroxybutyrate	Sigma-Aldrich	606030- 2.00g

Non-labeled metabolites

	Distributor	Catalog nr.
Glucose	Sigma-Aldrich	G8270-1Kg
Lactate	Sigma-Aldrich*	
Pyruvate	Sigma-Aldrich	P-5280
3-hydroxybutyrate	Sigma-Aldrich	54 965-10G-F

Chemicals and Reagents

	Distributor	Catalog nr.
3-(trimethylsilyl)propionic-2,2,3,3,d$_4$ acid sodium salt (TSP)	Sigma-Aldrich	269913
4-aminopyridine (4-AP)	Ascent Scientific	Asc-122
6-hydroxydopamine hydrochloride (6-OHDA)	Sigma	H4381
Calcium chloride (CaCl$_2$)	Fluka	21114
Carbogen gas	Linde Sogás, Lda	
Deutered water (D$_2$O)	CortecNet	Lot No. MKBG8156V
Dissodium phosphate Pentahydrated (Na$_2$HPO$_4$.5H$_2$O)	May&Baker LTD Dangenham England	S312/18/67-1
Fumarate	Sigma-Aldrich**	
Magnesium sulfate (MgSO$_4$)	Fluka	63126
Monossodium phosphate (NaH$_2$PO$_4$)	Merck	808 B 798170
Perchoric acid 70-72%	Merck	UN1873
Potassium chloride (KCl)	Riedel-de-Haën	31248
Potassium hydroxide (KOH)	Merck	UN1813
Pyrazine	Sigma-Aldrich**	
Sodium bicarbonate (NaHCO$_3$)	Sigma-Aldrich	S5761
Sodium chloride (NaCl)	Fluka	71381
Sodium phosphate monobasic monohydrate (NaH$_2$PO$_4$·H$_2$O)	Sigma-Aldrich	S9638-500G
Sodium hydroxide (NaOH)	Merck	1.06498.1000

*Kindly donated by Dr. Attila Köfalvi, Center for Neuroscience and Cell Biology of Coimbra (CNC), Universidade de Coimbra

**Kindly donated by Dr. Rui A. de Carvalho, Departamento de Ciências da Vida, Universidade de Coimbra

	Distributor
3mm NMR tubes	Wilmad LabGlass/CortecNet
Superfusion chambers	(67mm x 163mm x 118mm) Schlee GmbH & Co, Germany
Superfusion pump	Gilson

Animals

Male Wistar rats (Charles River, Barcelona, Spain) were used throughout this study and were handled according to the principles and procedures outlined as "3Rs" in the guidelines of European Union guidelines (86/609/EEC), FELASA and ARRIVE, and were approved by the Animal Welfare Committee of the Center for Neuroscience and Cell Biology of Coimbra. Animals were housed in a controlled animal facility (temperature 22°C and 12:12-h light:dark cycle) and given commercial food and water *ad libitum*.

3.2. Superfusion of hippocampus, cortex and striatum of WT Wistar Rats

Male (wild-type) Wistar rats, 8-11 weeks old, were anesthetized with halothane, sacrificed by decapitation and their brains excised and put in ice-cold artificial cerebral-spinal fluid (ACSF) containing 5mM glucose during 1 minute. The structures of interest (hippocampus, striatum and frontal cortex) were dissected and cut in 400µm slices with a McIlwain tissue chopper. For each structure, the slices were divided into 2 chambers and left to recover under superfusion (Fig.3.1) with re-circulating 700mL of ACSF 5 mM glucose continuously gassed with carbogen (pH7.4) at a rate of 3mL/min, for 1hour at room temperature. After, the chambers were submerged in a water bath at 35°C. For each structure, one chamber was superfused with re-circulating 300mL containing glucose, sodium lactate and sodium pyruvate, and the other chamber was superfused with the same volume of ACSF with the same substrates, plus sodium 3HB, to achieve metabolic stability under the new substrate conditions. After 1 hour, the superfusion media were replaced with identical concentrations of ^{13}C-enriched substrates: [1-^{13}C]glucose; [2-^{13}C]lactate and [2-^{13}C]pyruvate, all 99% enriched, and [U-^{13}C]3HB, 50% enriched. In addition, this new solution of labeled substrates also contained 50 µM of 4-aminopyridine (4-AP) to induce basal neuronal activity and achieve isotopic steady state within a 3 hour period, before tissue degradation starts (Duarte et al. 2007). The superfusate was sampled every 30minutes and the samples kept in ice (4ºC).
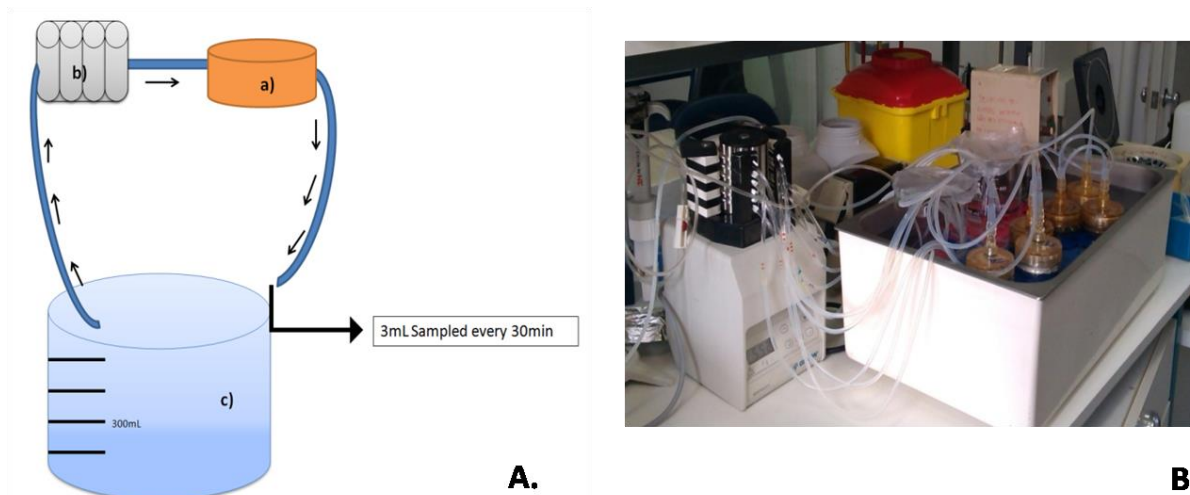
Fig.3.1 A. Schematic representation of the superfusion setup. **a)** superfusion chamber; **b)** pump (set to 3mL/min); **c)** ACSF container. Both the chambers and the ACSF are submerged in the water bath, as well as the extension of the tubes between the pump and the chamber, ensuring the ACSF reaches the right temperature before coming in contact with the tissue slices. **B.** Picture of the actual setup.

3.2.1. Supra-physiological saturating levels of glucose and 3-β hydroxybutyrate in hippocampus

Slices from the hippocampus of Wistar rats were prepared as described in point 3.2. The supra-physiological saturating concentrations used were 5mM glucose, 1/0.1mM lactate/pyruvate ±5mM 3HB.

3.2.2. Regional metabolism of *in situ* levels of glucose, lac/pyr and 3HB

Slices from the hippocampus, cortex and striatum of Wistar rats were prepared as described in point 3.2. The *in situ* concentrations used were 2mM glucose, 1/0.1mM lactate/pyruvate ±1.7mM 3HB.

3.2.3. Non-recirculating superfusion of hippocampal slices

Slices from the hippocampus of Wistar rats were prepared as described in point 3.2. The *in situ* concentrations used were 2mM glucose, 1/0.1mM lactate/pyruvate ±1.7mM 3HB. When the superfusion media were replaced by solutions with identical concentrations of ^{13}C-enriched substrates ([1-^{13}C]glucose; [2-^{13}C]lactate and [2-^{13}C]pyruvate ± [U-^{13}C]3HB, all 99% enriched plus 50 μM of 4-AP) they were left in a non-recirculating system for 90-120 minutes.

3.3. Regional metabolism of a 6-OHDA Rat Model of Parkinson's disease

Wistar rats of 12 weeks old, weighing ≥250g were anesthetized intraperitoneally (ip) with 75 mg/kg of ketamine (Bayer Healthcare) and 8mg/kg of xylazine (Rompun, Bayer Healthcare). They were also injected with a solution of dezipramine (20mg/kg), an inhibitor of norepinephrine transporters, assuring the selectivity of the 6-OHDA toxin for the dopamine transporters. Rats were then placed in a stereotaxic frame. From Bregma deep to the skull surface (AP=+0.2, ML=±3.5 and DV=-4.8), 10μg of 6-OHDA dissolved in sodium metabisulphite 0.1% were infused bilaterally in each striatum at a rate of 1 μL/min. After the injection, the cannula was left in place for 5minutes to avoid reflux of the toxin and afterwards it was removed slowly. Controls were submitted to the same procedure and injected with saline solution.

After 21 days of surgical procedure, the superfusion protocol was performed. This model has been reported as a pre-symptomatic stage of the disease, in which depressive and anxious behavior, as well as a mild cognitive impairment are already observed (Tadaiesky et al. 2008). Given the opportunity, we decided to test whether energetic metabolism changes also occurred. For the pilot studies in the 6-OHDA animal model of Parkinson's disease, superfusion of hippocampus, cortex and striatum was performed. Tissue preparation and recovery period were as described in point 3.2. The slices were presented with unlabeled metabolites for 1hour to adjust to the new substrates available, as already described above, and afterwards the solutions were switched for ones with similar concentrations but labeled substrates.

i) **Pilot study 1 - Provision of 5 mM [U-^{13}C]glucose and 1/0.1 mM sodium [3-^{13}C]lactate/unlabeled pyruvate**

ii) **Pilot study 2 - Provision of 5 mM [U-^{13}C]glucose, 1/0.1 mM sodium [3-^{13}C]lactate/unlabeled pyruvate and unlabeled 3HB**

3.4. Metabolite extraction

Metabolites were extracted using the perchloric acid (PCA) method. Ice-cold PCA 7.0-7.2% was added to the samples (~300 μL per hippocampus and striatum, ~500μL per cortex) and left at ~4ºC for 30 minutes. Samples were centrifuged for 15min at 16 000g, 10ºC (Sigma 3-18K centrifuge) and the protein in pellet stored at -80ºC for protein quantification. The supernatant was removed to a new vial and the pH was neutralized with KOH on ice-cold conditions; the precipitated salt was removed by centrifugation and the samples lyophilized.

3.5. Protein Quantification

The protein pellet was thawed and added to 5mL NaOH 0.5M and left to dissolve overnight. Protein was quantified by the bicinchoninic acid (BCA) method. Briefly, a calibration curve was built for each experimental set, with BSA (Bovine Serum Albumine) as protein standard (2, 1, 0.5, 0.25, 0.125, 0.0625 mg/mL) and r^2 value no less than 0.98 was used. To each well of a 96 multiwell-plate were added: 25µL H_2O, 25µL sample/calibration curve standard and 200µL of BCA reagent. The plate was protected from light and incubated at 37ºC for 60min. Absorbance values were measured at 562nm in a SpectraMax plus 384 spectrophotometer using SoftMaxPro5.2 software.

3.6. NMR sample preparation

Samples for NMR spectra analysis were dissolved in 250µL of phosphate buffer (NaH_2PO_4/Na_2HPO_4) made in D_2O, pD 7.0±0.2 containing TSP, fumarate and pyrazine as proton standards. Buffer added to each sample were normalized to mass. All samples, including the samples from the superfusate, were centrifuged for 10min, 13 500rcf, 10ºC (eppendorf centrifuge 5418R) to remove excess of salt. The supernatant (~200µL) was transferred to 3mm NMR tubes.

3.7. NMR spectra acquisition

Spectra (proton and ^{1}H-decoupled ^{13}C NMR) were obtained using an Agilent 600 MHz system with 3mm broadband probe. For ^{13}C spectrum, a 60-degree pulse, 30 kHz spectral width, 2.5 seconds acquisition time and 0.5 second pulse delay were used.

Quantitative ^{1}H spectra were acquired at 25°C with a 90° pulse and a 60 second acquisition time, as pyrazine T_1 was measured at 11.6±0.4sec. Typically 4-16 free induction decays were collected per sample.

3.8. NMR spectra analysis

All the acquired spectra were processed using the NUTS^{TM} software (Acorn NMR, Fremont, CA, USA). Free induction decays were baseline corrected and line broadening applied (0.5 Hz for ^{1}H and 1.0 Hz for ^{13}C) prior to Fourier transformation. For proton, chemical shifts were referenced to TSP at 0.0 ppm (Cerdan et al. 1990) and quantified relative to pyrazine (8.60 ppm) and fumarate (6.52ppm). ^{13}C chemical shifts were referenced to the C1 β-glucose peak at 96.9ppm.
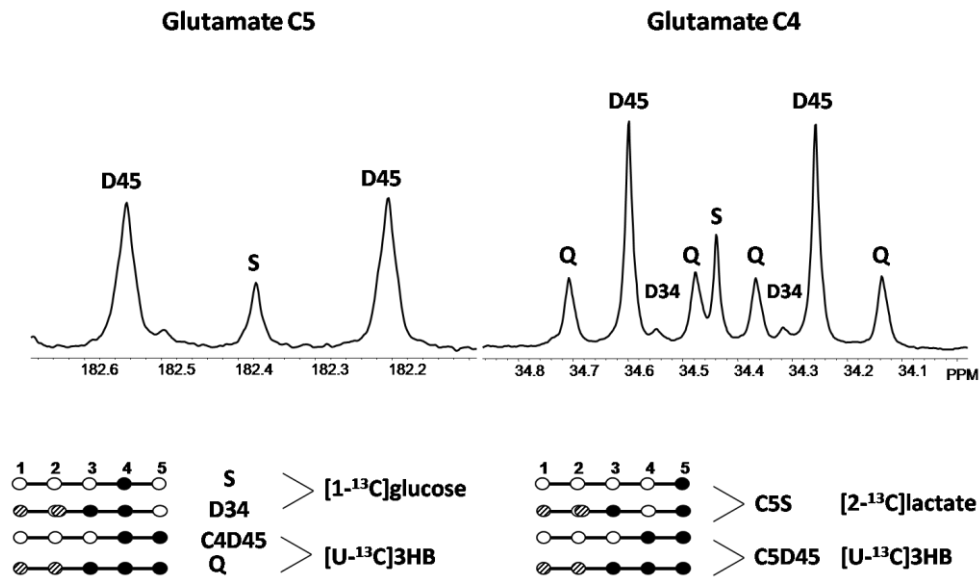
Fig.3.2 Peak assignment of the multiplets in the ¹³C spectra, in the regions corresponding to glutamate carbon 4 and 5.

The contribution to acetyl-coA entering the Krebs cycle from each labeled of the four possible acetyl-coA ^{13}C-isotopomers (designated as Fc0, Fc1, Fc2 and Fc3) was calculated using the nonsteady-state ^{13}C NMR isotopomer analysis from the glutamate carbon 4 and 5 multiplet ratios and the ratio of glutamate carbon 4 to carbon 3 enrichment (^{13}C4/^{13}C3) (Fig.3.2) according to equations 1 to 4 (Malloy et al. 1990). Each multiplet area was assigned as a fraction of the total area of that specific carbon resonance. The glutamate ^{13}C4/^{13}C3 ratio was corrected for partial saturation and nOe effects.

Glutamate enrichment was assumed to reflect the neuronal metabolic profile. Previous studies have shown that glial glutamate contributions are bellow the detection threshold of NMR (Chassain et al. 2005).

$$Fc1 = \frac{C5S}{C5D} \times Fc3 \qquad \textit{(eq1)}$$

$$Fc2 = \frac{C4}{C3} \times C4D34 \qquad \textit{(eq2)}$$

$$Fc3 = C4Q \times \frac{C4}{C3} \qquad \textit{(eq3)}$$

$$Fc0 = 1 - (Fc3 + Fc2 + Fc1) \qquad \textit{(eq4)}$$

33

3.8.1. Experiments using [2-¹³C]lactate/pyruvate, [1-¹³C]glucose, [U-¹³C]3HB

The fractional contribution to acetyl-coA of each labeled substrate was assigned as [2-¹³C]lactate/pyruvate (Fc1), [1-¹³C]glucose (Fc2), [U-¹³C]3HB (Fc3), and unlabeled endogenous substrates (Fc0) (Fig.3.3). Both glucose and unlabeled substrate concentration calculations are corrected for the 1:1 factor of [labeled lactate]:[unlabeled lactate] that comes from the breakdown of one molecule of [1-¹³C]glucose through the glycolytic pathway. 3HB is also corrected for the 50% fractional enrichment used.
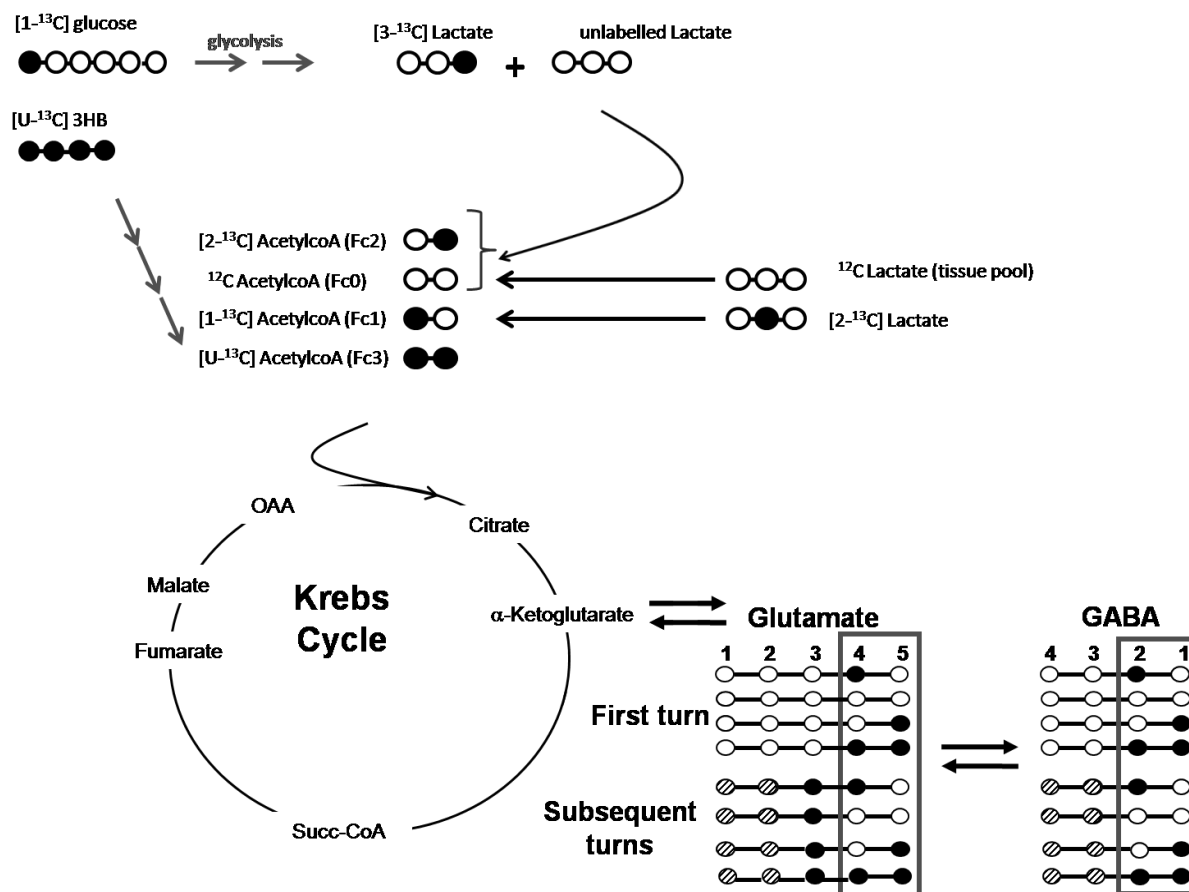

Fig.3.3 Expected labeling pattern in glutamate pool when using [2-¹³C]lactate/pyruvate (Fc1), [1-¹³C]glucose (Fc2) and [U-¹³C]3HB (Fc3) as precursors. Glutamate pool labeling is assumed to reflect the labeling in α-ketoglutarate and. Unlabeled and endogenous substrates are calculated as Fc0.

3.8.2. Experiments using, [U-¹³C]glucose, [3-¹³C]lactate and unlabeled pyruvate

The fractional contribution to acetyl-coA of each labeled substrate was assigned as [U-¹³C]glucose (Fc3), [3-¹³C]lactate (Fc2), and unlabeled pyruvate/endogenous substrates (Fc0) (Fig.3.4).The contribution of lactate is slightly underestimated, as contributions from the equilibrium with pyruvate may form some unlabeled lactate. This contribution, although significative, does not compromise any possible discoveries that would come from this pilot study.
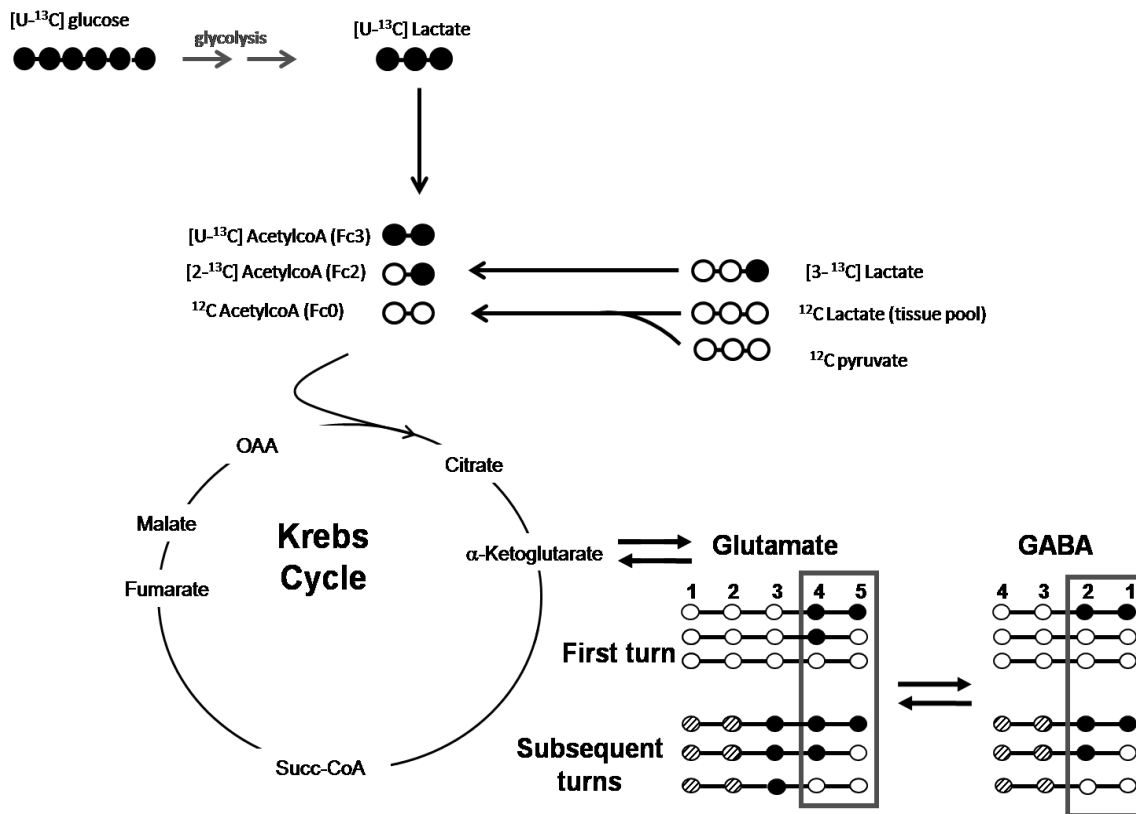
Fig.3.4 Expected labeling pattern in glutamate pool when using [U-¹³C]glucose (Fc3) and [3-¹³C]lactate (Fc2) as precursors. Glutamate pool labeling is assumed to reflect the labeling in α-ketoglutarate and, consequentially, the labeling throughout the cycle may be deduced. Unlabeled and endogenous substrates are calculated as Fc0.

3.8.3. Experiments using, [U-¹³C]glucose, [3-¹³C]lactate and unlabeled pyruvate and 3HB

The fractional contribution to acetyl-coA of each labeled substrate was assigned the same as in the previous pilot study (3.8.2): [U-¹³C]glucose (Fc3), [3-¹³C]lactate (Fc2). Unlabeled 3HB was assigned as Fc0, along with pyruvate and endogenous substrates (Fc0). Like in the previous pilot study, lactate contribution may be underestimated due to contributions from the pyruvate pool. Contribution of 3HB may not be accurately quantified, but big contributions in the unlabeled pool are assigned to this substrate.

3.8.4. Glutamate ^{13}C Natural Abundance Correction

Natural abundance for ^{13}C was measured for glutamate and included in isotopomer analysis as correction factor. A fresh solution of 20mM glutamate in D_2O phosphate buffer (NaH_2PO_4/Na_2HPO_4) pD 7.0 ± 0.1was made, and the ^{13}C spectrum acquired overnight. The following correction ratios were obtained:

C4/C3	C5/C4
0.912992	0.2125

3.9. Statistical analysis

The Welch unpaired t-test was used to test for statistical significance in substrate utilization profiles between groups assuming unequal variance.

4. Results and Discussion

4.1. Substrate contributions reported by glutamate ^{13}C-isotopomer analysis

As described in the previous section, ^{13}C glutamate isotopomer analysis can be used to evaluate different substrate contributions to the acetyl-coA pool (Fig.3.2, page 33), as it exists in high concentrations in most tissues and is in rapid exchange with Krebs cycle α-ketoglutarate (Carvalho et al. 1999). The non-steady state analysis allows this information to be obtained even if the[13]C-metabolite enrichment has not reached isotopomeric steady state (Malloy et al. 1990).
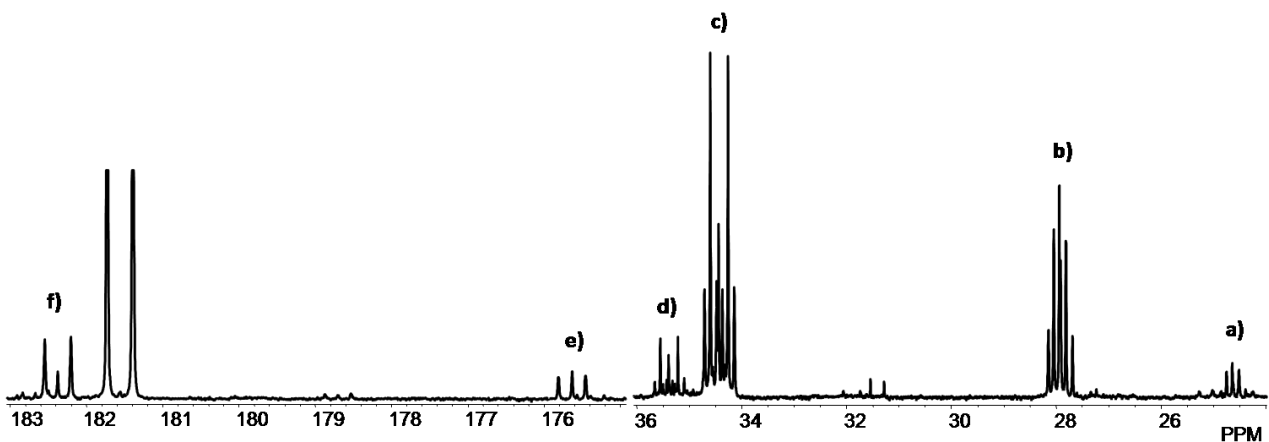

Fig.4.1 Typical carbon spectra of the extracts of hippocampal slices. Signal assignment was as follows: **a)** GABA C3; **b)** glutamate C3; **c)** glutamate C4; **d)** GABA C2; **e)** glutamate C1; **f)** glutamate C5

4.1.1. Supra-physiological saturating levels of glucose and 3-β hydroxybutyrate in hippocampus: 5mM glucose, 1/0.1mM lactate/pyruvate ±5mM3HB

At concentrations of 5mM glucose, 1/0.1mM lactate/pyruvate and 5mM 3-hydroxybutyrate (3HB), both the glucose transporters and monocarboxylate transporters are fully saturated, thus we can assess these substrates contributions to acetyl-coA under conditions of maximal cellular substrate uptake. One important rationale behind using such high concentrations (2-3 fold above their maximal cerebral concentrations) is due to the fact that the superfusion medium is typically recirculated and significant depletion of substrates could occur over the 3 hour duration period of these experiments if they were presented at lower physiological levels. As was evaluated by ^{1}H NMR, at the end of the superfusion period the concentrations of all substrates remained well above saturating values (see Fig.4.19b, page 63).

Fractional contribution of substrates to acetyl-coA pool at saturating conditions in hippocampal slices
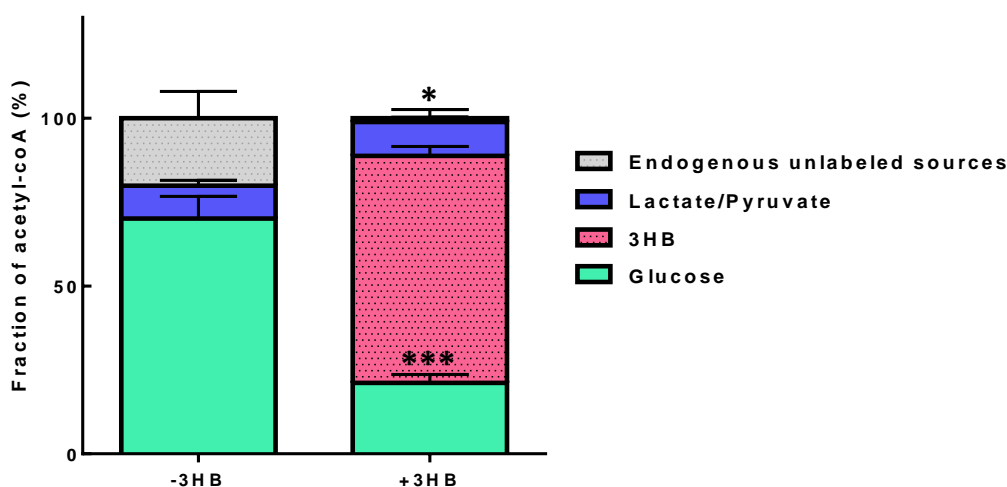

Fig.4.2 Fractional contribution of substrates to acetyl-coA pool entering the Krebs cycle in the absence (-3HB) and presence (+3HB) of 3-hydroxybutyrate, in rat hippocampus slices. Exogenous glucose*** is presented in green, lactate/pyruvate in blue, 3HB in pink and unlabeled endogenous sources in light grey*. Values are presented as means ±SEM of the results obtained from 6 independent experiments.
*p<0.05, *** p<0.0001 (presence *vs* absence of 3HB), unpaired t-test with Welch correction.

When the slices were presented with 5mM [1-^{13}C]glucose and 1/0.1mM [2-^{13}C]lactate/pyruvate, contributions to acetyl-CoA were 70±7% and 10±2%, respectively, with 20±8% from unlabeled endogenous sources (Fig.4.2, left). In the presence of 5mM [U-^{13}C]3HB, glucose contributions significantly fell (21±3%), lactate/pyruvate contributions were unchanged (10±1%) and endogenous contributions fell (1±3%), while [U-^{13}C]3HB became the major acetyl-coA contributor (68±3%) (Fig.4.2, right). These values are in agreement with recently reported contributions measured *in vivo* by ^{13}C NMR (Chowdhury et al. 2014).

These results indicate that when neither glucose nor 3HB were in limited supply, the hippocampal slices showed a clear preference for the ketone body as a source of acetyl-coA generation. While acetyl-coA flux from glucose was highly attenuated, contributions from exogenous lactate/pyruvate were not affected. This suggests that 3HB did not attenuate Krebs cycle glucose utilization by inhibition of pyruvate dehydrogenase (PDH), since PDH inhibition would also affect lactate/pyruvate contributions. This is also consistent with our observation of reduced output of glycolytic lactate (i.e. [3-^{13}C]lactate derived from [1-^{13}C]glucose) into the superfusion medium when 3HB was present (Fig.4.20d page 64; Fig.4.26b page 70). This metabolic alteration was also found previous studies of ketone body metabolism (Yudkoff et al. 2005; LaManna et al. 2009; Jiang et al. 2011).

The rate of 3HB (k) utilization relative to lactate/pyruvate (L) can be calculated from the glutamate carbon 5 (C5) doublet-to-singlet ratio (Fig.4.3, k/L). Our data shows that 3HB contribution to glutamate C5 enrichment was 7-fold higher than that of lactate/pyruvate. Following the same logic, 3HB (k) rate of utilization relative to glucose (G) can also be calculated analyzing the relative contributions to glutamate carbon 4 (Fig.4.3, k/G). 3HB contributed 3 times more to glutamate enrichment in comparison to glucose.
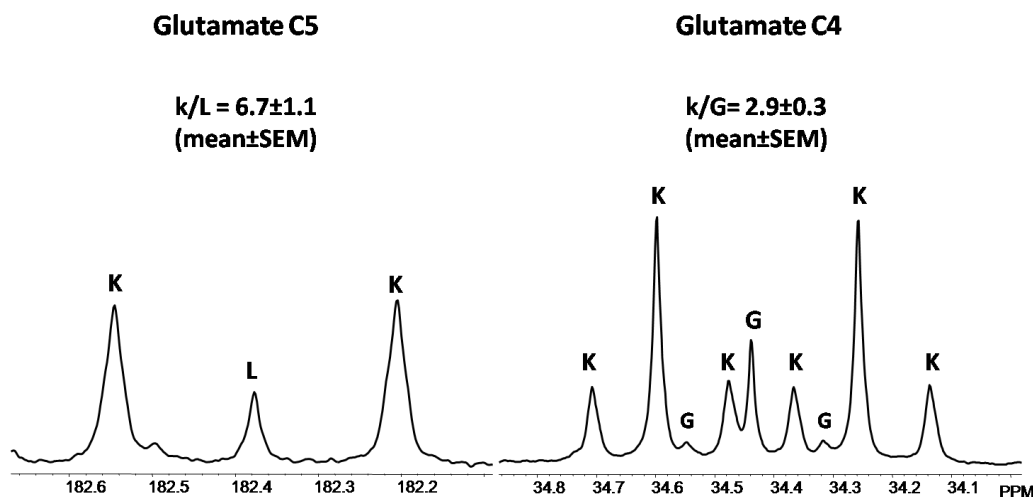
Glutamate C5

k/L = 6.7±1.1
(mean±SEM)

Glutamate C4

k/G= 2.9±0.3
(mean±SEM)

Fig.4.3 Relationship between glutamate carbon 4 and 5 ^{13}C isotopomers derived from different substrates: [2-^{13}C]lactate/pyruvate (**L**), [1-^{13}C]glucose (**G**) and [U-^{13}C]3HB (**k**). The letters above each ^{13}C signal component indicate the contributing ^{13}C-enriched substrate. **k/L** indicates the rate of 3HB utilization relative to lactate, **k/G** indicate the ratio of 3HB utilization relative to glucose. These ratios are adjusted for different enrichments of the precursor ^{13}C enriched substrates. Values are presented as mean±SEM for 6 individual experimental procedures.

The GABA ^{13}C-multiplet intensities were much lower than those of glutamate (Fig.4.1; Fig.4.4) due to a lower amount of GABA compared to glutamate, as seen by ^{1}H NMR (data not shown). This meant that some of the low-abundance GABA isotopomer signals, notably C2Q and C2D23 could not be reliably quantified for application of the nonsteady-state analysis to GABA as previously described (Duarte et al. 2007). Because of this, the k/G ratio was quantified from the ratio of the GABA C2D12 to C2S components on the basis that C2S is solely derived from [1-^{13}C]glucose while C2D12 can only originate from [U-^{13}C]3HB. We tested this method on glutamate by calculating k/G ratios from the analogous glutamate C4S and C4D45 signals, and compared with k/G ratios derived from the glutamate nonsteady state isotopomer analysis. The two methods yielded equivalent k/G ratios for glutamatergic neurons (2.9±0.3 using all isotopomers of 3HB *vs* 2.7±0.2 using only the C4D45). Using this approach, we found that the GABA k/G ratio was significantly lower than that of glutamate (mean±SEM 1.1±0.12 *vs* 2.7±0.2, *p < 0.0005) (Fig.4.4). These results indicate that for hippocampus slices, GABAergic neurons oxidized a lower fraction of ketone bodies relative to glucose in comparison to glutamatergic neurons.
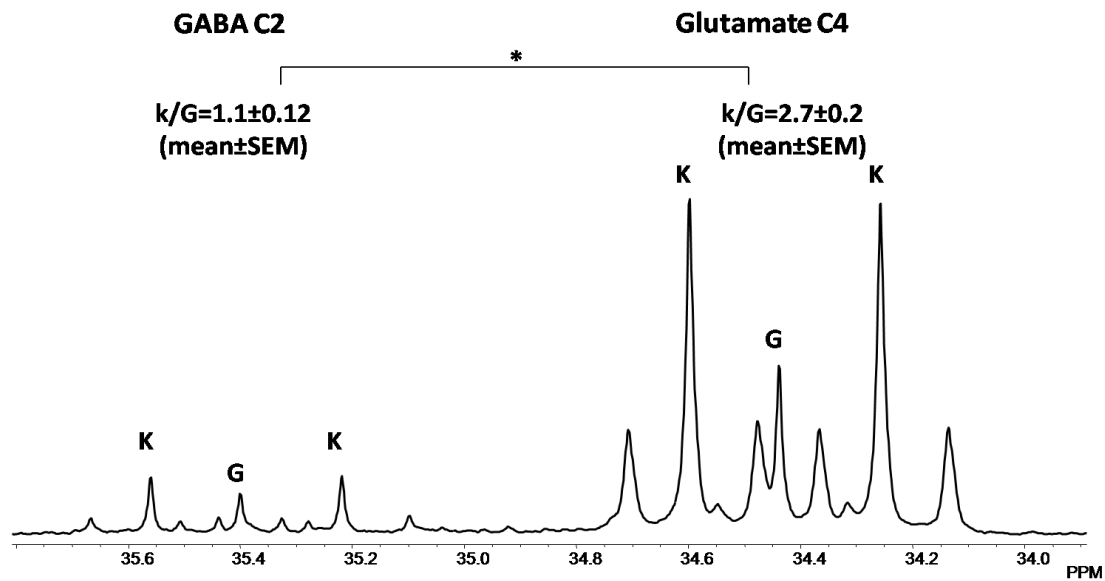
Fig.4.4 Relationship between glutamate carbon 4 and GABA carbon 2 ^{13}C isotopomers derived from[1-^{13}C]glucose (**G**) and [U-^{13}C]3HB (**k**).The letters above each ^{13}C signal component indicate the contributing ^{13}C-enriched substrate.**k/G** indicate the ratio of 3HB utilization relative do glucose, that is clearly higher in glutamate relative to GABA (*p<0.0005). These ratios are adjusted for different enrichments of the percursor^{13}C enriched substrates. Values are presented as mean±SEM for 6 individual experimental procedures.

In contrast to studies using *in situ* brain tissue provided with ^{13}C-substrates where in addition to glutamate and GABA, glutamine signals were also prominent (Kunnecke et al. 1993; Bouzier et al. 2000; Chowdhury et al. 2014), tissue glutamine ^{13}C-signals were generally absent in our brain slice preparations. There was no indication of glutamine washout into the superfusate. Duarte and colleagues have also reported a depletion of glutamine in superfused slices of hippocampus (Duarte et al. 2007), suggesting this might be related to the methodology used.

4.1.2. Regional metabolism of 2mM glucose, 1/0.1mM lac/pyr ± 1.7mM 3-hydroxybutyrate

Fractional contribution of substrates to acetyl-coA pool at maximal cerebral levels found *in situ*

a)

b)

c)

Fig.4.5 Fractional contribution of substrates to the acetyl-coA pool entering the Krebs cycle in the absence (-3HB) and presence (+3HB) of 3-hydroxybutyrate, in Wistar rat brain slices. **a)** hippocampal slices - *p<0.05 (presence *vs* absence of 3HB), unpaired t-test with Welch correction.; **b)** striatal slices; **c)** cortical slices. Exogenous glucose is presented in green, lactate/pyruvate in blue, 3HB in pink and unlabeled endogenous sources in light grey. Values are presented as mean±SEM of the results obtained from 4 independent experiments for hippocampus and mean±SD of 2 individual experiments for striatum and cortex.

For the *in situ* brain, there is a substantial gradient of glucose and ketone bodies across the blood-brain barrier (BBB) such that their true cerebral concentrations are far below that of blood with maximal levels considered to be about 2.0 and 1.7 mM, respectively. Since the BBB is abolished during brain slice preparation, the superfusate substrate concentration is directly

experienced by cerebral tissues in this setting. To recreate realistic cerebral glucose and ketone body concentrations, slices were perfused with 2.0 mM glucose, 1.0/0.1 mM lactate/pyruvate ± 1.7 mM 3HB. Under these conditions, contributions of glucose and lactate/pyruvate to acetyl-coA in hippocampus were (mean±SEM) 45±4% and 13±2%, respectively, with 43±4% from unlabeled endogenous sources. In the presence of 1.7mM [U-^{13}C]3HB, glucose contributions fell significantly (25±3%, *p<0.0053), lactate/pyruvate contributions were not significantly altered (20±5%), endogenous contributions significantly decreased to 18±7% (*p<0.027), while [U-^{13}C]3HB became the major acetyl-coA source (38±4%) Fig.4.5a.

In the striatum (Fig.4.5b), contributions of glucose in the absence and presence of 3HB were (mean±SD) 44±12% and 28±6%, respectively. Lactate/pyruvate contributions went from 13±2% (without 3HB) to 29±5% in the presence of 3HB. Endogenous contributions had a major decrease from 43±10% (without 3HB) to 3±8% in the presence of the ketone body. 3HB became the biggest contributor, accounting for 41±7% of the pool.

Surprisingly, in cortex slices (Fig.4.5c), glucose contributions did not seem to vary much when in the absence or presence of 3HB (mean±SD: 39±8 *vs* 33±0.6%, respectively). Lactate/pyruvate contributions also did not vary, contributing 21±13% in the absence and 22±13% in the presence of the ketone body. 3HB contributed 32±6% for the cortical acetyl-coA pool. Endogenous contributions follow the trend of the other structures, with 40±5% in the absence and 12±19% in the presence of 3HB.

Under these saturating physiological conditions in hippocampus slices, glucose contributions decreased in the presence of 3HB, with 3HB becoming an important but not a dominant source of acetyl-coA as was observed with supra-physiological substrate levels (5mM glucose ± 5mM 3HB). The striatum also seemed to follow this trend. However, 3HB oxidation and its displacement of glucose utilization was less pronounced in cortical slices, possibly due to different energetic requirements from different neuronal/astrocytic populations.

Although we failed to obtain statistical significant data for this test due to the small number of replicates, some tentative conclusions were reached. In the presence of the ketone body 3-hydroxybutyrate, lactate/pyruvate contributions seemed to increase in hippocampus and striatum. This could be due to the fact that these substrates are transported into the cells by a common set of transporters (MCT). The higher availability of substrates could have induced an upregulation of MCT expression, thus increasing the uptake of all the monocarboxylates available in the medium. This may have been feasible within the 4-hour incubation with lactate/pyruvate and ketone body, as significant increases (>50%) in MCT1 and MTC4 expression in rat muscle were observed after only 2hours of exercise (Coles et al. 2004). The fact that no apparent stimulation of lactate/pyruvate utilization was observed with supra-physiological levels could be due to a much higher availability of the ketone body (5mM) versus lactate/pyruvate (~1mM) resulting in more effective competition of ketone bodies for the transporters.

Another consistent observation regardless of the brain region was an unexpectedly high contribution of unlabeled endogenous substrates (accounting for over 40% of acetyl-coA) in slices

supplied with glucose and lactate/pyruvate, whereas in the presence of 3HB, endogenous contributions were only residual. It is known that brain glycogen storages exist (Lapidots & Gopher 1994; Choi et al. 2003; Gruetter 2003; Pierre & Pellerin 2005) mainly in glia, as there is evidence that glycogen is toxic to neurons (Pierre & Pellerin 2005). This reservoir is able to maintain function for 2hours of mild hypoglycemia (Choi et al. 2003), so one possible explanation would be that this stored glycogen was mobilized to compensate for the decreased glucose availability. Whether this could sustain a significant contribution to cerebral energy generation over a 4 hour period (1hour of adaptation period + 3hours of recirculated labeled compounds) is questionable based on typical brain glycogen concentrations. Alternatively, these data may simply represent outliers, and a that more realistic estimate of endogenous contributions would arise with more replicate measurements.

Ratios of 3HB relative to lactate utilization (k/L) and 3HB relative to glucose utilization (k/G) (see Fig.4.3) also show increased ketone body utilization relative to the other substrates (Table 4-1).

Table 4-1 k/L ratio indicates the rate of 3HB utilization (**k**) relative to lactate (**L**) and **k/G** represents 3HB (**k**) rate of utilization relative to glucose (**G**) evaluated by all ^{13}C isotopomers derived from different substrates, as represented in Fig.4.3 (page 40). Values are presented as mean±SD for 2 individual experimental procedures.

	Cortex	Hippocampus	Striatum
k/L	3.4±1.5	3.2±1.6	2.9±1
k/G	2.2±0.7	2.7±0.9	2.8±0.9

In the same fashion, when using only the C4D45/S of glutamate for k/G values, we get a good agreement to the values when using all multiplets (Table 4-2), allowing for a comparison of ketone bodies *vs* glucose contribution to glutamate and GABA pools. As was observed before, although the GABA pool has a significant contribution from 3HB (with striatum a possible exception), its utilization relative to glucose (k/G) is lower compared to that reported by glutamate (Table 4-2).

Table 4-2 k/G represents ketone bodies (**k**) rate of utilization relative to glucose (**G**) evaluated by C4D45/C4S for glutamate and C2D12/C2S for GABA, as represented in Fig.4.4 (page 41). Values are presented as mean±SD for 2 individual experimental procedures**.**

	Cortex	Hippocampus	Striatum
Glutamate k/G	2.4±0.8	2.6±0.9	2.8±1.2
GABA k/G	1.1±0.5	1.0±0.7	0.9±0.2

4.1.3. Regional metabolism of a 6-OHDA rat model of Parkinson's disease

Given that we had access to a 6-OHDA Parkinson's disease (PD) rat model in our lab, we decided to test if there were changes in cerebral substrate selection in this pre-symptomatic model (Tadaiesky et al. 2008), since previous studies have hinted at such modifications in other models (Chassain et al. 2005). First, we tested competition between glucose and lactate, and later included 3HB as a substrate. Due to the limited number of superfusion chambers available, these two experiments were conducted separately.

i)   Pilot study 1 – [U-13C]glucose (5mM) *vs* [3-13C]lactate (1mM)

Fractional contribution of substrates to acetyl-coA in a 6-OHDA Parkinson's disease model – pilot 1

a)

b)

c)
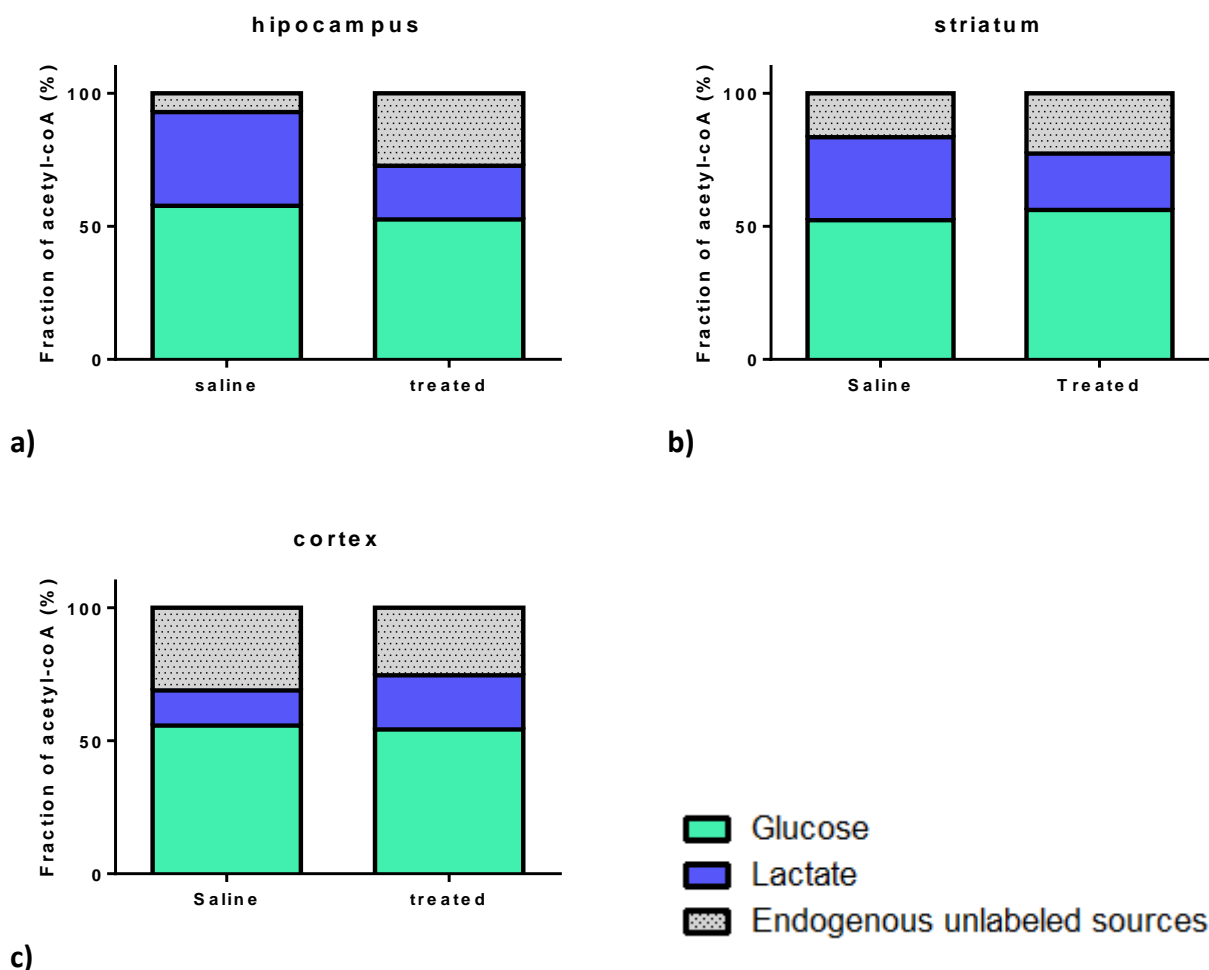
Fig.4.6 Fractional contribution of substrates to acetyl-coA pool entering the Krebs cycle in Wistar rat brain slices from animals that were injected with saline or 6-OHDA (treated). **a)** hippocampal slices; **b)** striatal slices; **c)** cortical slices. Exogenous glucose is presented in green, lactate in blue and unlabeled sources in light grey. Values are presented for a single experimental procedure.

In the presence of both glucose and lactate, there was no major difference in substrate selection when comparing slices from different structures or for slices obtained from saline *vs* treated animals, with glucose being the main contributor of acetyl-coA in glutamatergic neurons (Fig.4.6). In hippocampus, glucose and lactate contributions were 58% and 35% for saline, respectively, and 53% and 20% for treated. Endogenous contributions were 7% in control animals versus 27% for treated (Fig.4.6a). For striatum, glucose contribution was 52% in saline, with no change in the treated (56%). Lactate contributed 31% for saline and 21% for treated. Endogenous contributions were of 17% for saline injected animals, and 23% for the 6-OHDA treated (Fig.4.6b). In cortex, glucose and lactate contributed 56% and 13% for rats injected with saline, respectively, versus 54% and 20% in the ones injected with 6-OHDA. Endogenous substrates fill the remaining percentual gap, with 31% for saline and 25% for treated (Fig.4.6c). This sizable endogenous contribution in this experiment is at least partially accounted for by the 0.1 mM unlabeled pyruvate.

When slices were presented with glucose and lactate, while they preferred glucose for oxidation, exogenous lactate was also effectively utilized, in accordance with the literature (Bergersen et al. 2001; Pierre & Pellerin 2005; Bouzier-Sore et al. 2002; Dienel 2012; Pellerin 2010). In this pre-symptomatic 6-OHDA model of PD, our very preliminary data suggests no changes in relative utilization of these substrates.

ii) Pilot study 2 – [U-^{13}C]glucose (5mM) *vs* [3-^{13}C]lactate (1mM) *vs* unlabeled 3HB (5mM)

In this study, we supplemented the superfusing medium with 5mM of unlabeled 3HB. The rationale behind this was that a drop in either glucose or lactate contributions, accompanied by an increase in the contribution of unlabeled would indicate significant competition from 3HB for acetyl-coA production.

Fractional contribution of substrates to acetyl-coA in a 6-OHDA Parkinson's disease model – pilot 2
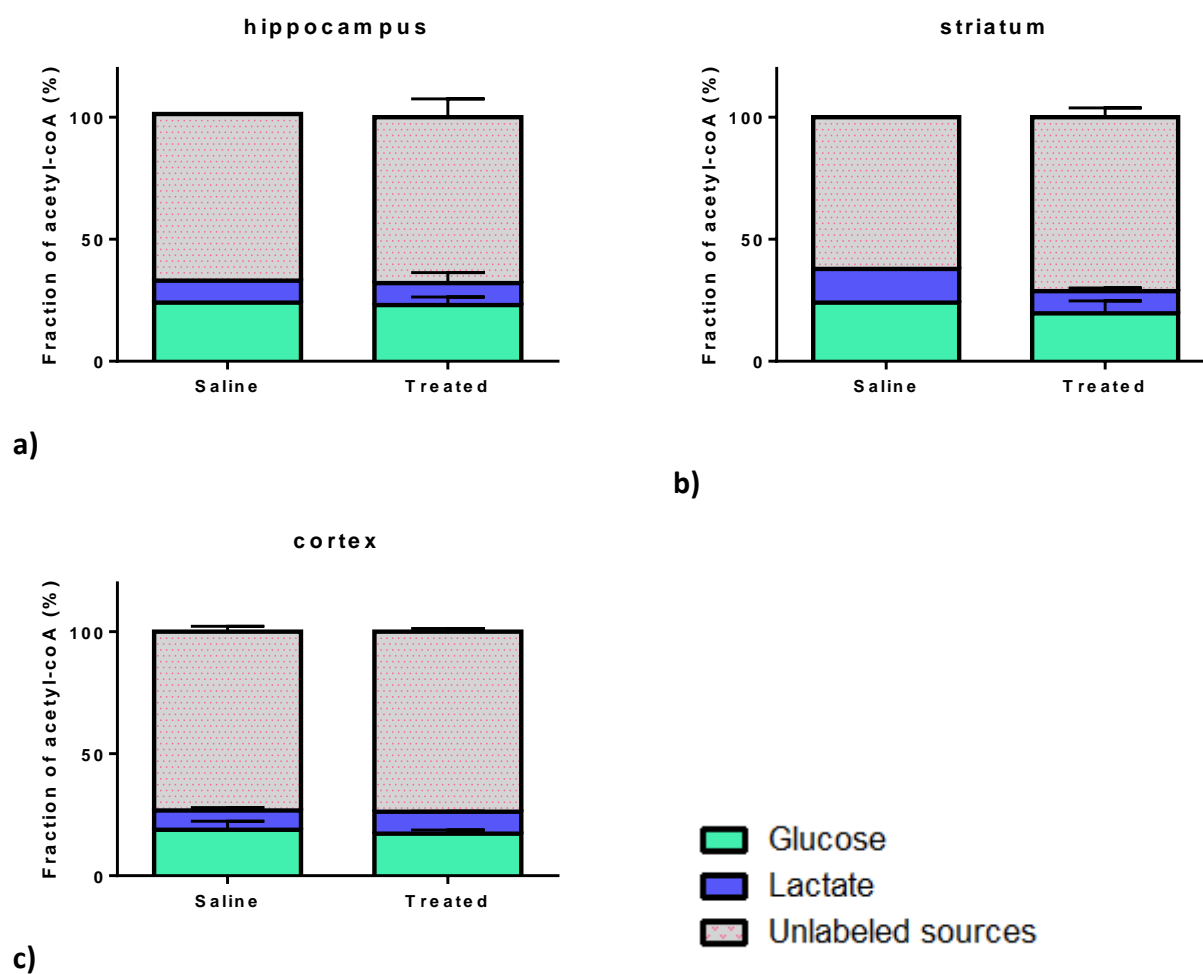

a)

b)

c)

Fig.4.7 Fractional contribution of substrates to acetyl-coA pool entering the Krebs cycle in Wistar rat brain slices that were injected with saline or 6-OHDA. **a)** hippocampal slices; **b)** striatal slices; **c)** cortical slices. Exogenous glucose is presented in green, lactate in blue and unlabeled sources (endogenous, pyruvate and 3HB) in grey with pink dots. Values are presented as mean±SD for 2 independent experiments for cortex (both saline and treated), treated striatum and treated hippocampus and for 1 experiment for saline striatum and saline hippocampus.

In the presence of unlabeled 3HB, no significant changes in substrate contribution to glutamatergic acetyl-coA generation were observed between saline-injected and 6-OHDA injected animals. In hippocampus, glucose and lactate contributed 23% and 9% for saline, respectively, versus (mean±SD) 23±3% and 9±4% for 6-OHDA treated animals. Unlabeled sources contributed 68% in saline and 68±8% in treated (Fig.4.7a). For striatum, glucose and lactate had contributions of 24% and 14% for saline, and 20±5% and 9±1% for treated. Unlabeled sources contributed 62% for saline and 71±4% for treated (Fig.4.7b). In cortex, glucose contributed 19±3% and 17±1% in saline-injected and treated, respectively. Lactate contributed 8±1% in saline and 9±0.1% in treated, while unlabeled sources contributed 73±2% in saline and 74±1% in treated animals (Fig.4.7c).

There were no significant changes in substrate preference between saline and 6-OHDA injected animals, for either of the pilot experiments. Comparing both experiments, in the presence of 3HB the glucose contributions seem to decrease, with 3HB becoming the major contributor, as happened in the previous experiments using WT animals. However, and contradicting the WT results, lactate contributions seem to decrease when in the presence of 3HB. One possible explanation could be that in the WT experiments, lactate was supplemented in a 1:10 ratio with pyruvate of similar labeling, due to the close isotopic equilibrium between these two molecules. In the 6-OHDA animals experiments, [3-^{13}C]lactate was supplemented in a 1:10 ratio with unlabeled pyruvate, since no [3-^{13}C]pyruvate was available at the time. Another possibility could be an impaired metabolism of this pathway due to the lesion suffered from the injection.

The rate of glucose (G) utilization relative to lactate (L) contributions to glutamate and GABA can be calculated similarly to what was done before (see Fig.4.4, page 41). Since in this experiment [U-^{13}C]glucose and [3-^{13}C]lactate were used, relative contributions of each substrate were corrected for the isotopomers generated (Fig.4.8). While the GABA signals were lower than that of glutamate, we were still able to quantify all multiplets from contributing isotopomers (Table 4-3; Table 4-4).
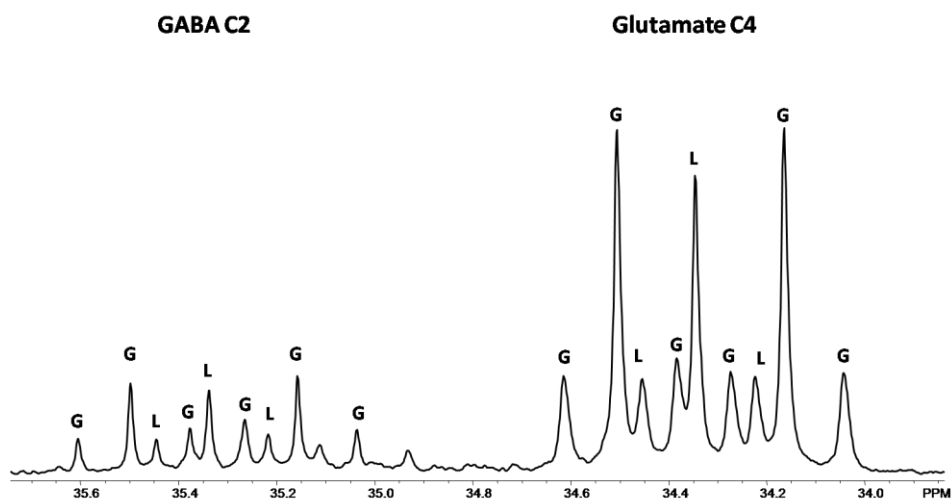

Fig.4.8 Relationship between glutamate carbon 4 and GABA carbon 2 ^{13}C isotopomers derived from [U-^{13}C]glucose (**G**) and [3-^{13}C]lactate (**L**).The letters above each ^{13}C signal component indicate the contributing ^{13}C-enriched substrate.

Table 4-3 Ratio of glucose utilization relative to lactate (**G/L**) in glutamate and GABA pools for the three brain structures analyzed in pilot study 1. These ratios are adjusted for different enrichments of the precursor ^{13}C enriched substrates. Values are presented for a single experimental procedure.

Pilot 1	Cortex		Hippocampus		Striatum	
	Glutamate	GABA	Glutamate	GABA	Glutamate	GABA
Saline	3.63	2.46	2.02	2.19	1.95	2.36
Treated	2.62	2.87	2.4	2.4	2.61	2.06

Table 4-4 Ratio of glucose utilization relative to lactate (**G/L**) in glutamate and GABA pools for the three brain structures analyzed in pilot study 2. These ratios are adjusted for different enrichments of the precursors ^{13}C enriched substrates. Values are presented as mean±SD for 2 individual experimental procedures for cortex (both saline and treated), treated striatum and treated hippocampus. Saline striatum and saline hippocampus values are presented for a single experimental procedure.

Pilot 2	Cortex		Hippocampus		Striatum	
	Glutamate	GABA	Glutamate	GABA	Glutamate	GABA
Saline	2.8±0.6	3.1±1.1	2.51	2.11	1.7	1.49
Treated	2.6±0.5	2.8±0.6	3.4±0.6	2.6±1.3	2.6±1.3	2.4±0.8

According to the data from the tables 4-3 and 4-4, for slices from a given brain structure, glucose was preferred over lactate for both glutamate and GABA formation, either in the presence or absence of 3HB. G/L values obtained from glutamate and GABA analyses were similar to each other, suggesting equal preference of substrates, and were also similar between saline and 6-OHDA injected animals, suggesting no changes at this level for this particular model of PD.

4.1.4. C4/C3 glutamate ratios

Table 4-5 Glutamate C4/C3 ratio of WT Wistar rats different brain structures superfused with different concentrations of substrates.

	5mM glucose, 1/0.1mM lac/pyr ± 5mM 3HB recirculating conditions	2mM glucose, 1/0.1mM lac/pyr, ± 1.7mM 3HB recirculating conditions			2mM glucose, 1/0.1mM lac/pyr, ± 1.7mM 3HB non - recirculating conditions
	hippocampus (mean ± SEM) (n=6)	cortex (mean±SD) (n=2)	striatum (mean±SD) (n=2)	hippocampus (mean±SD) (n=2)	hippocampus (mean±SD) (n=2)
-3HB	2.2 ± 0.2	1.6±0.5	1.7±0.1	1.7±0.4	2.5±0.02
+3HB	2 ± 0.1	1.8±0.03	2±0.1	1.8±0.04	2.7±0.2

Table 4-6 Glutamate C4/C3 ratio of tissue extracts from Wistar rats injected with saline/6-OHDA and superfused with glucose, lactate and pyruvate (Pilot 1). Values are presented for one individual experiment.

	hippocampus (n=1)	striatum (n=1)	cortex (n=1)
Saline	2.9	2	2.4
Treated	1.8	1.8	1.9

Table 4-7 Glutamate C4/C3 ratio of tissue extracts from Wistar rats injected with saline/6-OHDA and superfused with glucose, lactate, pyruvate and 3HB (Pilot 2). Values are presented as one individual experiment (n=1) or mean±SD for 2 individual experiments (n=2).

	hippocampus (n=1)s; (n=2)t	striatum (n=1)s; (n=2)t	cortex (n=2)
Saline	1.3	1.3	1.4±0.05
Treated	1.3±0.02	1.3±0.17	1.7±0.3

The glutamate C4/C3 ratio is sensitive to both the extent of isotopic enrichment of Krebs cycle intermediates - converging to a minimum value at isotopic steady-state - as well as anaplerotic flux. The effects of anaplerosis on the C4/C3 ratio depend on the extent to which the anaplerotic substrate is labeled. To the extent that the anaplerotic substrate is unlabeled, the glutamate C4/C3 ratio is increased by anaplerotic activity. Previous experiments have shown that in the presence of 50µM 4-AP, a C4/C3 ratio of 1.4 was achieved after 3hours (Duarte et al. 2007). However, the C4/C3 ratios derived from our experiments were consistently above this value (Table 4-5, Table 4-6 and Table 4-7). There are several reasons for this. Perhaps the most likely is **that isotopic steady state was not achieved.** The *ex-vivo* nature of the experiment means that the basal functioning of neuronal transmission no longer occurs on its own, resulting in a slower turnover of the cycle since very little neurotransmitters need to be produced. This is the reason why we supply the medium with 4-AP, which obligates neurons to have some activity and increases cycle flux, but other stimuli options should be explored if more appropriate. **A second factor that could contribute to higher C4/C3 ratios is increased anaplerotic activity**. Anaplerotic substrates supply the Krebs cycle at points other than acetyl-coA; for example propionate supplies the cycle at the level of succinyl-coA while pyruvate may supply the cycle at the level of oxaloacetate (see Fig.1.2 page 13). Pyruvate (re)cycling, by conversion of pyruvate to oxaloacetate through pyruvate carboxylase (PC) has been reported in brain glia (Kunnecke et al. 1993; Lapidots & Gopher 1994; Beckmann et al. 1995). In our study, we used [1-^{13}C]glucose, from which derives one unlabeled pyruvate and one [3-^{13}C]pyruvate. If we consider them entering the PC pathway at the same rate, we would get 50% unlabeled oxaloacetate, 25% oxaloacetate labeled at C2 and 25% labeled at C3 due to scrambling of the label via malate and fumarate. If this oxaloacetate pool condenses with [2-^{13}C]acetyl-coA, only 25% of the resulting glutamate/glutamine would be labeled in both C3 and C4, while the remaining 75% would not be labeled in C3, even at steady state.

Some authors (Chowdhury et al. 2014) have suggested that in the presence of ketone bodies, these become the main acetyl-coA producer while glucose is diverted to anaplerotic oxaloacetate synthesis and Krebs cycle flux upregulation. Since we did not perform a longitudinal study to determine if the glutamate C4/C3 ratio had converged to a constant value at the time of tissue harvesting, we cannot determine to what extent the elevated glutamate C4/C3 ratios that we observed reflect anaplerotic activity or isotopic nonsteady-state.

4.2. ¹H extract analysis: cell content quantification

¹H analysis of extracts allows us to quantify the metabolites present (Fig.4.9), a complementary data for the selection of substrates for acetyl-coA generation. By using internal standards of known concentration, we are able to determine absolute amounts of the substances analyzed.
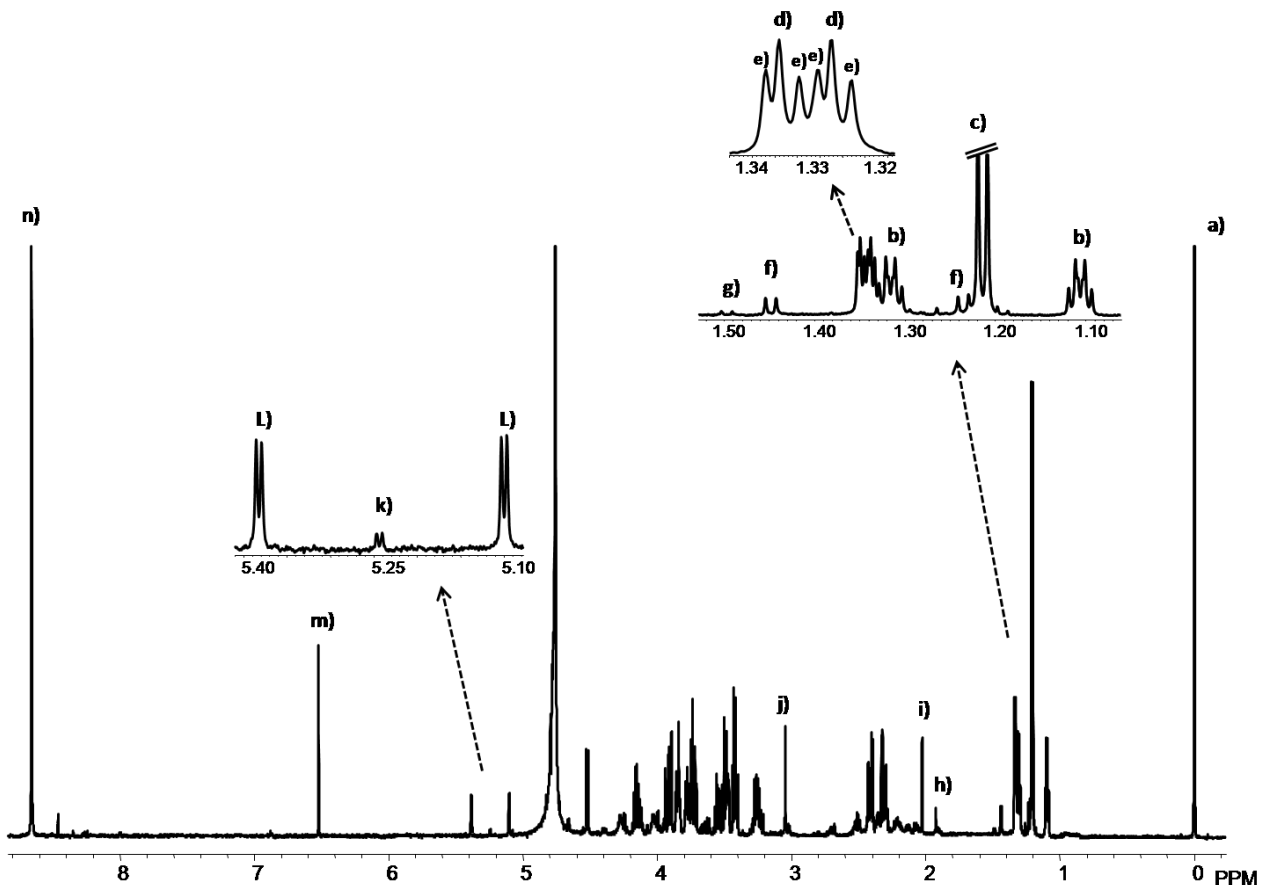
Fig.4.9 Representative 1H spectra of an extract. **a)** TSP standard; **b)** [U-¹³C]3HB; **c)** unlabelled 3HB; **d)** unlabelled lactate; **e)** [2-¹³C]lactate; **f)** [3-¹³C]lactate; **g)** alanine; **h)** acetate; **i)** N-acetyl-aspartate (NAA);
j) creatine/phosphocreatine; **k)** unlabelled glucose; **L)** [1-¹³C]glucose; **m)** fumarate standard; **n)** pyrazine standard.

4.2.1. Supra-physiological saturating levels of glucose and 3-β hydroxybutyrate in hippocampus: 5mM glucose, 1/0.1mM lactate/pyruvate ±5mM 3HB

All metabolites were efficiently uptaken and retained in the cells (Fig.4.10). We can also infer glycolytic contributions to total lactate pool, as [3-^{13}C]lactate is only produced by the breakdown of [1-^{13}C]glucose. The breakdown of one molecule of [1-^{13}C]glucose originates one [3-^{13}C]lactate and one unlabeled lactate (Fig.3.3, page 34), so the actual contribution of glycolytic lactate pool is the value represented in the graphic. The bars represented as "unlabeled endogenous lactate" are also corrected for this contribution. The glycolytic contribution to the lactate pool did not change significantly between the two conditions, with (mean± SEM) 57±8% contribution in the presence of 3HB and 57±6% in the absence of the ketone body. A residual amount of unlabeled glucose representing the 1% unlabeled fraction in the 99%-enriched commercial [1-^{13}C]glucose and/or incomplete washout of unlabeled glucose from the preceding stabilization solutions.

Different metabolites and their isotopomers present in PCA extracts

a)

b)

c)
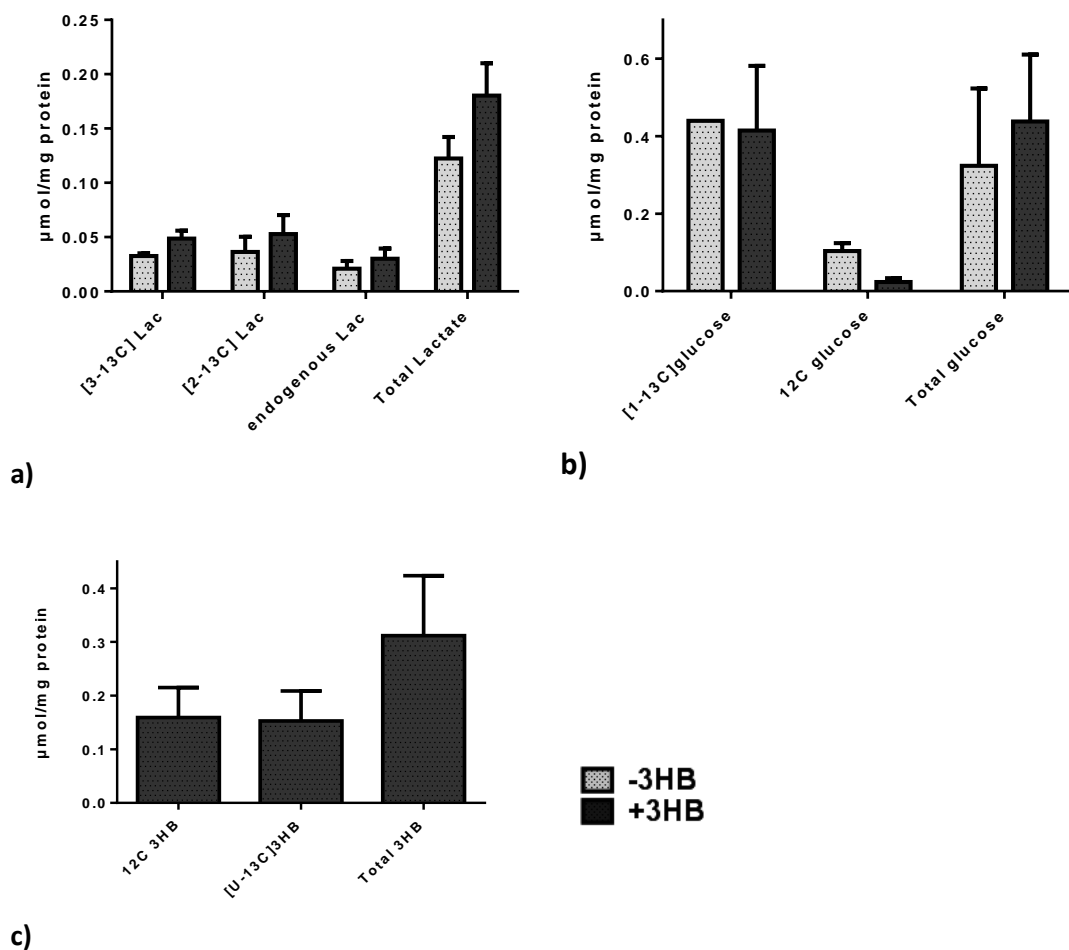
Fig.4.10 Different substrates isotopomers observed by ^{1}H NMR analysis of tissue extracts of slices superfused with 5mM [1-^{13}C]glucose, 1/0.1mM [2-^{13}C]lactate/pyruvate ± 5mM [U-^{13}C]3HB.
a) lactate; **b)** glucose; **c)** 3-hydroxybutyrate. Values are presented as mean±SEM of the results obtained from 5 independent experiments.

Of note, not all substrates were found in all extracts. For example, NAA (see Fig.4.11) was only found in 3 sets of experiments (and in those, both in -3HB and +3HB groups) and glucose was sometimes absent from some extracts. One possible explanation for this would be the extraction method used; PCA at 7% drops the pH to levels close to 0. This acidic environment for a considerable period of time like the one used (aprox.30minutes) may result in degradation of some of these compounds. In some cases, glucose signals were buried in the water peak (at 4.8ppm) and also suffer the effect spectral artifacts arising from the ^{1}H NMR water suppression procedure, making their quantification more unreliable.

Cell activity markers: NAA, total creatine and lactate/alanine ratio of PCA tissue extracts
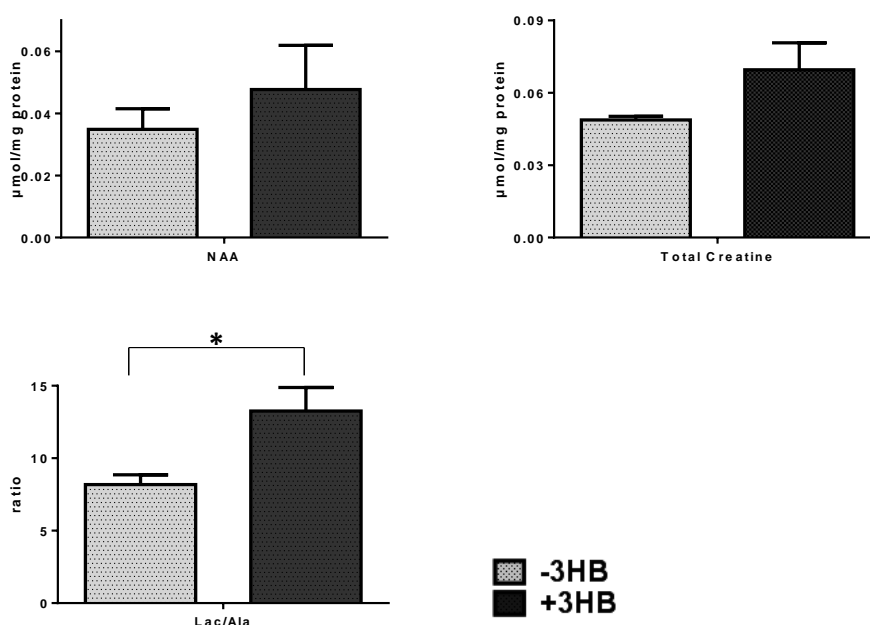
Fig.4.11 Quantification of NAA, total creatine and lactate/alanine ratio (*p<0.05, multiple t-tests) from tissue extracts of slices superfused with 5mM [1^{13}C]glucose, 1/0.1mM [2-^{13}C]lactate/pyruvate ± 5mM [U-^{13}C]3HB. Values are presented as mean±SEM of the results obtained from 3 independent experiments for NAA and 4 independent experiments for total creatine and lac/ala ratio.

The neuronal marker NAA showed no significant changes between conditions, and total creatine levels also showed no alterations (Fig.4.11). We did not observe any labeled NAA, in agreement with previous reports of NAA being a pool that does not exchange with other cell metabolites over the timeframe of the experiment (Lapidots & Gopher 1994). We were not able to measure metabolic energy indicators such as PCre/ATP and ATP/ADP, due to technical difficulties in acquiring ^{31}P spectra. PCre/Cre was theoretically possible to measure by ^{1}H, but the spectral resolution was insufficient to distinguish both signals separately, as they resonate too close to each other (3.0360ppm for creatine and 3.0280ppm for phosphocreatine) (Duarte et al. 2007; Govindaraju et al. 2000).

Pyruvate and lactate reflect the cytosolic redox state, and their ratio is usually found to be around 1:10, but may be as low as 1:50 (Barros 2013). Lactate dehydrogenase (LDH) is an enzyme that regulates lactate and pyruvate in a manner to reflect the cytosolic pair NADH/NAD$^+$ (eq 5, where K is the equilibrium constant of PDH and [H$^+$] is the cytosolic proton concentration). Alanine is in close equilibrium with pyruvate and often substitutes pyruvate in the equation, as alanine has a defined isolated resonance in the ^{1}H, unlike pyruvate that is usually buried under glucose peaks (Cruz et al. 2001; Ben-Yoseph et al. 1993; Duarte et al. 2007; Alves et al. 2011).

$$\frac{[Lac]}{[Pyr]} = \frac{[NADH]}{[NAD^+]}.K.[H^+]$$ **(eq5)**

This ratio was slightly increased in the +3HB group, when comparing to the -3HB condition (Fig.4.11, *p<0.05). This increased ratio reflects a more reduced redox cytosolic environment within the cells, resulting from increased NADH availability from increased glycolytic production (Cruz et al. 2001). These results are in agreement with the literature that shows ketone bodies to be effective anti-oxidants (Veech et al. 2001; Cheng et al. 2009).

As was mentioned, alanine is usually in close isotopomer equilibrium with pyruvate. In the ^{13}C spectra, a small amount of [3-^{13}C]alanine was observed, as well as a very small amount of [2-^{13}C]alanine. In the ^{1}H spectra, the signal-to-noise resolution is too low for any isotopomers quantification.

4.2.2. Regional metabolism of 2mM glucose, 1/0.1mM lac/pyr ± 1.7mM 3-hydroxybutyrate

In Fig.4.12 are represented the lactate and 3HB isotopomers quantified from tissue extracts of hippocampus, cortex and striatum slices superfused in 2mM [1-^{13}C]glucose, 1/0.1mM [2-^{13}C]lac/pyr, ± 1.7mM [U-^{13}C]3HB at recirculating conditions, and for hippocampus slices at non-recirculating conditions. As was observed before, we can see that all labeled substrates are efficiently taken up by the cells. In some extracts, some metabolites were unmeasurable and repetition of this protocol is likely to supply the missing data.

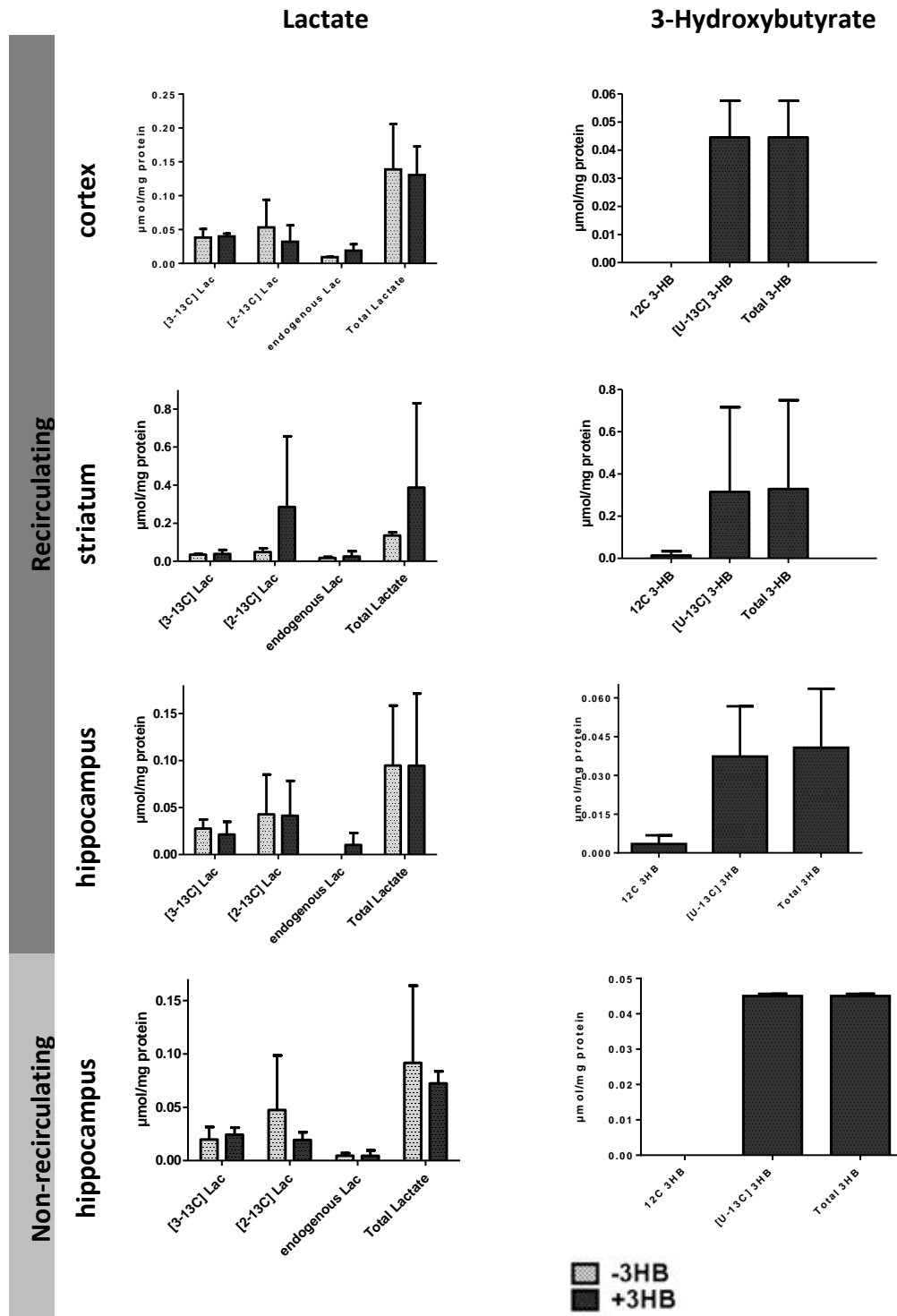# Different metabolites and their isotopomers present in PCA extracts

Fig.4.12 Substrate isotopomers observed by ^{1}H NMR analysis of tissue extracts of slices from WT wistar rats. Slices were superfused with 2mM [1-^{13}C]glucose, 1/0.1mM [2-^{13}C]lac/pyr, ± 1.7mM [U-^{13}C]3HB at either recirculating or non-recirculating conditions. Values are presented as mean±SD of the results obtained from 2 independent experiments.

Fig.4.13 shows the quantification of NAA, total creatine and the lactate/alanine ratio from tissue extracts of hippocampus, cortex and striatum slices superfused in 2mM [1-^{13}C]glucose, 1/0.1mM [2-^{13}C]lac/pyr, ± 1.7mM [U-^{13}C]3HB at recirculating conditions, and for hippocampus slices at non-recirculating conditions. The values are in accordance with the ones observed before.

Cell activity markers: NAA, total creatine and lactate/alanine ratio of PCA tissue extracts
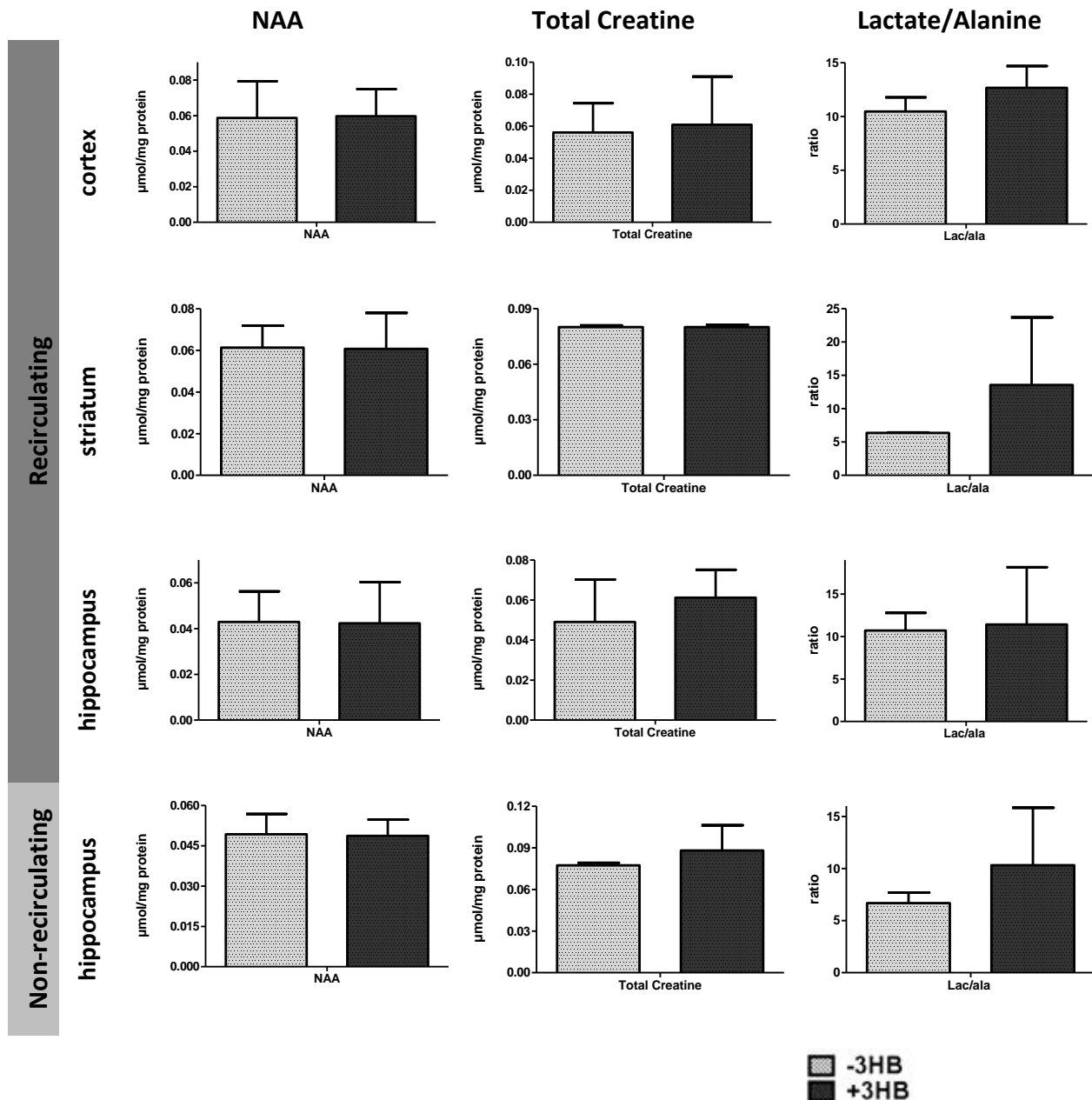
Fig.4.13 Quantification of NAA, total creatine and lac/ala ratio in tissue extracts of slices from WT Wistar rats. Slices were superfused with recirculating 2mM [1-^{13}C]glucose, 1/0.1mM [2-^{13}C]lac/pyr, ± 1.7mM [U-^{13}C]3HB (top 3 rows) and same concentrations put at non-recirculating conditions (bottom row). Values are presented as mean ± SD of the results obtained from 2 independent experiments.

4.2.3. Regional metabolism of a 6-OHDA rat model of Parkinson's disease

i)   Pilot study 1 – [U-^{13}C] Glucose (5mM) *vs* [3-^{13}C] Lactate (1mM)
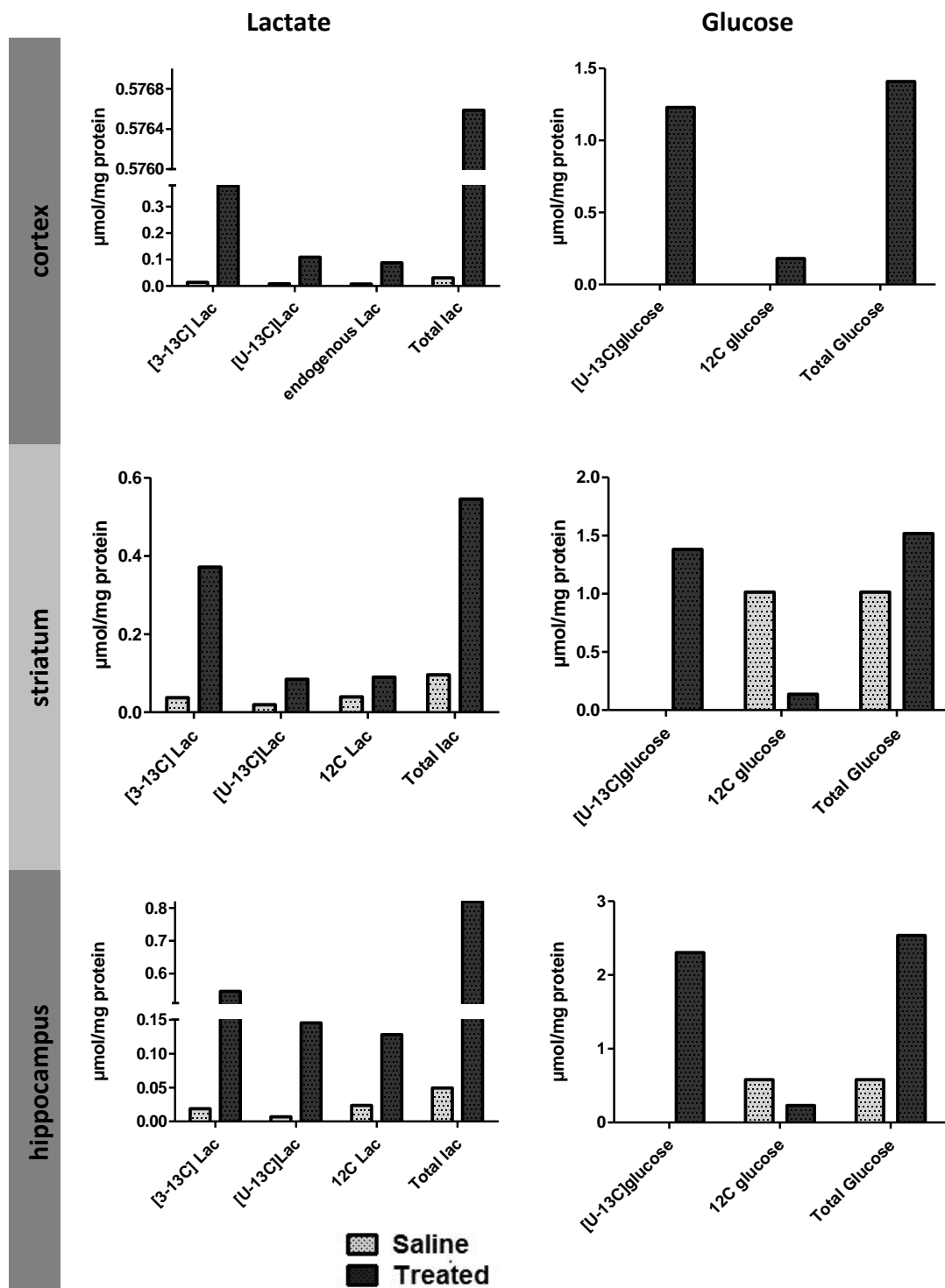

Fig.4.14 Substrate isotopomers observed by ^{1}H NMR analysis of tissue extracts of slices from the pre-sympotmatic 6-OHDA rats. Slices were superfused with recirculating 5mM [U-^{13}C]glucose, 1/0.1mM [3-^{13}C]lac/unlab.pyr. Presented values are from a single experimental procedure.

In Fig.4.14 are represented the various metabolites and their isotopomers quantified from tissue extracts of hippocampus, cortex and striatum slices from saline or 6-OHDA injected rats (treated) superfused in 5mM [U-^{13}C]glucose and 1/0.1mM [3-^{13}C]lac/unlabeled pyruvate. As was observed before, we can see that all labeled substrates are efficiently taken up by the cells. In some extracts, some metabolites could not be measured with adequate precision.

Cell activity markers: NAA and total creatine of PCA tissue extracts
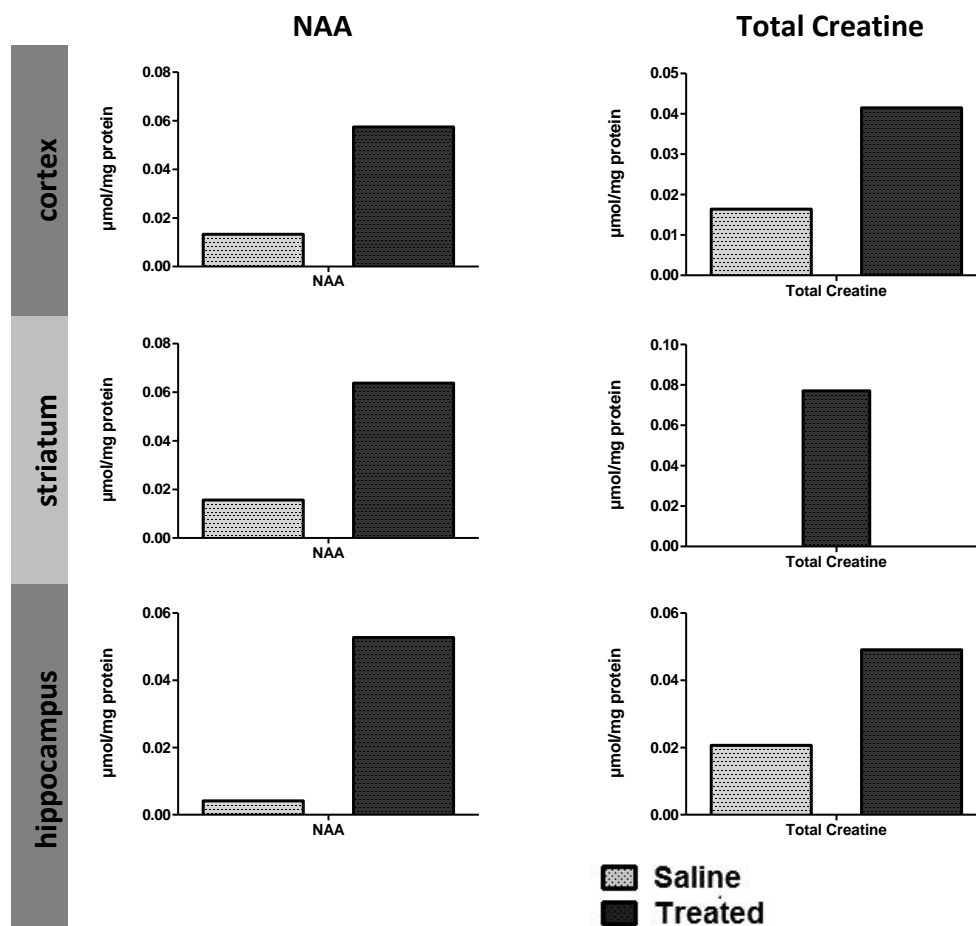
Fig.4.15 Quantification of NAA and total creatine in tissue extracts of slices from the pre-sympotmatic 6-OHDA rats. Slices were superfused with recirculating 5mM [U-^{13}C]glucose, 1/0.1mM [3-^{13}C]lac/unlabeled pyruvate. Presented values are from a single experimental procedure.

The quantification of the cell activity markers NAA and total creatine in both the 6-OHDA PD model pilot studies (Fig.4.15 and Fig.4.17) were very difficult in these samples as these spectra exhibited a particularly poor signal-to-noise ratio and were more contaminated. In fact, some markers (for example, total creatine in the saline-injected striatum) were not possible at all to quantify as it overlap with some contaminant that obliterated the signal. Alanine was also particularly difficult to quantify, translating in low precision and high uncertainties in estimates of

the lac/ala ratio (not shown). As these were pilot samples with n=1 and n=2, no attempt conclusions could be taken from these measurements, except that these molecules were present.

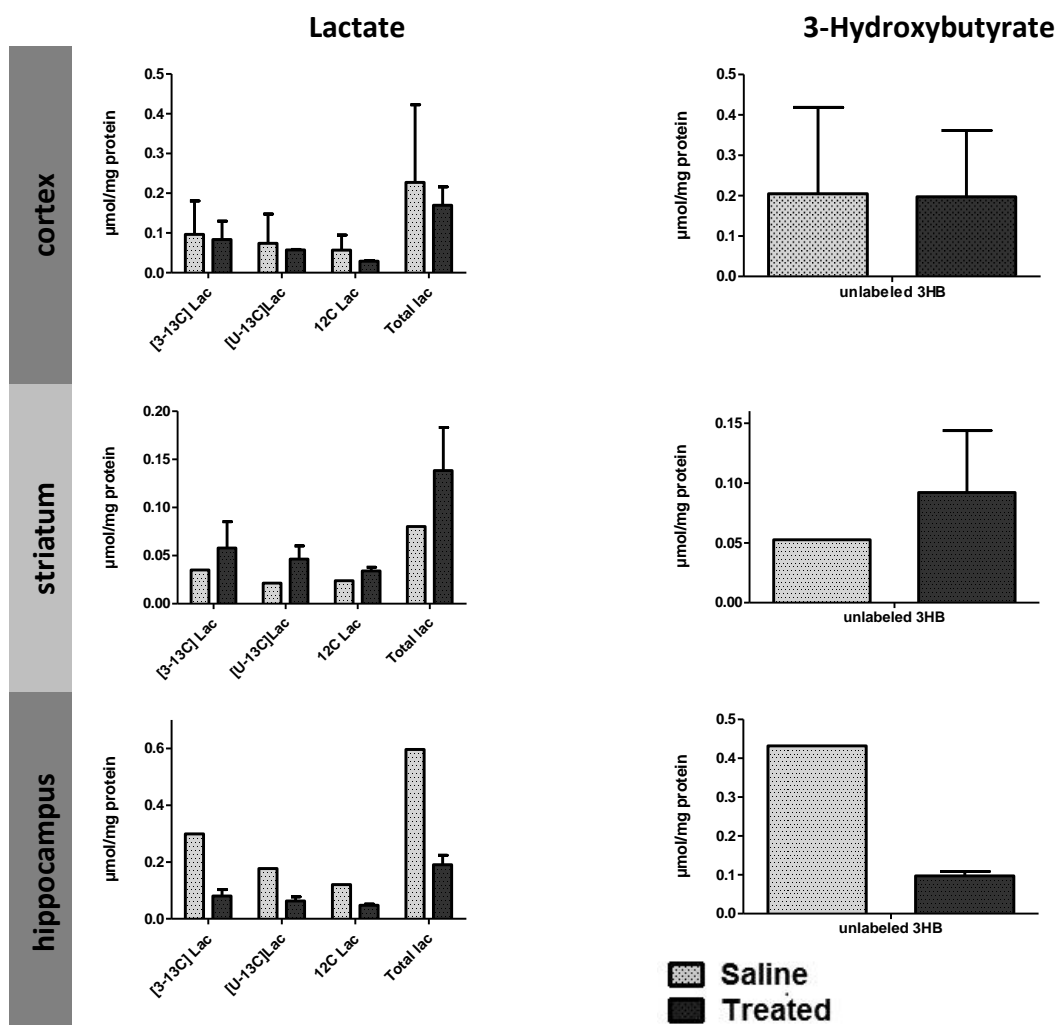ii) **Pilot study 2 – [U-13C]glucose (5mM) *vs* [3-13C]lactate (1mM) *vs* unlabeled 3HB (5mM)**

Fig.4.16 Different substrates isotopomers observed by ^{1}H NMR analysis of tissue extracts of slices from the pre-sympotmatic 6-OHDA rats. Slices were superfused with recirculating 5mM [U-13C]glucose, 1/0.1mM [3-13C]lac/unlab.pyr, 5mM unlab.3HB. Values are presented as mean±SD of the results obtained from 2 independent experiments for cortex (both saline and treated), treated striatum and treated hippocampus and for 1 experiment for saline striatum and saline hippocampus.

In Fig.4.16 are represented the various metabolites and their isotopomers quantified from tissue extracts of hippocampus, cortex and striatum slices from saline or 6-OHDA injected rats (treated) superfused in 5mM [U-^{13}C]glucose, 1/0.1mM [3-^{13}C]lac/unlabeled pyruvate and 5mM unlabeled 3HB. As in the previous pilot, quantification of some metabolite signals such as alanine was imprecise because of low signal-to-noise.
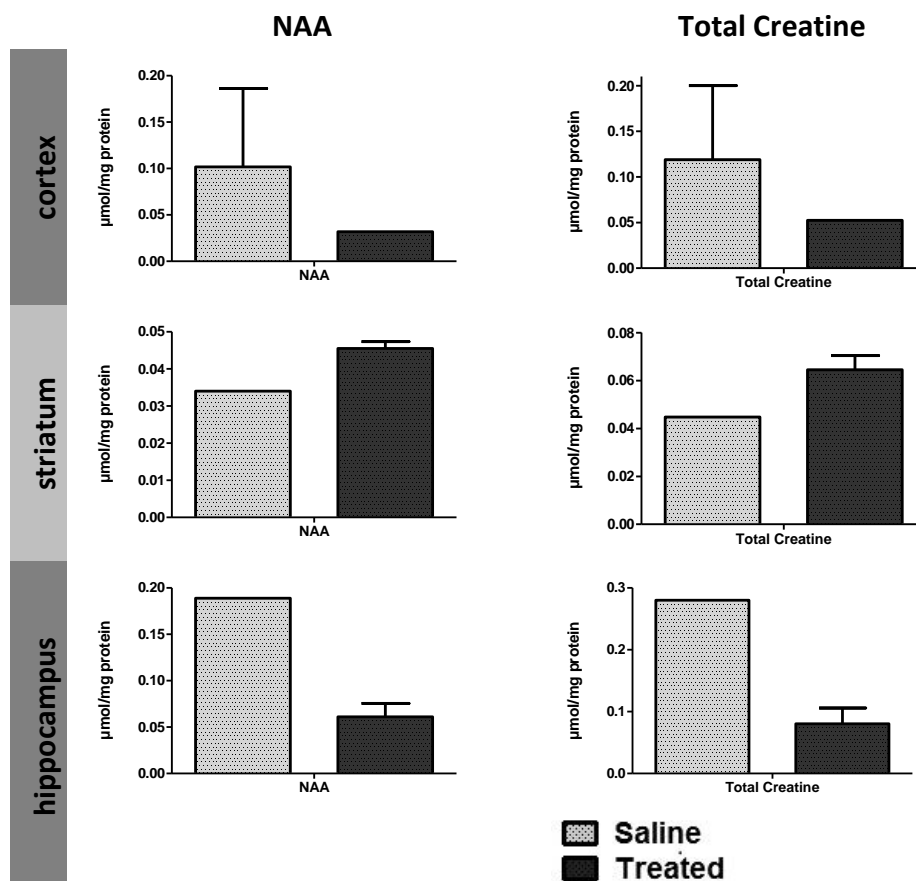
Cell activity markers: NAA and total creatine of PCA tissue extracts

Fig.4.17 Quantification of NAA and total creatine in tissue extracts of slices from the pre-sympotmatic 6-OHDA rats. Slices were superfused with recirculating 5mM [U-^{13}C]glucose, 1/0.1mM [3-^{13}C]lac/unlab.pyr, 5mM unlab.3HB. Values are presented as mean±SD of the results obtained from 2 independent experiments for cortex (both saline and treated), treated striatum and treated hippocampus and for 1 experiment for saline striatum and saline hippocampus.

4.3. ¹H analysis of superfusates

Samples from the superfusate coming out of the slice chambers were collected every 30minutes (Fig.3.1 page 30 and Fig.4.18, below) to quantify the output of metabolites over time. The ¹H NMR spectra of the superfusating medium allows us to analyze most metabolites being output and not just the ones we were expecting. We scanned these spectra for molecules like alanine and NAA, which are typically intracellular and are not expected to appear in the extracellular medium in measurable amounts. The appearance of these molecules in the superfusate would be taken as a signal of cell disrupture and of loss of tissue integrity.
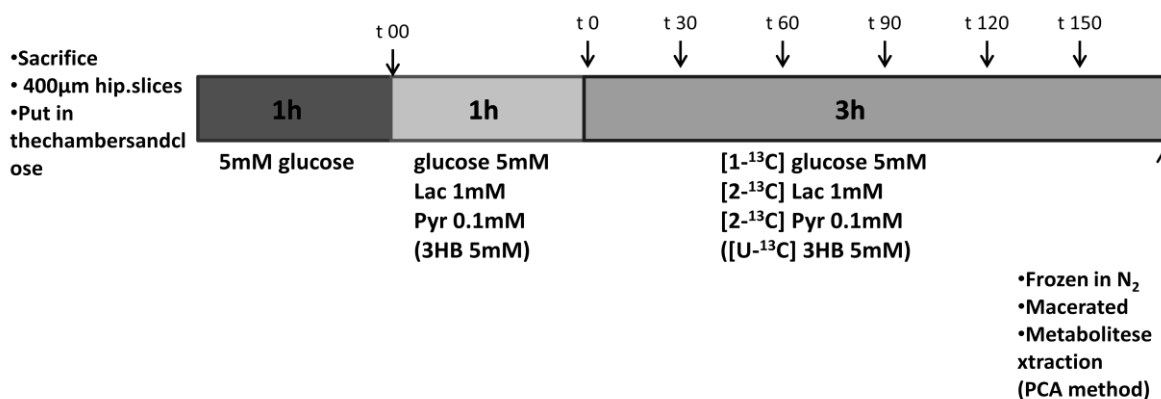

Fig.4.18 Schematic representation of the experimental timeline, with the timepoints of superfusate collection.

4.3.1. Supra-physiological saturating levels of glucose and 3-β hydroxybutyrate in hippocampus: 5mM glucose, 1/0.1mM lactate/pyruvate ± 5mM 3HB

In all the timepoint spectra for all the experiments performed, neither alanine nor NAA were observed, suggesting the conditions provided (temperature, oxygen, pH, energetic substrates) were sufficient to keep functional activity of the slices. In some samples from the end of the "recovery period" (timepoint 00 in Fig.4.18), small peaks in the region of alanine and/or NAA would appear, but would disappear throughout the experiment. We consider this to be normal as the slicing process causes some cell damage, but the analysis of the remaining timepoints reveals that this was not a systemic problem, and the death of some cells did not compromise the activity of the remaining ones.

At the end of the recovery period (Fig.4.18, timepoint 00), when the slices only had contact with the ACSF medium containing 5mM glucose, and before the new solution was added (5mMglucose + 1/0.1mM lac/pyr ± 5mM 3HB), one sample was taken from the superfusate and analyzed by ¹H NMR (Fig.4.19a). The purpose of this sample was to evaluate the uptake of glucose in this recovery.
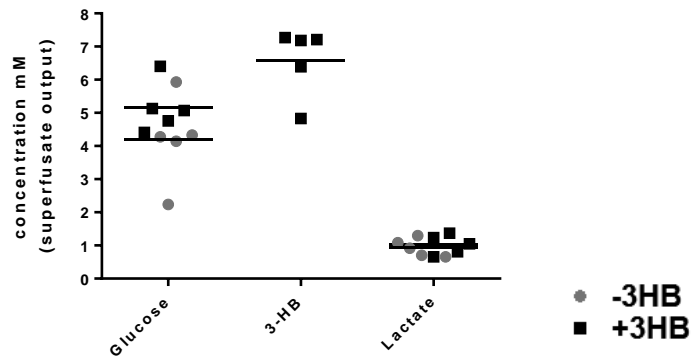
Substrate concentration at the first and last time-points

Substrate concentration after recovery period
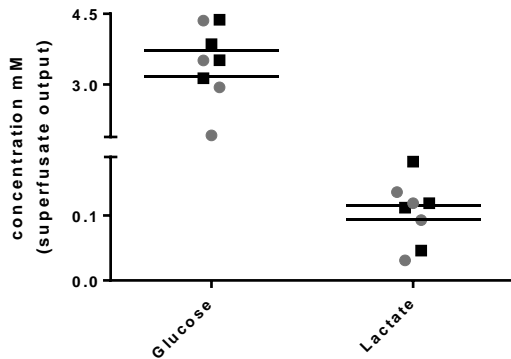
Substrate concentration at timepoint "150 minutes"

a)

b)

Fig.4.19 a) Glucose and lactate concentrations in the medium after the recovery period of 1 hour (ACSF with 5mM glucose) and before the new substrates are introduced (lactate, pyruvate ± 3-hydroxybutyrate). **b)** Substrate concentrations in the medium after the slices being in contact with the labeled substrates for 150 minutes. Each dot corresponds to an independent experiment (with *vs* without 3HB) of 4 independent experiments.

From Fig.4.19a) we can conclude that there is a significant uptake of glucose from the medium for the recovery of the slices, as the initial glucose concentration given was 5mM and after 1hour it can decrease to as low as 2mM. As such, for all the experiments, even the ones at low glucose concentration (2mM, see point 3.2.2) the recovery solution will always contain 5mM glucose, as a lower concentration might compromise the viability of the slices at later times. Not surprisingly, there is also some output of lactate; since this superfusing solution has only glucose, this lactate is originated from the cells, indicating an active glycolytic pathway.

As was mentioned before, the high concentrations of glucose and 3HB given relate to the recirculating nature of the experiment, and the need for the continuous saturation of the transporters over time, which would not be achieved if there was depletion in substrate availability. The ^{1}H analysis of the last timepoint collected, 150minutes after the labeled substrates are introduced (Fig.4.19b) shows that all substrates are still at saturating levels at this time.

Lactate isotopomers output in the superfusate of hippocampal slices superfusated at supra-physiological saturating conditions
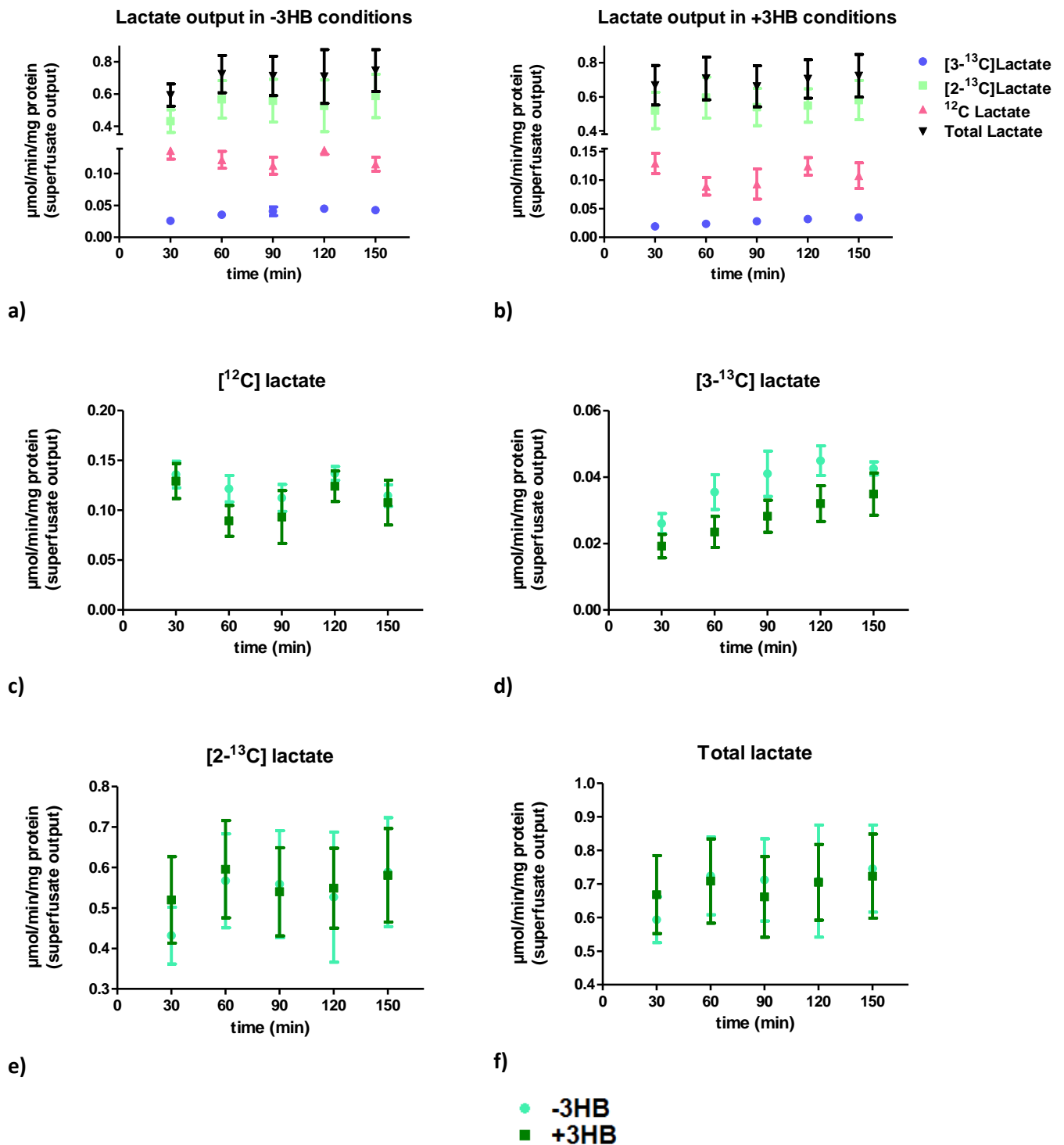

Fig.4.20 Comparison of output over time of lactate isotopomers of hippocampal slices superfused with 5mM glucose, 1/0.1mM lactate/pyruvate in the absence (-3HB) and presence (+3HB) of 5mM 3-Hydroxybutyrate. **a)** all isotopomers output in -3HB conditions; **b)** all isotopomers output in +3HB conditions; **c)** comparison of endogenous and unlabeled sources (12C) in both conditions, **d)** comparison of [3-^{13}C]lactate output in both conditions, **e)** comparison of [2-^{13}C]lactate in both conditions **f)** comparison of total lactate in both conditions. Values are presented as mean±SEM for 5 individual experiments.

Fig.4.20 shows the correlation of lactate isotopomers output over time. [3-^{13}C]lactate output was lower in the presence of 3HB comparing to the control (-3HB) conditions at all timepoints, supporting the idea that 3HB inhibited glycolysis upstream of PDH. This analysis should not be used for quantification of output metabolites purposes, since the recirculating conditions induce an accumulation of metabolites that is not negligible as is shown in Fig.4.25 (page 69).

Amongst the expected metabolites (lactate, glucose, etc) in the medium, we observed a peak at 1.92ppm, consistent with theCH₃ resonance of acetate (Fig.4.21). This peak also had two satellites (J=~7Hz) consistent with the signal from labeled ^{13}C in C1 ([2]J$_{C-H}$), and two other satellites (J=~127Hz) consistent with signal from labeled ^{13}C of C2 ([1]J$_{C-H}$). In experiments with [U-^{13}C]3HB, no signals corresponding to [U-^{13}C]acetate were ever observed, indicating that the origin of the acetate isotopomers did not include the acetyl-coA pool that was fed by 3HB (Fig.4.21b).
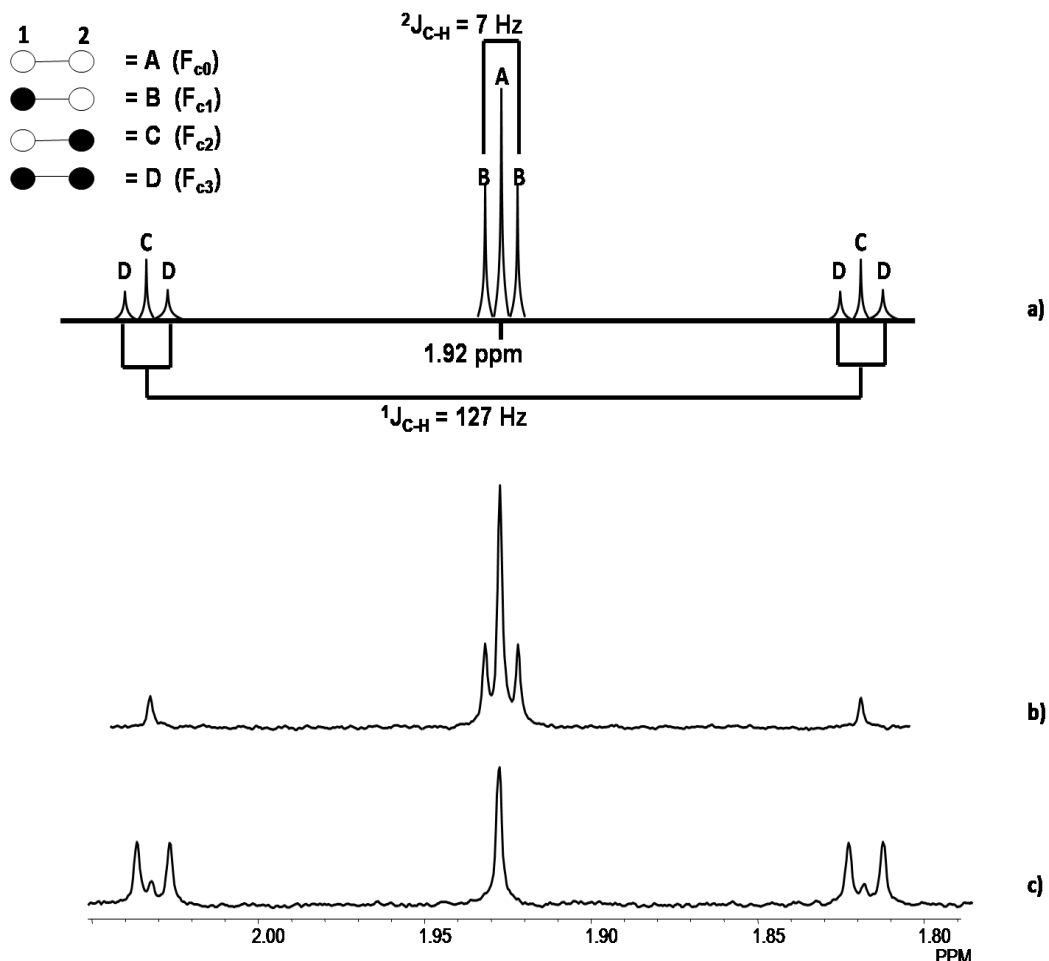

Fig.4.21 ^{1}H spectra close-up on the acetate region. **a)** schematic representation of different expected labels and their correspondence to acetyl-coA label (Fc0, Fc1, Fc2 or Fc3). **b)** example of a[1]H spectrum from slices superfused with [1-^{13}C]glucose, [2-^{13}C]lactate/pyruvate and [U-^{13}C]3HB. **c)** example of a ^{1}H spectrum from slices of rats injected with 6-OHDA/saline superfused with [U-^{13}C]glucose, and [3-^{13}C]lactate/pyruvate.

Acetate has long been known to be a selective substrate for astrocytes and has been used extensively as a substrate to distinguish astrocytic from neural metabolism (Badar-Goffer et al. 1990; Cerdan et al. 1990; Beckmann et al. 1995; Zwingmann & Leibfritz 2003; Melø et al. 2006; Duarte et al. 2007). However, no acetate was used as an exogenous substrate in this work, so its appearance (and labeling) means that it was produced by the tissue (Fig.4.22).
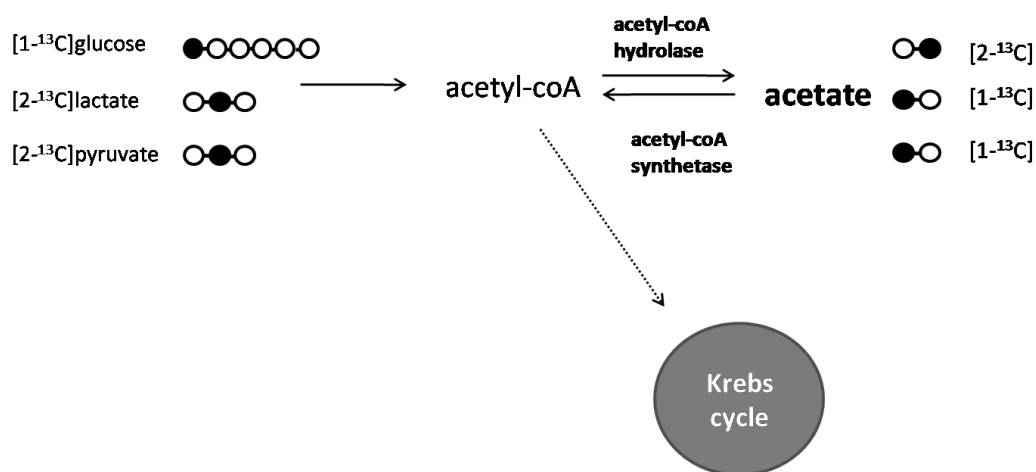

Fig.4.22 Acetate isotopomer synthesis from lactate/pyruvate and glucose precursors.

We only observe labeling from cytosolic substrates, i.e., there is some contribution of [1-^{13}C]glucose to [2-^{13}C]acetate, and a significant contribution of [2-^{13}C]lactate/pyruvate to [1-^{13}C]acetate, but no contribution from [U-^{13}C]3HB, as no [U-^{13}C]acetate is observed (Fig.4.21b). This is also in agreement with Rae and colleges' findings, as they have shown that pyruvate is the main contributor for acetate formation (Rae et al. 2012). We therefore concluded that acetate can be produced from glucose-, lactate- and pyruvate-derived acetyl-coA via acetyl-coA hydrolase (Fig.4.22). The cytosolic isoform of the counterpart enzyme of this reaction (acetyl-coA synthetase -AceSS1), which is responsible for the production of acetyl-coA for fatty acid synthesis, is found in all brain regions. The mitochondrial isoform of acetyl-coA synthetase (AceSS2) exists in very low amounts in the brain (Rae et al. 2012).

Further confirmation of the acetate isotopomer signals was provided from superfusion experiments using [U-^{13}C]glucose and [3-^{13}C]lactate, where the predicted [U-^{13}C]acetate and [2-^{13}C]acetate products were observed (Fig.4.21c).

4.3.2. Regional metabolism of 2mM glucose, 1/0.1mM lac/pyr ± 1.7mM 3-hydroxybutyrate

Fig.4.23 shows glucose and lactate concentrations after recovery period for all 3 structures studied. As expected, for some experiments the consumption of glucose was considerable. As before, lactate was observed after this recovery period and within the same range.
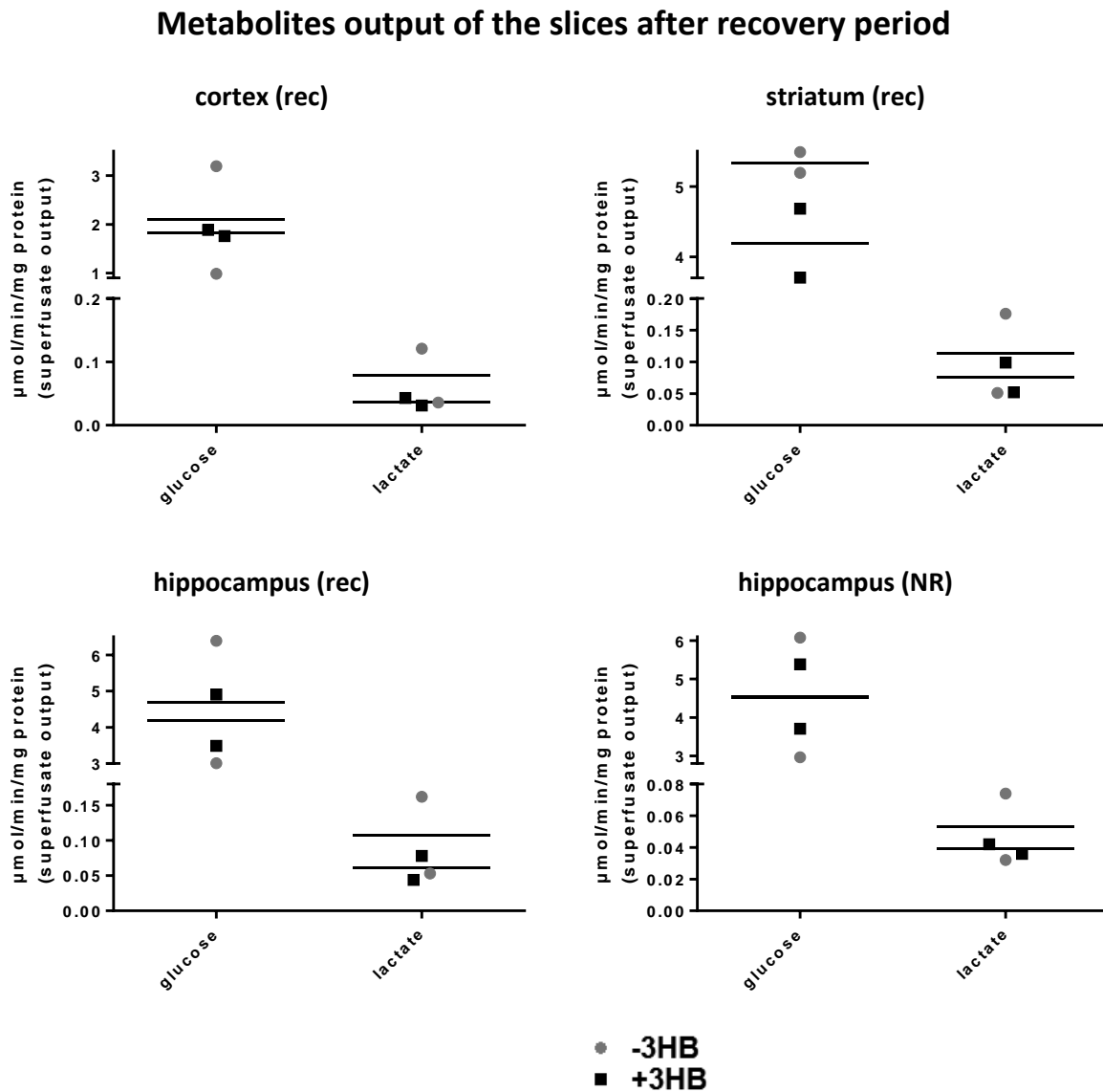

Fig.4.23 Glucose and lactate concentrations in the medium after the recovery period of 1hour (ACSF with 5mM glucose) and before the new substrates are introduced (lactate, pyruvate ± 3-hydroxybutyrate). Each point corresponds to an independent experiment (with *vs* without 3HB) of 2 independent experiments.

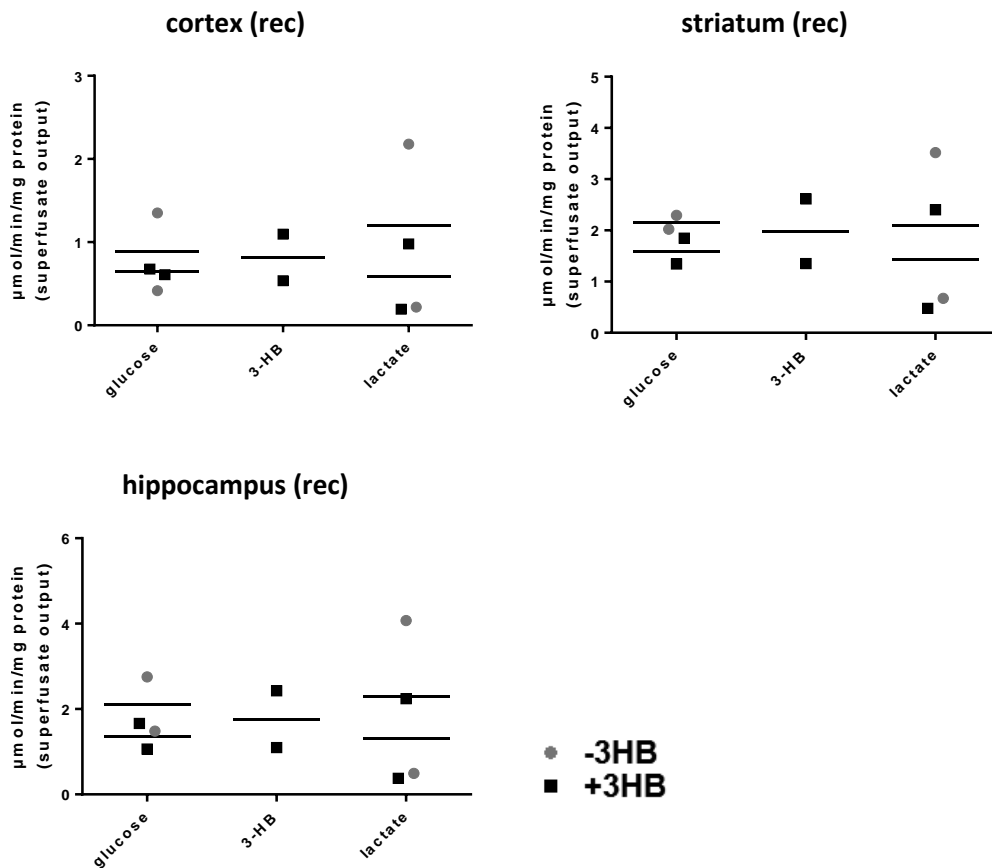## Substrate concentration at timepoint "150min"

Fig.4.24 Substrate concentrations in the medium after the slices being in contact with the labeled substrates for 150minutes in recirculating (rec) conditions. Each point corresponds to an independent experiment (with *vs* without 3HB) of 2 independent experiments.

The analysis of the superfusate after 150 minutes of re-circulating superfusion with the labeled metabolites (Fig.4.24) shows that while there was a tendency for starting substrate concentrations to be lower at 150 min compared to 0 min, they were nevertheless sufficient to maintain tissue viability. Lactate and acetate formation was also quantified (Fig.4.25) under both circulating and non-recirculating conditions.

Comparison of hippocampal slices output of lactate and acetate over time in recirculating and non-recirculating conditions
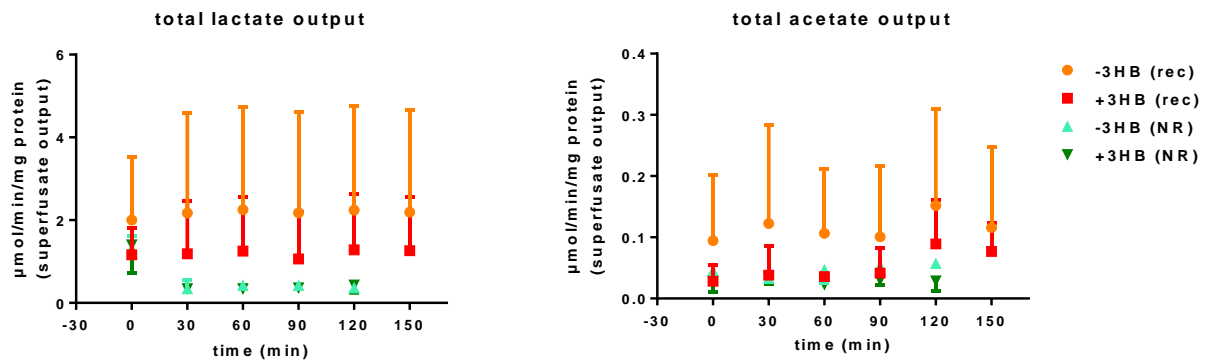

Fig.4.25 Comparison of output over time of total lactate and acetate for recirculating (rec) and non-recirculating (NR) conditions, for hippocampal slices superfused with 2mM glucose, 1/0.1mM lactate/pyruvate in the absence (-3HB) and presence (+3HB) of 3-hydroxybutyrate. Values are presented as mean±SD for 2 individual experiments.

Although highly preliminary with only two replicates, we estimate that under recirculating conditions, the cumulative amount of acetate that was secreted was about 5% that of lactate (i.e. approximately 0.1 versus 2.0 µmol/min/mg tissue protein.

Total lactate output increased over time indicating that overall, more lactate was secreted into the medium than was taken up and oxidized by the tissue (Fig.4.26d). Levels of [2-^{13}C]lactate (Fig.4.26c) remained constant while unlabeled and endogenous sources (Fig.4.26a) decreased over time, possibly due to a more effective washout under non-recirculating conditions. The amount of [3-^{13}C]lactate (Fig.4.26b) resulting from the breakdown of [1-^{13}C]glucose appeared to be greater in the absence than in the presence of 1.7 mM 3HB.

Lactate isotopomers output of hippocampal slices superfused in non-recirculating conditions

[¹²C] lactate   a)

[3-¹³C] lactate   b)

[2-¹³C] lactate   c)
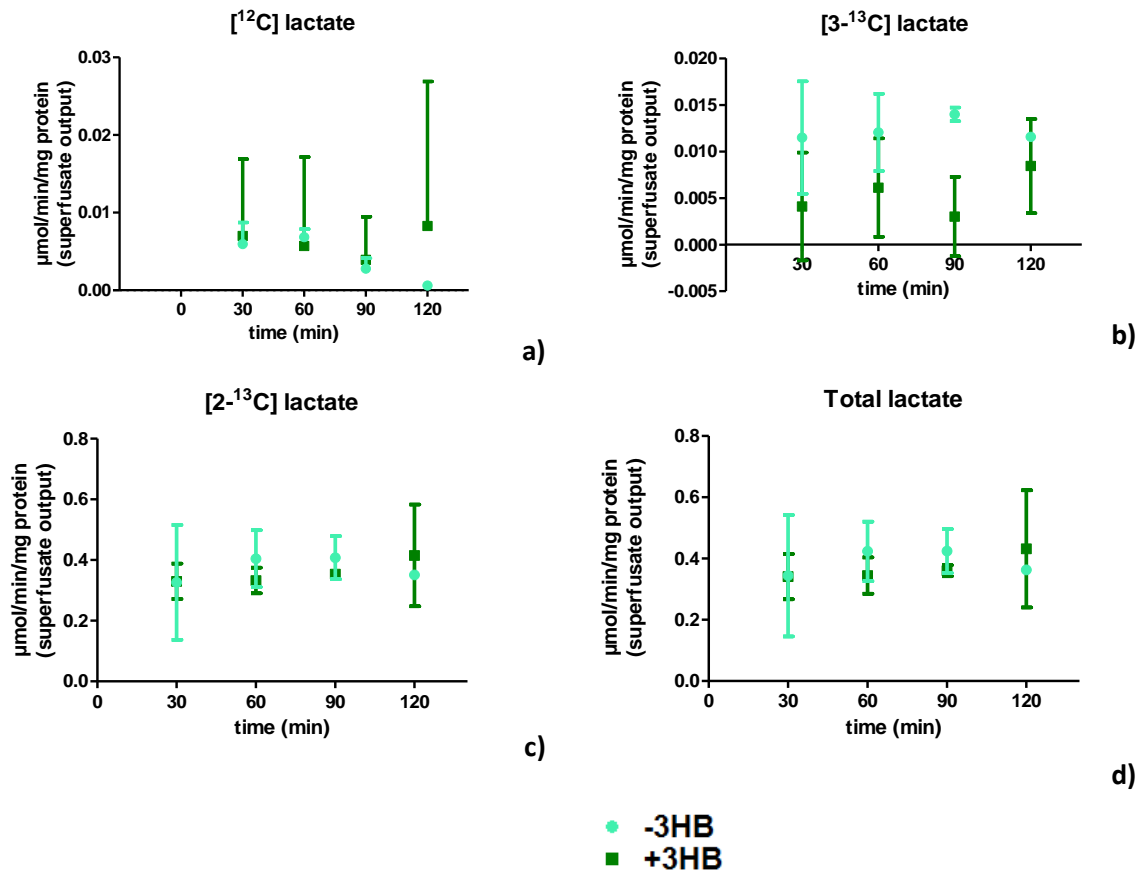
Total lactate   d)

● -3HB
■ +3HB

Fig.4.26 Comparison of output over time of lactate isotopomers for hippocampal slices superfused with 2mM glucose, 1/0.1mM lactate/pyruvate in the absence (-3HB) and presence (+3HB) of 3-hydroxybutyrate.
a) Endogenous and unlabeled sources, **b)** [3-¹³C]lactate, **c)** [2-¹³C]lactate, **d)** total lactate. Values are presented as mean±SD for 2 individual experiments

Both labeled and unlabeled acetate output showed a tendency to increase over time with the unlabeled isotopomer being the predominant species (Fig.4.27a,b). The production of [1-¹³C]acetate, presumably derived from [2-¹³C]lactate (see Fig.4.22, page 66), tended to be higher in the absence than in the presence of 3HB (Fig.4.27d). Meanwhile, levels of [2-¹³C]acetate, presumably derived from [1-¹³C]glucose via [3-¹³C]pyruvate were low, but detectable in experiments with recirculated medium while under non-recirculating conditions it was not detectable (Fig.4.28).

Acetate isotopomers output of hippocampal slices superfused in non-recirculating conditions
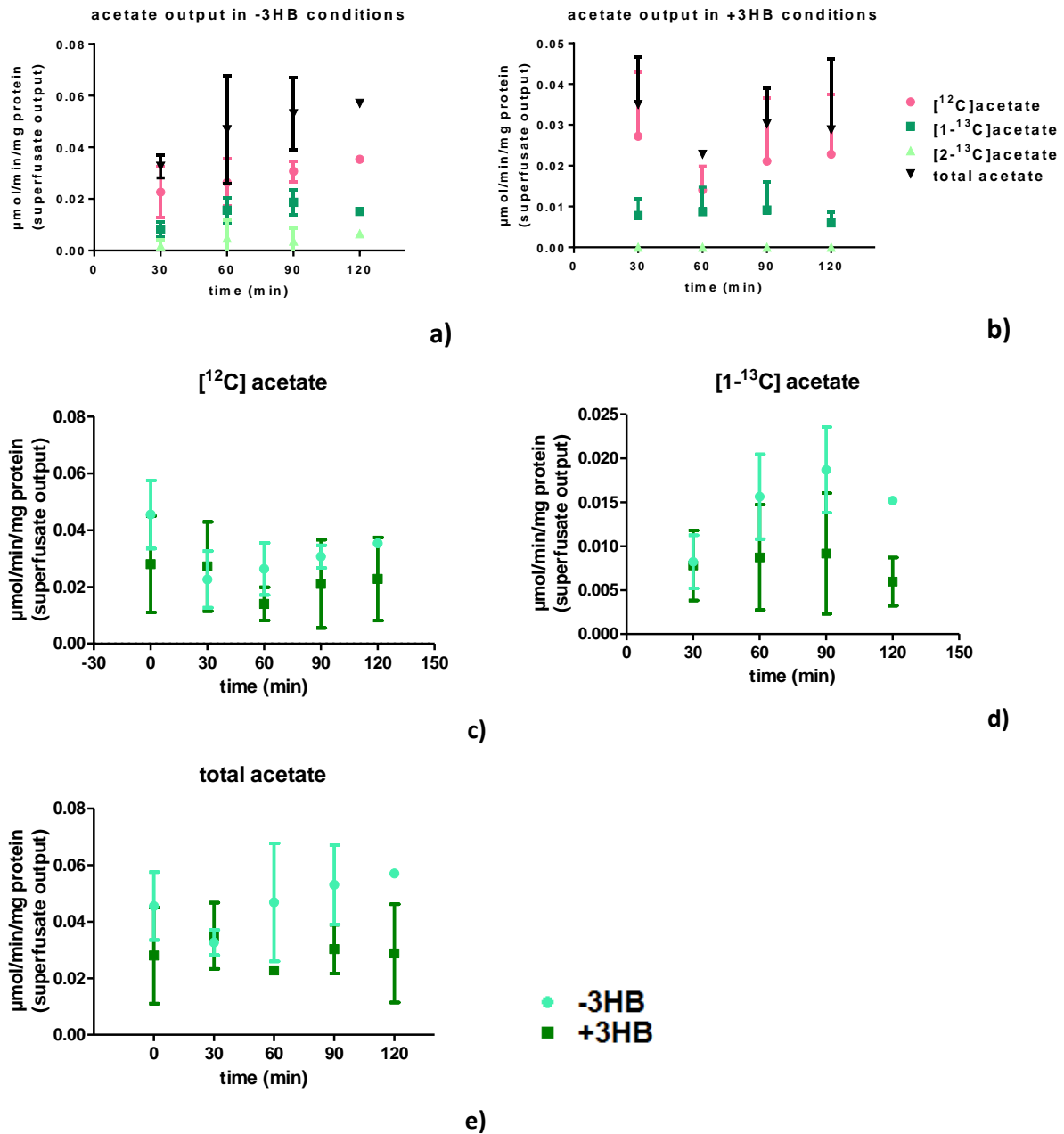

Fig.4.27 Comparison of output over time of acetate isotopomers of hippocampal slices superfused with 2mM glucose, 1/0.1mM lactate/pyruvate in the absence (-3HB) and presence (+3HB) of 3-hydroxybutyrate. **a)** all isotopomers output in -3HB conditions; **b)** all isotopomers output in +3HB conditions; **c)** comparison of endogenous and unlabeled sources (^{12}C) in both conditions, **d)** comparison of [1-^{13}C]acetate output in both conditions, **e)** comparison of total acetate in both conditions. Values are presented as mean±SD for 2 individual experiments

Comparison of hippocampal slices [2-^{13}C]Acetate output over time in recirculating and non-recirculating conditions
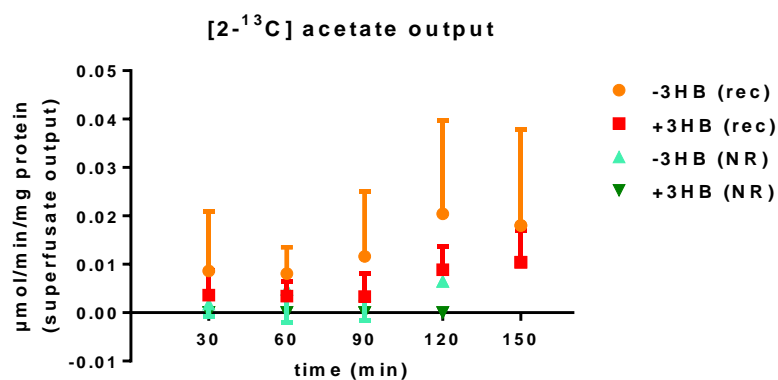

Fig.4.28 Comparison of output over time of [2-^{13}C]acetate for recirculating (rec) and non-recirculating (NR) conditions, for hippocampal slices superfused with 2mM glucose, 1/0.1mM lactate/pyruvate in the absence (-3HB) and presence (+3HB) of 3-hydroxybutyrate. Values are presented as mean±SD for 2 individual experiments

5. Concluding Remarks and Future Work

In conclusion, ketone bodies are an effective substrate for hippocampal oxidative metabolism and, surprisingly, seem to be preferred over glucose when both substrates are available becoming the major contributor for acetyl-coA formation as evaluated by Glutamate ^{13}C isotopomer analysis. They also seem to be more extensively metabolized by glutamatergic neurons than GABAergic neurons, suggesting a subtle but significant neuron-type compartmentation.

The significant output of acetate to the superfusing medium was a surprise by itself, and even more by the fact that it does not seem to be labeled by the ketone bodies at all. Furthermore, even though ketone bodies do not contribute to this acetate pool, their presence seems to downregulate acetate production. Acetyl-coA hydrolase is the most likely candidate for acetate formation, but the reasons for this high activity rate is yet to be determined.

The pilot studies with the pre-symptomatic PD model suggest that no changes occur at the metabolic flux and substrate selection. However, a more detailed study would be of use, namely exploring glutamate and GABA pool absolute quantification values, which may be altered. Some studies have suggested that the use of ketone bodies for PD patients relies more on their anti-oxidant properties rather than fuel properties, so an analysis exploring this hypothesis may shed some light on this matter.

A pressing issue is the increase of repetition of the experiments at physiological saturating conditions and at non-recirculating conditions, to achieve significance in any findings related to substrate selectivity at this concentrations and acetate output. An increase in the number of scans acquired of the ^{13}C NMR samples may also provide enough signal-to-noise ratio to better quantify GABA signaling, and to evaluate if any glutamine signals are visible, since it was oddly missing from our data.

Our findings may be useful for future applications of the ketogenic diet as a co-therapy for numerous neuronal and neurodegenerative diseases that compromise metabolic function, whether this aspect is a cause or a consequence of the disease.

References

Alves, M.G., Oliveira, P.J. & Carvalho, R. a, 2011. Substrate selection in hearts subjected to ischemia/reperfusion: role of cardioplegic solutions and gender. *NMR in biomedicine*, 24(9), pp.1029–37.

Bach, A. et al., 1977. Ketogenic Response to Medium-Chain Triglyceride Load in the Rat. *The Journal of Nutrition*, pp.1863–1870.

Badar-Goffer, R.S., Bachelard, H.S. & Morris, P.G., 1990. Cerebral metabolism of acetate and glucose studied by 13C-n . m . r . spectroscopy. *Biochemistry Journal*, 266, pp.133–139.

Barros, L.F., 2013. Metabolic signaling by lactate in the brain. *Trends in neurosciences*, 36(7), pp.396–404.

Bates, M.W., Krebs, H. a & Williamson, D.H., 1968. Turnover rates of ketone bodies in normal, starved and alloxan-diabetic rats. *The Biochemical journal*, 110(4), pp.655–61.

Beckmann, N. et al., 1995. *Carbon-13 NMR spectroscopy of Biological Systems* United Kin. N. Beckmann, ed., San Diego, California: Academic Press Limited.

Ben-Yoseph, O. et al., 1993. Glycerol 3-phosphate and lactate as indicators of the cerebral cytoplasmic redox state in severe and mild hypoxia respectively: a 13C- and 31P-n.m.r. study. *The Biochemical journal*, 291 Pt 3, pp.915–9.

Bergersen, L. et al., 2001. A novel postsynaptic density protein: the monocarboxylate transporter MCT2 is co-localized with δ-glutamate receptors in postsynaptic densities of parallel fiber-Purkinje cell synapses. *Experimental Brain Research*, 136(4), pp.523–534.

Bergersen, L., Rafiki, A. & Ottersen, O.P., 2002. Immunogold cytochemistry identifies specialized membrane domains for monocarboxylate transport in the central nervous system. *Neurochemical research*, 27(1-2), pp.89–96.

Bergersen, L.H., 2007. Is lactate food for neurons? Comparison of monocarboxylate transporter subtypes in brain and muscle. *Neuroscience*, 145(1), pp.11–9.

Bouzier, A.-K. et al., 2000. The metabolism of [3-(13)C]lactate in the rat brain is specific of a pyruvate carboxylase-deprived compartment.

Bouzier-Sore, A.-K. et al., 2002. Feeding active neurons: (re)emergence of a nursing role for astrocytes. *Journal of physiology, Paris*, 96(3-4), pp.273–82.

Cahill, G.F. & Aoki, T.T., 1980. Alternate fuel utilization by brain. In J. V. Passonneau et al., eds. *Cerebral metabolism and neuronal function*. Baltimore: Williams & Wilkins, pp. 234–42.

Carvalho, R. a et al., 1999. Multiple bond 13C-13C spin-spin coupling provides complementary information in a 13C NMR isotopomer analysis of glutamate. *Magnetic resonance in*

medicine : official journal of the Society of Magnetic Resonance in Medicine / Society of Magnetic Resonance in Medicine, 42(1), pp.197–200.

Castro, M.A. et al., 2009. A metabolic switch in brain: glucose and lactate metabolism modulation by ascorbic acid. *Journal of neurochemistry*, 110(2), pp.423–40.

Cerdan, S., Kunnecke, B. & Seelig, J., 1990. Cerebral Metabolism of [1 ,2-13C2] Acetate as Detected by in Vivo and in Vitro 13C NMR. *Journal of Biological Chemistry*, 265(22), pp.12916–12926.

Chassain, C. et al., 2005. Cerebral glutamate metabolism in Parkinson's disease: an in vivo dynamic (13)C NMS study in the rat. *Experimental neurology*, 191(2), pp.276–84.

Cheng, B. et al., 2009. Ketogenic diet protects dopaminergic neurons against 6-OHDA neurotoxicity via up-regulating glutathione in a rat model of Parkinson's disease. *Brain research*, 1286, pp.25–31.

Choi, I.-Y., Seaquist, E.R. & Gruetter, R., 2003. Effect of hypoglycemia on brain glycogen metabolism in vivo.

Chowdhury, G.M. et al., 2014. The contribution of ketone bodies to basal and activity-dependent neuronal oxidation in vivo. *Journal of cerebral blood flow and metabolism : official journal of the International Society of Cerebral Blood Flow and Metabolism*, 34(7), pp.1233–42..

Coles, L. et al., 2004. Exercise rapidly increases expression of the monocarboxylate transporters MCT1 and MCT4 in rat muscle. *The Journal of physiology*, 561(Pt 1), pp.253–61.

Cruz, F. et al., 2001. Intracellular Compartmentation of Pyruvate in Primary Cultures of Cortical Neurons As Detected by 13C NMR Spectroscopy With Multiple 13C Labels. *Journal of neuroscience research*, 781, pp.771–781.

Daikhin, Y. & Yudkoff, M., 1998. Ketone bodies and brain glutamate and GABA metabolism. *Developmental neuroscience*, 20(4-5), pp.358–64.

Dienel, G. a, 2012. Brain lactate metabolism: the discoveries and the controversies. *Journal of cerebral blood flow and metabolism : official journal of the International Society of Cerebral Blood Flow and Metabolism*, 32(7), pp.1107–38.

Duarte, J.M.N., Cunha, R. a & Carvalho, R. a, 2007. Different metabolism of glutamatergic and GABAergic compartments in superfused hippocampal slices characterized by nuclear magnetic resonance spectroscopy. *Neuroscience*, 144(4), pp.1305–13.

Erecińska, M. et al., 1996. Regulation of GABA level in rat brain synaptosomes: fluxes through enzymes of the GABA shunt and effects of glutamate, calcium, and ketone bodies. *Journal of neurochemistry*, 67(6), pp.2325–34.

Gamble, J.L., Ross, G.S. & Tisdall, F.F., 1923. THE METABOLISM OF FIXED BASE DURING FASTING. *The Journal of biological chemistry*, 57, pp.633–695.

Govindaraju, V., Young, K. & Maudsley, a a, 2000. Proton NMR chemical shifts and coupling constants for brain metabolites. *NMR in biomedicine*, 13(3), pp.129–53.

Greene, A.E. et al., 2001. Caloric restriction inhibits seizure susceptibility in epileptic EL mice by reducing blood glucose. *Epilepsia*, 42(11), pp.1371–8.

Gruetter, R., 2003. Glycogen: the forgotten cerebral energy store. *Journal of neuroscience research*, 74(2), pp.179–83.

Hallböök, T. et al., 2012. The effects of the ketogenic diet on behavior and cognition. *Epilepsy research*, 100(3), pp.304–9.

Hasebe, N. et al., 2010. Anticonvulsant effects of methyl ethyl ketone and diethyl ketone in several types of mouse seizure models. *European journal of pharmacology*, 642(1-3), pp.66–71.

Hashim, S.A. & Vanitallie, T.B., 2014. Ketone Body therapy: From the ketogenic Diet to the Oral Administration of Ketone Ester. *Journal of lipid research*, pp.1–35.

Hassel, B. & Bråthe, a, 2000. Cerebral metabolism of lactate in vivo: evidence for neuronal pyruvate carboxylation. *Journal of cerebral blood flow and metabolism : official journal of the International Society of Cerebral Blood Flow and Metabolism*, 20(2), pp.327–36.

Hattingen, E. et al., 2009. Phosphorus and proton magnetic resonance spectroscopy demonstrates mitochondrial dysfunction in early and advanced Parkinson's disease. *Brain : a journal of neurology*, 132(Pt 12), pp.3285–97.

Hawkins, R. a, Williamson, D.H. & Krebs, H. a, 1971. Ketone-body utilization by adult and suckling rat brain in vivo. *The Biochemical journal*, 122(1), pp.13–8.

Henderson, S.T., 2008. Ketone Bodies as a Therapeutic for Alzheimer ' s Disease. *The Journal of the American Society for Experimental NeuroTherapeutics*, 5(July), pp.470–480.

Henderson, S.T. & Poirier, J., 2011. Pharmacogenetic analysis of the effects of polymorphisms in APOE, IDE and IL1B on a ketone body based therapeutic on cognition in mild to moderate Alzheimer's disease; a randomized, double-blind, placebo-controlled study. *BMC medical genetics*, 12(1), p.137.

Hove, J.L.K. Van et al., 2003. D , L-3-hydroxybutyrate treatment of multiple acyl-CoA dehydrogenase deficiency (MADD). *Lancet*, 361, pp.1433–1435.

Jiang, L. et al., 2011. Cortical substrate oxidation during hyperketonemia in the fasted anesthetized rat in vivo. *Journal of cerebral blood flow and metabolism*, 31(12), pp.2313–23.

Johnson, R.E., Sargent, F.I. & Passmore, R., 1958. Normal Variantions in total Ketone Bodies in Serum and Urine of Healthy Young Men. *Journal of Experimental Phisiology*, (43), pp.339–344.

Kang, J.-Q. & Macdonald, R.L., 2009. Making sense of nonsense GABA(A) receptor mutations associated with genetic epilepsies. *Trends in molecular medicine*, 15(9), pp.430–8.

Kashiwaya, Y. et al., 2000. D-B-Hydroxybutyrate protects neurons in models of Alzheimer's and Parkinson's disease. *Proceedings of the National Academy of Sciences of the United States of America*, 97(10), pp.5440–5444.

Kernig, K. et al., 2012. The afterhyperpolarizing potential following a train of action potentials is suppressed in an acute epilepsy model in the rat Cornu Ammonis 1 area. *Neuroscience*, 201, pp.288–96.

Kinsman, S.L. et al., 1992. Efficacy of the ketogenic diet for intractable seizure disorders: review of 58 cases. *Epilepsia*, 33(6), pp.1132–6.

Koper, J.W. et al., 1984. Acetoacetate and glucose as substrates for lipid synthesis by rat brain oligodendrocytes and astrocytes in serum-free culture. *Biochimica et biophysica acta*, 796, pp.20–26.

Kunnecke, B., Cerdan, S. & Seelig, J., 1993. Cerebral Metabolism of [1,2-13C2] Glucose and [U-13C4]3-Hydroxybutyrate in Rat Brain as Detected by 13C NMR Spectroscopy. *NMR in biomedicine*, 6(October 1992), pp.264–277.

Laffel, L., 1999. Ketone bodies: a review of physiology, pathophysiology and application of monitoring to diabetes. *Diabetes/metabolism research and reviews*, 15(6), pp.412–26.

LaManna, J.C. et al., 2009. Ketones supress brain glucose consumption P. Liss et al., eds. *Advances in Experimental Medicine and Biology*, 645, pp.301–306.

Lapidots, A. & Gopher, A., 1994. Cerebral metabolic compartmentation. Estimation of glucose flux via pyruvate carboxylase/pyruvate dehydrogenase by 13C NMR isotopomer analysis of D-[U-13C]glucose metabolites. *The Journal of biological chemistry*, 269, pp.27198–27208.

Leino, R.L. et al., 1997. Ultrastructural localization of GLUT 1 and GLUT 3 glucose transporters in rat brain. *Journal of neuroscience research*, 49(5), pp.617–26.

Lindon, J.C. et al., 2007. *Handbook of Metabonomics and Metabolomics* 1st editio. J. C. Lindon, J. K. Nicholson, & E. Holmes, eds., Oxford, UK.

Ma, W., Berg, J. & Yellen, G., 2007. Ketogenic diet metabolites reduce firing in central neurons by opening K ATP channels. *The Journal of neuroscience : the official journal of the Society for Neuroscience*, 27(14), pp.3618–25.

Malloy, C.R. et al., 1990. Contribution of exogenous substrates to acetyl coenzyme A: measurement by 13C NMR under non-steady-state conditions. *Biochemistry*, 29(29), pp.6756–61.

Marin-Valencia, I. et al., 2012. Glut1 deficiency (G1D): epilepsy and metabolic dysfunction in a mouse model of the most common human phenotype. *Neurobiology of disease*, 48(1), pp.92–101.

McNally, M. a & Hartman, A.L., 2012. Ketone bodies in epilepsy. *Journal of neurochemistry*, 121(1), pp.28–35.

Melø, T.M., Nehlig, A. & Sonnewald, U., 2006. Neuronal-glial interactions in rats fed a ketogenic diet. *Neurochemistry international*, 48(6-7), pp.498–507.

Owen, O.E. et al., 1967. Brain metabolism during fasting. *The Journal of clinical investigation*, 46(10), pp.1589–95.

Pan, J.W. et al., 2002. [2,4-13 C2]-β-Hydroxybutyrate Metabolism in Human Brain. *Journal of cerebral blood flow and metabolism*, 22(7), pp.890–898.

Patel, M.S. & Owen, O.E., 1976. Lipogenesis from Ketone Bodies in Rat Brain. Evidence for conversion of acetoacetate into acetyl-coenzyme A in the cytosol. *Biochemistry Jounal*, 156, pp.603–607.

Pellerin, L. et al., 2005. Cellular and subcellular distribution of monocarboxylate transporters in cultured brain cells and in the adult brain. *Journal of neuroscience research*, 79(1-2), pp.55–64.

Pellerin, L., 2010. Food for thought: the importance of glucose and other energy substrates for sustaining brain function under varying levels of activity. *Diabetes & metabolism*, 36 Suppl 3, pp.S59–63.

Pierre, K. & Pellerin, L., 2005. Monocarboxylate transporters in the central nervous system: distribution, regulation and function. *Journal of neurochemistry*, 94(1), pp.1–14.

Prins, M.L., 2008. Cerebral Metabolic Adaptation and Ketone Metabolism after Brain Injury. *Journal of cerebral blood flow and metabolism*, 28(1), pp.1–16.

Puchades, M. et al., 2013. Unaltered lactate and glucose transporter levels in the MPTP mouse model of Parkinson's disease. *Journal of Parkinson's disease*, 3(3), pp.371–85.

Puchowicz, M.A. et al., 2000. Dog model of therapeutic ketosis induced by oral administration of R,S-1,3-butanediol diacetoacetate. *Journal of Nutritional Biochemistry*, 11, pp.281–287.

Rae, C. et al., 2012. Metabolism, compartmentation, transport and production of acetate in the cortical brain tissue slice. *Neurochemical research*, 37(11), pp.2541–53.

Seymour, K.I. et al., 1999. Identification of Cerebral Acetone by 1H MRS in Patients with Seizures Controlled by Ketogenic Diet . *MAGMA*, (8), pp.33–42.

Silver, I. a & Erecińska, M., 1994. Extracellular glucose concentration in mammalian brain: continuous monitoring of changes during increased neuronal activity and upon limitation in oxygen supply in normo-, hypo-, and hyperglycemic animals. *The Journal of neuroscience : the official journal of the Society for Neuroscience*, 14(8), pp.5068–76.

Simpson, I. a, Carruthers, A. & Vannucci, S.J., 2007. Supply and demand in cerebral energy metabolism: the role of nutrient transporters. *Journal of cerebral blood flow and metabolism*, 27(11), pp.1766–1791.

Suzuki, M. et al., 2001. Effect of beta-hydroxybutyrate, a cerebral function improving agent, on cerebral hypoxia, anoxia and ischemia in mice and rats. *Japanese journal of pharmacology*, 87(2), pp.143–50.

Tadaiesky, M.T. et al., 2008. Emotional, cognitive and neurochemical alterations in a premotor stage model of Parkinson's disease. *Neuroscience*, 156(4), pp.830–40.

Thavendiranathan, P. et al., 2003. The effect of the "classic" ketogenic diet on animal seizure models. *Brain research*, 959(2), pp.206–13.

Thio, L.L., Wong, M. & Yamada, K. a., 2000. Ketone bodies do not directly alter excitatory or inhibitory hippocampal synaptic transmission. *Neurology*, 54(2), pp.325–325.

Vanitallie, T.B. & Nufert, T.H., 2003. Ketones : Metabolism ' s Ugly Duckling. *Nutrition Reviews*, 61(10), pp.327–341.

Vannucci, S.J. & Simpson, I. a, 2003. Developmental switch in brain nutrient transporter expression in the rat. *American journal of physiology, Endocrinology and metabolism*, 285(5), pp.E1127–34.

Veech, R.L. et al., 2001. Ketone bodies, potential therapeutic uses. *IUBMB life*, 51(4), pp.241–7.

Veech, R.L., 2004. The therapeutic implications of ketone bodies: the effects of ketone bodies in pathological conditions: ketosis, ketogenic diet, redox states, insulin resistance, and mitochondrial metabolism. *Prostaglandins, leukotrienes, and essential fatty acids*, 70(3), pp.309–19.

Wilder, R., 1921. The effects of ketonemia on the course of epilepsy. *Mayo Clinic Proceedings*.

Yang, L. et al., 2007. Anesthetic properties of the ketone bodies beta-hydroxybutyric acid and acetone. *Anesthesia and analgesia*, 105(3), pp.673–9.

Yeh, Y.-Y. & Zee, P., 1975. Relation of Ketosis to Metabolic Changes Induced by Acute Medium-Chain Triglyceride Feeding in Rats. *The Journal of Nutrition*, (3), pp.58–67.

Yudkoff, M. et al., 2005. Response of brain amino acid metabolism to ketosis. *Neurochemistry international*, 47(1-2), pp.119–28.

Zhang, Y. et al., 2013. Contribution of Brain Glucose and Ketone Bodies to Oxidative Metabolism. In W. J. Welch et al., eds. *Oxygen Transport to Tissue XXXIV, Advances in Experimental Medicine and Biology*. Advances in Experimental Medicine and Biology. New York, NY: Springer New York, pp. 365–370.

Zwingmann, C. & Leibfritz, D., 2003. Regulation of glial metabolism studied by 13C-NMR. *NMR in biomedicine*, 16(6-7), pp.370–99.